complexes is chromatin remodeling, which involves the ATP-dependent dynamic remodeling of chromatin structure [9–13]. Chromatin remodeling complexes utilize energy from ATP hydrolysis to rearrange nucleosomal arrays in a non-covalent manner. For VDR, a specific ATP-dependent chromatin remodeling complex, WINAC, has been biochemically identified [11]. A second co-regulator complex class regulates transcriptional control directly, through physical interaction with general transcription factors and RNA polymerase II [14,15]. The DRIP/TRAP co-activator complex has been well-described as a representative of this complex class to co-activate liganded NRs in vivo and in vitro.

Members of a third co-regulator complex class are classified to modify histone tails covalently, for example, by acetylation, methylation and phosphorylation, in promoter nucleosomal arrays [16–19]. p160 family members/p300/CBP histone acetylase (HAT) co-activator complex has been well characterized as a typical member of this class. This type of HAT co-activator complex harbors one of three p160 HAT family members (SRC-1 [18], TIF2 [20,21], AIB1 [22–26]) and one of CBP/p300 HAT [27] together with other components. In addition of such co-regulator complexes to define histone acetylation state, the other histone modifying enzyme complexes to methylate histones appear to support the ligand-dependent transcriptional activation by NRs [28,29]. Though the DRIP/TRAP non-HAT and the p160/CBP HAT complexes have been described to co-activate VDR [7,30], it remains to be addressed if the other histone modifying enzyme complexes are required for VDR transactivation.

Ligand-dependent interaction of NRs with co-activator complexes are mediated through physical interaction of consensus LXXLL and related motifs present on specific complex components and the C-terminal helix 12 (H12) of the NR LBD domain [31]. The ligand-induced association of NRs with complexes is stabilized by ligand binding-induced shifting of NR H12. The molecular basis of this ligand-induced association has been deduced by X-ray analysis [32,33].

Considering the tissue-specific gene regulation by VDR from a variety of phenotypic abnormalities seen in VDR KO mice [34], the present study was undertaken to examine whether VDR requires multiple types of transcriptional co-regulator complexes. To address this issue, we generated a series of VDR H12 mutants and tested co-activation of the VDR mutants by two classes of different co-activator complexes (DRIP/TRAP and p160/CBP complexes). A VDR H12-point mutant, that selectively lost its ability to physically interact with the TRAP/DRIP complex, was still potent in ligand-induced transactivation. Another VDR H12-point mutant, that was unable to associate with either co-activator in vitro, still retained ligand-induced transactivation. Thus, taken together, our results suggest that multiple known and unknown types of co-activator complex support ligand-induced transactivation by VDR.

Material and methods

Materials

Rat VDR cDNA in pSG5 [30] was applied to generate a series of alanine point replaced mutants in the VDR H12. Mutagenesis was performed through PCR with specific sets of oligonucleotide primers. For GST fusion proteins of the VDR point mutants, the cDNAs of VDR LBD point mutants were inserted into pGEX-4T-1. For one-hybrid analysis of the VDR mutants with TIF2, TIF2 cDNA was fused with a cDNA of VP16 activation domain to generate a TIF2 chimeric protein with VP16.

Cell culture and transient transfection

COS-1 cells (derived from monkey kidney) and 293T cells (derived from human kidney) were maintained in DMEM supplemented with 5% FBS (Gibco) at 37 °C, 5% CO_2. For transfection, cells were cultured in DMEM (phenol red-free) supplemented with 5% charcoal-stripped FBS. Cells were transfected with expression vectors of either VDR, RXR, co-activators, or the combined and were harvested for 24 h, after treatment with vehicle or 1, $25(OH)_2D_3$ (1×10^{-8} M). For one-hybrid analysis, the expression vectors of VDR mutants and VP16-TIF2 chimeric protein were transfected and incubated for 24 h in the presence of 1, $25(OH)_2D_3$ (1×10^{-8} M). The total cell extracts prepared from the transfectants were applied for a luciferase assays as described [11].

Western blotting

The transfected COS-1 cells used for the luciferase assay were also utilized for Western blotting analysis to measure the expression levels of the VDR mutants. Briefly the transfectants were lysed in TNE (10 mM Tris–HCl, pH 7.8, 1% Nonidet P-40, 0.15 M NaCl, 1 mM EDTA, 1 mM phenylmethylsulfonyl fluoride, 1 μg/ml aprotini) buffer. Cell lysates were separated by 8% SDS-polyacrylamide gel eletrophoresis, transferred onto polyvinylidene difluoride membranes (Milliopore) and detected with rat anti-VDR monoclonal antibody (NeoMarkers) and anti-rat IgG antibody conjugated with horseradish peroxidase (Dako).

GST pull-down assay

For the GST pull-down assay, TIF2 and DRIP205 were in vitro-translated and incubated with GST-fused a series of VDR point mutants deleting the A/B and C domain as illustrated in Fig. 3, immobilized on glutathione–Sepharose beads, in the absence or presence of 1, $25(OH)_2D_3$ (1×10^{-6} M) [35].

Chromatin immunoprecipitation

Soluble chromatin from 293T cells derived from human kidney, prepared using the chromatin immunoprecipitation assay kit (Upstate), was immunoprecipitated with antibodies against the indicated proteins [11,36]. Specific primer pairs were designed to amplify the promoter region of human vitamin D 24 hydroxylase (5′-GGGAGGCGCGTTCGAA-3′ and 5′-TCCTATGCCCAGGGAC-3′), from genomic DNA. PCR conditions were optimized to allow semi-quantitative measurement and PCR products were visualized on 2% agarose/TAE gels.

Results

Several, but not all, point mutations in VDR helix 12 impair ligand-induced transactivation function

As illustrated in Fig. 1, a series of alanine replacements were introduced into the transactivation core domain (AD core) in the VDR H12 domain. The amino acid

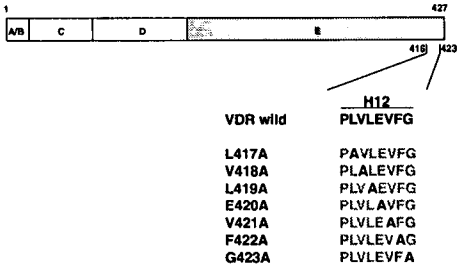

Fig. 1. Schematic representation of VDR point mutants. Rat VDR protein is schematically displayed, and alanine point replacement in H12 domains are indicated in the lower panel.

residue number of rat VDR H12 is adjusted to those of human VDR, since the length and amino acid residues of H12 is identical between rat and human. We then examined the ligand-induced transactivation function of the VDR mutants by a transient expression assay with their expression vectors and a luciferase reporter plasmid containing a consensus VDRE (DR3) in its promoter. The plasmids were transfected with a renal cell line, COS-1 cells as indicated in Fig. 2.

Ligand-induced transactivation of VDR in the presence of RXR was severely impaired by alanine replacement at 417Leu, 420Glu, 422Phe, while only partial reductions in transactivation were observed in V418A, L419A and V421A VDR H12 mutants. Unexpectedly, the 423 glycine replacement (G423A) rather potentiated ligand-induced transactivation of VDR. Thus, the loss of ligand-induced transactivation of 417, 420 and 422 VDR point mutations was expected to be caused by abrogation of co-activator interaction through H12. In contrast, the

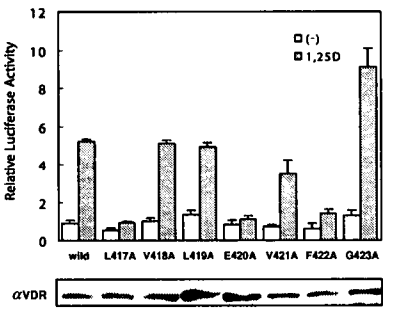

Fig. 2. H12 point mutations of VDR caused altered transactivation function of liganded VDR. The expression vectors of VDR mutants were transfected with COS-1 cells in the presence of 1, $25(OH)_2D_3$ (1×10^{-8} M). The transfected cells were applied for a luciferase analysis. The averages of the results from three independent experiments are shown with ±SD (upper panel). The expression levels of the VDR mutants were verified by Western blotting with a specific antibody for VDR (lower panel).

retained though diminished activities of the other mutants suggest there was still a retained ability to interact with co-activators in a ligand-dependent manner in some mutants. The transcriptional activities of the VDR mutants appeared unlikely due to the mutant expression levels, when the expression levels were estimated by Western blot analysis (see lower panel in Fig. 2). Note that we could confirm the same observations in human kidney cell line 293T cells (data not shown).

Different usage of co-activators for VDR H12-point mutants

To verify whether transcriptionally active VDR H12 mutants are capable of interacting with the best characterized co-activators, ligand-induced interaction of VDR mutants with DRIP205/TRAP220 and TIF2 co-activators was tested. DRIP205/TRAP220 was originally identified to physically interact in vitro with liganded VDR as a non-HAT DRIP/TRAP co-activator complex component. This complex then co-activated VDR as observed by an in vitro transcription assay [15]. TIF2, one of three p160 HAT co-activator family members, has been well described to associate with VDR in a ligand-dependent manner. By a GST pull-down assay, the inactive VDR mutants (L417A, E420A and F422A) were expectedly seen to lose their co-activator interactions (Fig. 3). Surprisingly, a transcriptionally active VDR mutant (V421A) was also unable to associate with either co-activator, and the V418A mutant interacted with only TIF2, but not DRIP205. To confirm these observations, a one-hybrid system with the VDR mutants and a TIF2 chimeric protein fused with a VP16 activation domain for a sensitive detection, was used to detect ligand-induced interaction of the VDR mutants with TIF2. Reflecting the observation in vitro, TIF2 interactions were observed in the V418A, L419A, and G423A mutants, but not in the V421A mutant in COS-1 cells (Fig. 4) and 293T cells (data not shown).

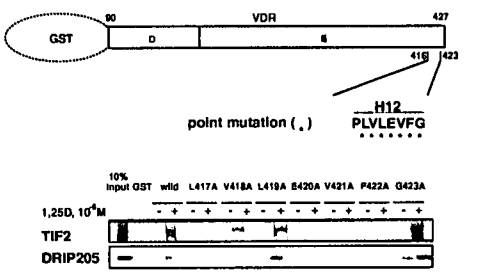

Fig. 3. Differential associations of VDR mutants with co-activators. Singular print mutations (•) introduced into H12 in the GST-VDR were the same as shown in Fig. 1. Two best known co-activators (TIF2 and DRIP205) were in vitro translated and incubated with the bacterially expressed VDR chimeric mutants fused with GST in the absence (−) or presence (+) of 1, $25(OH)_2D_3$ (1×10^{-6} M). The association was visualized on SDS PAGE.

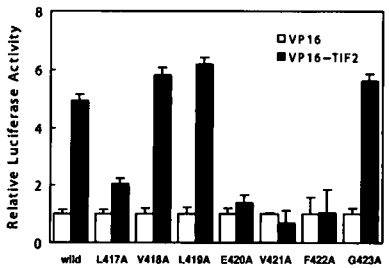

Fig. 4. The V421A VDR mutant failed to functionally associate with TIF2. As described in Fig. 2, a luciferase assay was performed for one-hybrid assay to detect ligand-dependent association of the VDR mutants with TIF2. Although V421A mutant was only partially impaired in the ligand-induced transactivation, this mutant failed to interact with TIF2, in accordance with in vitro GST-pull down assay (see Fig. 3).

VDR H12 mutants are recruited to the target promoter in vivo

We could not still exclude the possibility that several H12 point-mutations disable VDR from associating with the target promoter, leading to impaired transactivation in the transient expression assay, even though the expression levels of the VDR mutants were unaltered by the point mutations. To address this issue, we tested if these mutants are recruited to the endogenous target promoter of human vitamin D 24 hydroxylase [24(OH)ase] gene, that is well known to contain typical VDRE [37] by ChIP analysis. As shown in Fig. 5, V418A and V421A were recruited to the promoters, and the transcriptionally inactive VDR mutants were also recruited (data not shown). These findings clearly suggest that promoter targeting of VDR/RXR heterodimer to the target promoter does not directly couple with transactivation function of liganded VDR. As the HAT co-activators recruited to ligand VDR are presumed to acetylate histones for histone modification, histone modification may be dispensable for promoter targeting of VDR.

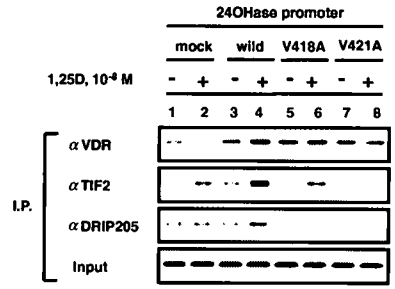

Fig. 5. The VDR point mutants were recruited to the human vitamin D 24-hydroxylase gene promoter. ChIP analysis was performed in the human vitamin D 24-hydroxylase gene promoter in 293T cells transfected with the indicated plasmids shown in the figure. The immobilized chromatin immunoprecipitated by a specific antibody was used for PCR to detect the factor bindings as described in Materials and methods.

Discussion

Is chromatin remodeling and histone modification independent from VDR-mediated gene regulation?

In our study, we have already reported that ligand-induced transactivation and transrepression mediated VDR requires chromatin remodeling through one class of ATP-dependent chromatin remodeling complex, WINAC [11,38]. Ligand-independent association of VDR with WSTF protein in the WINAC complex as well as non-specific but significant interaction of the WSTF bromo domain with acetylated histone appear to assist targeting of VDR to specific DNA binding regions in the VDR target gene promoters [38]. At the present time it is unclear whether chromatin remodeling is coupled with histone modification in VDR-mediated gene regulations. For sex steroid hormone receptors, histone modification appears indispensable prior to chromatin remodeling since steroid receptor recruitment to the target promoter is dependent on ligand binding [39]. This is presumably accompanied by recruitment of histone modifying enzyme co-regulator complexes that undergo histone modification. However, unlike steroid receptors, we observed ligand-independent recruitment of VDR to the target promoters, implying a possibility that promoter targeting of VDR does not require histone modification. This idea was further supported by the observations that the V421A VDR H12 mutant is unable to associate with the p160 HAT co-activators, but was still recruited to the promoter (Fig. 5). Thus, it is more likely that WINAC associating with VDR remodels the target chromosomal areas to expose VDREs, leading to stable DNA binding of VDR/RXR.

The two classes of co-activator have distinct sites of direct contact with VDR AF-2

By generating a series of VDR mutants, we have shown in this study that point-mutations in VDR H12 regions result in loss of ligand binding-dependent ability to associate with the tested co-activators, DRIP205 and TIF2. This would agree with the recent view that H12 serves as a direct interface for co-activator interaction through physical interaction with LXXLL motifs of the co-activators [40,41]. By detailed analysis of the interaction of VDR H12 mutants with co-activators in vitro, we found that a VDR H12 mutant (V418A) lacking ligand-induced ability to associate with DRIP205 is still capable of interacting with the other class of co-activator TIF2 (Figs. 3 and 4). These findings were unexpected, since the H12 domain is well established to serve as the direct interface to recruit DRIP205 in the DRIP/TRAP co-activator complex [42]. Indeed, loss of the interaction with DRIP205 was also confirmed to impair ligand-induced transactivation of VDR in vitro. As this V418A mutant was still transcriptionally ligand-inducible, this mutation appears unlikely to abrogate the indispensable H12 property of ligand-induced H12 shifting. Moreover, ligand-induced recruitment to VDR was seen in the VDR target gene promoter by ChIP analysis (Fig. 5). Thus, together with these findings, it is most likely that ligand-induced transactivation of VDR is supported by multiple classes of co-activator complex.

A third co-activator complex for VDR?

Accumulating evidence of co-regulator/co-regulator complex identification suggests that ligand-induced transactivation of nuclear receptors is supported by a number of co-regulators/co-regulator complexes [43,44]. Each co-regulators complex is believed to govern a distinct process in gene regulation.

However, at least among co-activators, functional redundancy is observed in our in vitro transactivation assays. In the present study, the V421A VDR H12 mutant was unexpectedly transcriptionally active even though this mutant lost its ability to interact with either class of co-activator complexes, both of which have been shown indispensable for ligand-induced transactivation of VDR in vitro [12,14,15]. These findings indicate the possible existence of other co-activator complexes. Although histone acetylation is well described to trigger chromatin activation for following gene expression, methylation of specific residues of histone tails has recently proposed to also enable chromatin active for transcription [28,29]. In this respect, like the other NR members, histone methylase complex(es) recruited to liganded VDR may be potent enough to activate chromatin through functional association with HAT complexes, leading co-activation of liganded VDR. To verify this idea, identification of the third critical co-activator/co-activator complex using several distinct approaches is required. Such studies would enhance our understanding of the spatial and temporal function of VDR in various target tissues.

Acknowledgments

We thank Teijin Pharma Ltd. for the 1α, 25(OH)$_2$D$_3$. We also thank H. Higuchi for manuscript preparation. This work was supported in part by the Program for Promotion of Basic Research Activities for Innovative Biosciences (PROBRAIN) and priority areas from the Ministry of Education, Culture, Sports, Science and Technology (to S.K.).

References

[1] H.F. DeLuca, Adv. Exp. Med. Biol. 196 (1986) 361–375.
[2] R. Bouillon, W.H. Okamura, A.W. Norman, Endocr. Rev. 16 (1995) 200–257.
[3] M.R. Walters, Endocr. Rev. 13 (1992) 719–764.
[4] D.J. Mangelsdorf, C. Thummel, M. Beato, P. Herrlich, G. Schutz, K. Umesono, B. Blumberg, P. Kastner, M. Mark, P. Chambon, R.M. Evans, Cell 83 (1995) 835–839.
[5] M.R. Hughes, P.J. Malloy, D.G. Kieback, R.A. Kesterson, J.W. Pike, D. Feldman, B.W. O'Malley, Science 242 (1988) 1702–1705.
[6] M.R. Haussler, G.K. Whitfield, C.A. Haussler, J.C. Hsieh, P.D. Thompson, S.H. Selznick, C.E. Dominguez, P.W. Jurutka, J. Bone Miner. Res. 13 (1998) 325–349.
[7] S. Kim, N.K. Shevde, J.W. Pike, J. Bone Miner. Res. 20 (2005) 305–317.
[8] C.K. Glass, M.G. Rosenfeld, Genes Dev. 14 (2000) 121–141.
[9] D.V. Fyodorov, J.T. Kadonaga, Cell 106 (2001) 523–525.
[10] T. Ito, M. Bulger, M.J. Pazin, R. Kobayashi, J.T. Kadonaga, Cell 90 (1997) 145–155.
[11] H. Kitagawa, R. Fujiki, K. Yoshimura, Y. Mezaki, Y. Uematsu, D. Matsui, S. Ogawa, K. Unno, M. Okubo, A. Tokita, T. Nakagawa, T. Ito, Y. Ishimi, H. Nagasawa, T. Matsumoto, J. Yanagisawa, S. Kato, Cell 113 (2003) 905–917.
[12] B. Lemon, C. Inouye, D.S. King, R. Tjian, Nature 414 (2001) 924–928.
[13] G.J. Narlikar, H.Y. Fan, R.E. Kingston, Cell 108 (2002) 475–487.
[14] W. Gu, S. Malik, M. Ito, C.X. Yuan, J.D. Fondell, X. Zhang, E. Martinez, J. Qin, R.G. Roeder, Mol. Cell 3 (1999) 97–108.
[15] C. Rachez, Z. Suldan, J. Ward, C.P. Chang, D. Burakov, H. Erdjument-Bromage, P. Tempst, L.P. Freedman, Genes Dev. 12 (1998) 1787–1800.
[16] T. Heinzel, R.M. Lavinsky, T.M. Mullen, M. Soderstrom, C.D. Laherty, J. Torchia, W.M. Yang, G. Brard, S.D. Ngo, J.R. Davie, E. Seto, R.N. Eisenman, D.W. Rose, C.K. Glass, M.G. Rosenfeld, Nature 387 (1997) 43–48.
[17] Y. Kamei, L. Xu, T. Heinzel, J. Torchia, R. Kurokawa, B. Gloss, S.C. Lin, R.A. Heyman, D.W. Rose, C.K. Glass, M.G. Rosenfeld, Cell 85 (1996) 403–414.
[18] S.A. Onate, S.Y. Tsai, M.J. Tsai, B.W. O'Malley, Science 270 (1995) 1354–1357.
[19] J. Yanagisawa, H. Kitagawa, M. Yanagida, O. Wada, S. Ogawa, M. Nakagomi, H. Oishi, Y. Yamamoto, H. Nagasawa, S.B. McMahon, M.D. Cole, L. Tora, N. Takahashi, S. Kato, Mol. Cell 9 (2002) 553–562.
[20] H. Hong, K. Kohli, A. Trivedi, D.L. Johnson, M.R. Stallcup, Proc. Natl. Acad. Sci. USA 93 (1996) 4948–4952.
[21] J.J. Voegel, M.J. Heine, C. Zechel, P. Chambon, H. Gronemeyer, EMBO J. 15 (1996) 3667–3675.
[22] S.L. Anzick, J. Kononen, R.L. Walker, D.O. Azorsa, M.M. Tanner, X.Y. Guan, G. Sauter, O.P. Kallioniemi, J.M. Trent, P.S. Meltzer, Science 277 (1997) 965–968.
[23] H. Chen, R.J. Lin, R.L. Schiltz, D. Chakravarti, A. Nash, L. Nagy, M.L. Privalsky, Y. Nakatani, R.M. Evans, Cell 90 (1997) 569–580.
[24] H. Li, P.J. Gomes, J.D. Chen, Proc. Natl. Acad. Sci. USA 94 (1997) 8479–8484.
[25] A. Takeshita, G.R. Cardona, N. Koibuchi, C.S. Suen, W.W. Chin, J. Biol. Chem. 272 (1997) 27629–27634.
[26] J. Torchia, D.W. Rose, J. Inostroza, Y. Kamei, S. Westin, C.K. Glass, M.G. Rosenfeld, Nature 387 (1997) 677–684.
[27] V.V. Ogryzko, R.L. Schiltz, V. Russanova, B.H. Howard, Y. Nakatani, Cell 87 (1996) 953–959.
[28] E. Metzger, M. Wissmann, N. Yin, J.M. Muller, R. Schneider, A.H. Peters, T. Gunther, R. Buettner, R. Schule, Nature 437 (2005) 436–439.
[29] Y. Sedkov, E. Cho, S. Petruk, L. Cherbas, S.T. Smith, R.S. Jones, P. Cherbas, E. Canaani, J.B. Jaynes, A. Mazo, Nature 426 (2003) 78–83.
[30] K. Takeyama, Y. Masuhiro, H. Fuse, H. Endoh, A. Murayama, S. Kitanaka, M. Suzawa, J. Yanagisawa, S. Kato, Mol. Cell. Biol. 19 (1999) 1049–1055.
[31] D.M. Heery, E. Kalkhoven, S. Hoare, M.G. Parker, Nature 387 (1997) 733–736.
[32] A.K. Shiau, D. Barstad, P.M. Loria, L. Cheng, P.J. Kushner, D.A. Agard, G.L. Greene, Cell 95 (1998) 927–937.
[33] A.K. Shiau, D. Barstad, J.T. Radek, M.J. Meyers, K.W. Nettles, B.S. Katzenellenbogen, J.A. Katzenellenbogen, D.A. Agard, G.L. Greene, Nat. Struct. Biol. 9 (2002) 359–364.
[34] T. Yoshizawa, Y. Handa, Y. Uematsu, S. Takeda, K. Sekine, Y. Yoshihara, T. Kawakami, K. Arioka, H. Sato, Y. Uchiyama, S. Masushige, A. Fukamizu, T. Matsumoto, S. Kato, Nat. Genet. 16 (1997) 391–396.
[35] T. Imai, K. Matsuda, T. Shimojima, T. Hashimoto, Y. Masuhiro, T. Kitamoto, A. Sugita, K. Suzuki, H. Matsumoto, S. Masushige, Y. Nogi, M. Muramatsu, H. Handa, S. Kato, Biochem. Biophys. Res. Commun. 233 (1997) 765–769.

[36] Y. Shang, X. Hu, J. DiRenzo, M.A. Lazar, M. Brown, Cell 103 (2000) 843–852.
[37] K.S. Chen, H.F. DeLuca, Biochim. Biophys. Acta 1263 (1995) 1–9.
[38] R. Fujiki, M.S. Kim, Y. Sasaki, K. Yoshimura, H. Kitagawa, S. Kato, EMBO J. 24 (2005) 3881–3894.
[39] V. Kumar, P. Chambon, Cell 55 (1988) 145–156.
[40] J.J. Voegel, M.J. Heine, M. Tini, V. Vivat, P. Chambon, H. Gronemeyer, EMBO J. 17 (1998) 507–519.
[41] C.X. Yuan, M. Ito, J.D. Fondell, Z.Y. Fu, R.G. Roeder, Proc. Natl. Acad. Sci. USA 95 (1998) 7939–7944.
[42] C. Rachez, B.D. Lemon, Z. Suldan, V. Bromleigh, M. Gamble, A.M. Naar, H. Erdjument-Bromage, P. Tempst, L.P. Freedman, Nature 398 (1999) 824–828.
[43] B. Belandia, R.L. Orford, H.C. Hurst, M.G. Parker, EMBO J. 21 (2002) 4094–4103.
[44] L.P. Freedman, Cell 97 (1999) 5–8.

nature medicine

Central control of bone remodeling by neuromedin U

Shingo Sato[1], Reiko Hanada[2], Ayako Kimura[1], Tomomi Abe[3], Takahiro Matsumoto[4,5], Makiko Iwasaki[1], Hiroyuki Inose[1], Takanori Ida[2], Michihiro Mieda[3], Yasuhiro Takeuchi[6], Seiji Fukumoto[7], Toshiro Fujita[7], Shigeaki Kato[4,5], Kenji Kangawa[8], Masayasu Kojima[2], Ken-ichi Shinomiya[1] & Shu Takeda[1]

Bone remodeling, the function affected in osteoporosis, the most common of bone diseases, comprises two phases: bone formation by matrix-producing osteoblasts[1] and bone resorption by osteoclasts[2]. The demonstration that the anorexigenic hormone leptin[3–5] inhibits bone formation through a hypothalamic relay[6,7] suggests that other molecules that affect energy metabolism in the hypothalamus could also modulate bone mass. Neuromedin U (NMU) is an anorexigenic neuropeptide that acts independently of leptin through poorly defined mechanisms[8,9]. Here we show that *Nmu*-deficient (*Nmu*$^{-/-}$) mice have high bone mass owing to an increase in bone formation; this is more prominent in male mice than female mice. Physiological and cell-based assays indicate that NMU acts in the central nervous system, rather than directly on bone cells, to regulate bone remodeling. Notably, leptin- or sympathetic nervous system–mediated inhibition of bone formation[6,7] was abolished in *Nmu*$^{-/-}$ mice, which show an altered bone expression of molecular clock genes (mediators of the inhibition of bone formation by leptin). Moreover, treatment of wild-type mice with a natural agonist for the NMU receptor decreased bone mass. Collectively, these results suggest that NMU may be the first central mediator of leptin-dependent regulation of bone mass identified to date. Given the existence of inhibitors and activators of NMU action[10], our results may influence the treatment of diseases involving low bone mass, such as osteoporosis.

Bone mass is maintained at a constant level between puberty and menopause by a succession of bone-resorption and bone-formation phases[11,12]. The discovery that neuronal control of bone remodeling is mediated by leptin[6] shed light on a new regulatory mechanism of bone remodeling and also suggested that bone mass may be regulated by a variety of neuropeptides[13]. In line with this observation, cannabinoids and pituitary hormones have been shown to be intimately involved in bone remodeling[14,15]. Leptin inhibits bone formation by binding to its receptors located in hypothalamus and thereby activating the sympathetic nervous system (SNS), which requires the adrenergic β2 receptors (Adrb2) expressed in osteoblasts[7,16]. Downstream of Adrb2, leptin signaling activates molecular clock genes that regulate osteoblast proliferation and hence bone formation[17]. In addition, leptin regulates bone resorption through two distinct pathways[16].

NMU is a small peptide produced by nerve cells in the submucosal and myenteric plexuses in the small intestine, and also by structures in the brain, including the dorsomedial nucleus of the hypothalamus[9]. It is generally assumed that NMU acts as a neuropeptide to regulate various aspects of physiology, including appetite, stress response and SNS activation[9]. Indeed, NMU-deficient (*Nmu*$^{-/-}$) mice develop obesity due to increased food intake and reduced locomotor activity that is believed, at least in part, to be leptin independent[8]. In addition, expression of NMU is diminished in leptin-deficient (*Lep*^{ob}) mice[18], but can be induced in these mice by leptin treatment[19]. In search of additional neuropeptides that regulate bone remodeling, we analyzed *Nmu*$^{-/-}$ mice.

When assessed at 3 and 6 months of age, both male and female *Nmu*$^{-/-}$ mice showed a high bone mass phenotype as compared to the wild type (WT), with male mice more severely affected than female mice (**Fig. 1a** and data not shown). The presence of a uniform increase in bone mineral density (BMD) along the femurs of *Nmu*$^{-/-}$ mice suggested that both trabecular and cortical bone were equally affected (**Supplementary Fig. 1** online). Microcomputed tomography analysis confirmed this observation (**Fig. 1b,c**). To determine whether this phenotype was secondary to the obesity of the *Nmu*$^{-/-}$ mice, we restricted their food intake for 1 month starting at 2 months of age. This manipulation normalized the body weight and serum insulin level of the *Nmu*$^{-/-}$ mice but did not affect their high bone mass phenotype (**Fig. 1d** and data not shown). Of note, when *Nmu*$^{-/-}$ mice were backcrossed to the C57BL/6J genetic background, their body weight became similar to that of their WT littermates; however, their BMD remained high (data not shown). These results suggest that NMU regulates bone mass independently of its regulation of energy metabolism, just as leptin does[7]. To better characterize the cellular nature of the bone phenotype in the *Nmu*$^{-/-}$ mice, we

[1]Department of Orthopaedic Surgery, Graduate School, 21st Century Center of Excellence Program, Tokyo Medical and Dental University, 1-5-45 Yushima, Bunkyo-ku, Tokyo 113-8519, Japan. [2]Division of Molecular Genetics, Institute of Life Science, Kurume University, 1-1 Hyakunen-kohen, Kurume, Fukuoka 839-0842, Japan. [3]Department of Molecular Neuroscience, Tokyo Medical and Dental University 1-5-45 Yushima, Bunkyo-ku, Tokyo 113-8519, Japan. [4]Institute of Molecular and Cellular Biosciences, University of Tokyo, 1-1-1 Yayoi, Bunkyo-ku, Tokyo 113-0032, Japan. [5]Exploratory Research for Advanced Technology, Japan Science and Technology Agency, 4-1-8 Honcho, Kawaguchi, Saitama 332-0012, Japan. [6]Toranomon Hospital Endocrine Center, 2-2-2 Toranomon, Minato-ku, Tokyo 105-8470, Japan. [7]Division of Nephrology and Endocrinology, Department of Internal Medicine, University of Tokyo Hospital, 7-3-1 Hongo, Bunkyo-ku, Tokyo 113-8655, Japan. [8]Department of Biochemistry, National Cardiovascular Center Research Institute, 5-7-1 Fujishiro-dai, Suita-shi, Osaka 565-8565, Japan. Correspondence should be addressed to S.T. (shu-tky@umin.ac.jp).

Received 4 June; accepted 8 August; published online 16 September 2007; doi:10.1038/nm1640

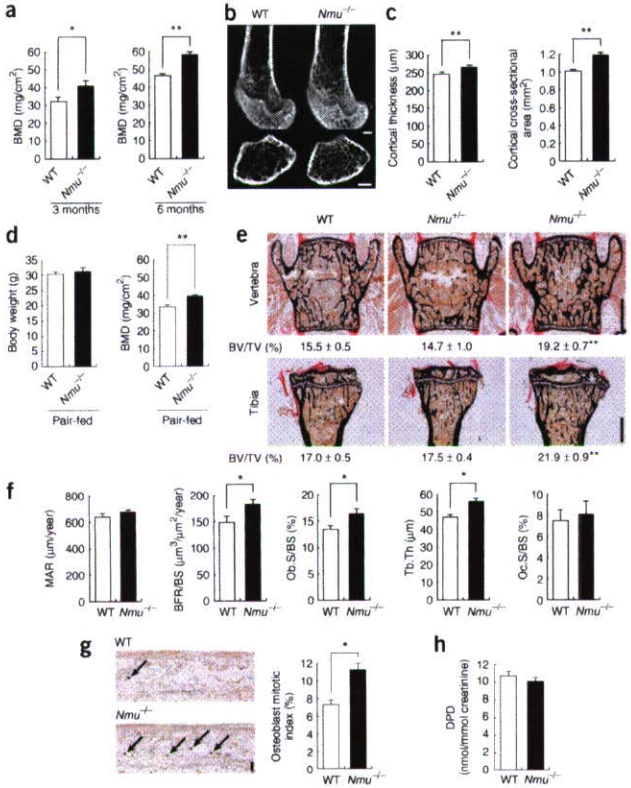

Figure 1 High bone mass in *Nmu*$^{-/-}$ mice due to increased bone formation. (**a**) Bone mineral density (BMD) of the femurs of 3 (left)- and 6 (right)-month-old male wild-type (WT) and *Nmu*$^{-/-}$ mice. (**b**) Micro-computed tomography (μCT) analysis of the distal femurs of male mice at 3 months. Scale bars, 500 μm. (**c**) Cortical thickness and cross-sectional area of the femurs of 3-month-old male mice. (**d**) Body weight and BMD of 3-month-old male mice with restricted food intake. (**e**) Histological analysis of the vertebrae and tibiae of 3-month-old male WT, *Nmu*$^{+/-}$ and *Nmu*$^{-/-}$ mice. Bone volume per tissue volume (BV/TV). Scale bars, 1 mm. (**f**) Histomorphometric analysis of the vertebrae of 3-month-old male mice. Mineral apposition rate (MAR), bone formation rate over bone surface area (BFR/BS), osteoblast surface area over bone surface area (Ob.S/BS), trabecular thickness (Tb. Th) and osteoclast surface area over bone surface area (Oc.S/BS). (**g**) Increased osteoblast proliferation in newborn *Nmu*$^{-/-}$ mice. Immunolocalization of BrdU incorporation (arrows) in the calvariae of WT and *Nmu*$^{-/-}$ mice (left). Osteoblast mitotic index (right). Scale bar, 20 μm. (**h**) Urinary elimination of deoxypyridinoline (DPD) in WT and *Nmu*$^{-/-}$ mice. **, $P < 0.01$; *, $P < 0.05$.

performed histological and histomorphometric analyses of vertebrae and tibiae in both male and female animals (**Fig. 1e** and **Supplementary Fig. 1**). At 3 and 6 months of age, *Nmu*$^{-/-}$ mice showed greater bone volume in both vertebrae and tibiae than did WT littermates, with male mice having a more pronounced phenotype (**Fig. 1e** and **Supplementary Fig. 1**). At the present time we do not have a clear explanation of the difference in phenotype severity between male and female mice. Bone formation rates (WT mice, 146.9 ± 12.3, *Nmu*$^{-/-}$ mice, 183.7 ± 10.3, $P < 0.05$) and osteoblast numbers were both significantly greater in the vertebrae and tibiae of *Nmu*$^{-/-}$ mice (**Fig. 1f** and **Supplementary Fig. 1**). The higher osteoblast numbers in the presence of a normal mineral apposition rate (**Fig. 1f** and **Supplementary Fig. 1**), which reflects the function of individual osteoblasts[20], suggested that osteoblast proliferation may be increased in *Nmu*$^{-/-}$ mice. Indeed, 5-bromo-2-deoxyuridine (BrdU)-positive proliferative osteoblast counts were significantly increased in *Nmu*$^{-/-}$ mice *in vivo* (**Fig. 1g**), demonstrating that NMU affects osteoblast proliferation. In contrast, *Nmu*$^{-/-}$ and WT mice showed comparable osteoclast numbers and osteoclast surface areas (**Fig. 1f** and **Supplementary Fig. 1**), suggesting that NMU does not affect bone resorption. This observation was further supported by the normal level of urinary elimination of deoxypyridinoline in *Nmu*$^{-/-}$ mice (**Fig. 1h**). Taken together, these results demonstrate that NMU deficiency results in an isolated increase in bone formation leading to high bone mass. *Nmu*-heterozygote mice did not have an overt bone abnormality at any age analyzed (**Fig. 1e**).

Two cognate G protein–coupled receptors have been reported to be NMU receptors: NMUR1, which is expressed in various tissues, including the small intestine and lung (data not shown), and NMUR2, which is predominantly expressed in the hypothalamus and the small intestine (**Fig. 2a**)[18]. Both receptors and NMU itself were barely detectable in bone (**Fig. 2a**). To further exclude the possibility of a direct action of NMU on osteoblasts, we treated mouse primary osteoblasts with varying concentrations of NMU. Alkaline phosphatase activity, mineralization and expression of osteoblastic genes were all unaffected by this treatment (**Fig. 2b,c**). In addition, there were no differences between WT mice and *Nmu*$^{-/-}$ mice in the expression of osteoblastic genes *in vivo* (**Fig. 2d**). Moreover, both WT and *Nmu*$^{-/-}$ osteoblasts proliferated normally *in vitro* in response to NMU treatment (**Fig. 2e**), though *Nmu*$^{-/-}$ osteoblasts proliferated more than WT osteoblasts *in vivo* (**Fig. 1g**). Osteoclastic differentiation from bone marrow macrophages was unchanged by NMU treatment (**Fig. 2f**), as expected from the absence of a bone resorption defect *in vivo* (**Fig. 1f,h**). Taken together, these results strongly suggest that NMU's effect on bone may not come from its direct action on osteoblasts, but rather through another relay.

Because the anorexigenic effect of NMU requires a hypothalamic relay[8,19] and because hypothalamic neurons have been shown to regulate bone mass, we tested whether NMU's regulation of bone formation could involve a central relay. Continuous intracerebroventricular (i.c.v.) infusion of NMU into *Nmu*$^{-/-}$ mice decreased their fat mass and fat pad weight significantly, although body weight was not affected (**Fig. 2g** and **Supplementary Fig. 2** online). In addition, NMU i.c.v. infusion eliminated the high bone mass phenotype in *Nmu*$^{-/-}$ mice (**Fig. 2g** and **Supplementary Fig. 2**), suggesting that NMU inhibits bone formation through the central nervous system.

The central nature of bone remodeling regulation by NMU, along with the notion that the anorexigenic effect of NMU may be independent of leptin[8], prompted us to examine whether leptin could be involved in the regulation of bone formation by NMU. To address this question, we performed i.c.v. infusion of NMU or leptin in *Lep*^{ob} mice. NMU decreased fat pad weight significantly, albeit to a milder extent than that achieved by leptin (**Fig. 3a** and **Supplementary Fig. 3** online). Body weight was not significantly changed by the NMU infusion, indicating that this treatment had only a mild effect on energy metabolism (data not shown). In contrast, NMU decreased bone mass in *Lep*^{ob} mice as efficiently as leptin did (**Fig. 3a**). These results indicate that NMU inhibits bone formation in a leptin-independent manner. Next, we asked whether leptin could correct the high bone mass phenotype of *Nmu*$^{-/-}$ mice. Leptin i.c.v. infusion decreased bone volume and bone formation in WT mice, as previously reported (**Fig. 3b** and **Supplementary Fig. 3**)[6]. However, the leptin paradoxically increased bone volume and osteoblast number in *Nmu*$^{-/-}$ mice (**Fig. 3b,c** and **Supplementary Fig. 3**). The fact that leptin decreased fat mass and fat pad weight in *Nmu*$^{-/-}$ mice and increased urinary elimination of normetanephrine, a metabolite of noradrenaline[17], verified that the administration of leptin was properly performed (**Fig. 3b,d** and **Supplementary Fig. 3**). Therefore, taken together, these results suggest that NMU acts downstream of leptin to regulate bone formation.

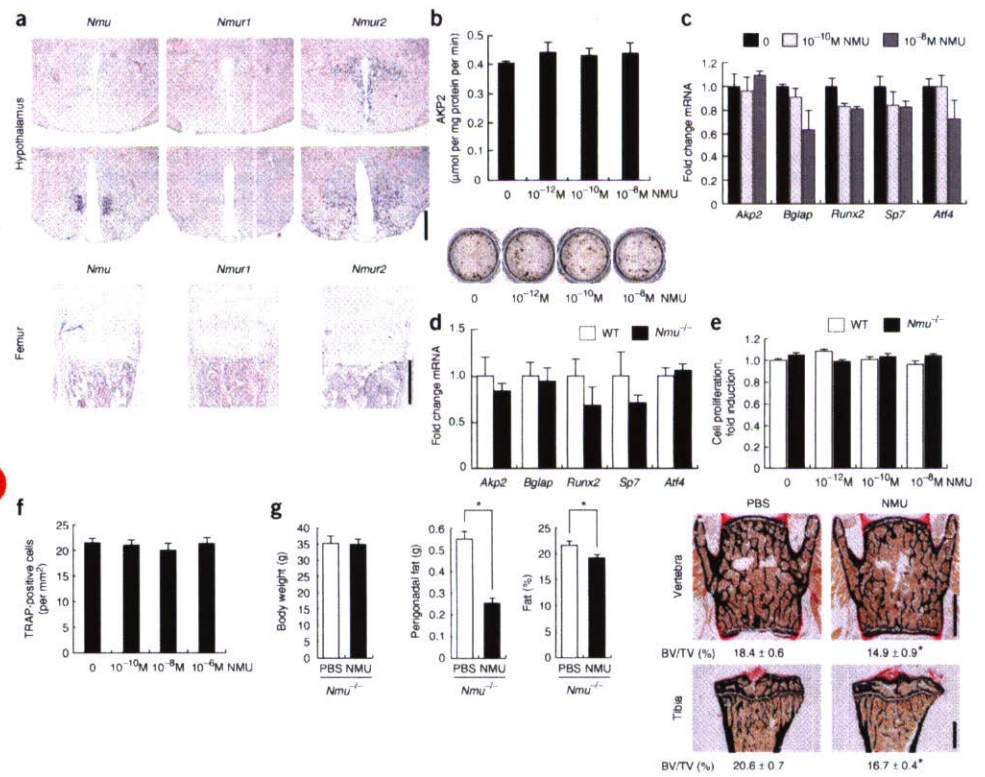

Figure 2 Absence of NMU's direct effect on osteoblasts; decrease in bone mass by NMU i.c.v. infusion. (**a**) Expression of *Nmu*, *Nmur1* and *Nmur2* in the hypothalamus at the atlas-levels of 38 (top) and 43 (bottom) and in the femur as shown by *in situ* hybridization. Note the expression of *Nmu* in the dorsomedial nucleus of the hypothalamus (DMH) (bottom) and *Nmur2* in paraventricular nucleus (top), arcuate nucleus and DMH (bottom). Scale bars, 500 μm. (**b–d**) Effect of NMU on osteoblast differentiation. (**b,c**) WT osteoblasts treated with NMU. (**b**) Alkaline phosphatase (AKP2) activity (top), mineralized nodule formation (bottom). (**c**) Expression of osteoblastic genes (*Akp2*, *Bglap*, *Runx2*, *Sp7* and *Atf4*), depicted as fold change over WT expression. (**d**) Expression of osteoblastic genes in WT and *Nmu*$^{-/-}$ femurs. (**e**) Effect of NMU on osteoblast proliferation. WT or *Nmu*$^{-/-}$ osteoblasts treated with NMU. (**f**) Effect of NMU on osteoclast differentiation. Bone marrow–derived osteoclasts treated with NMU. (**g**) Effect of NMU i.c.v. infusion on body weight, fat pad weight (perigonadal fat) and fat mass (left). Histological analysis of the vertebrae (top right) and tibiae (bottom right). Male mice at 3 months of age were used. Scale bars, 1 mm. *, $P < 0.05$.

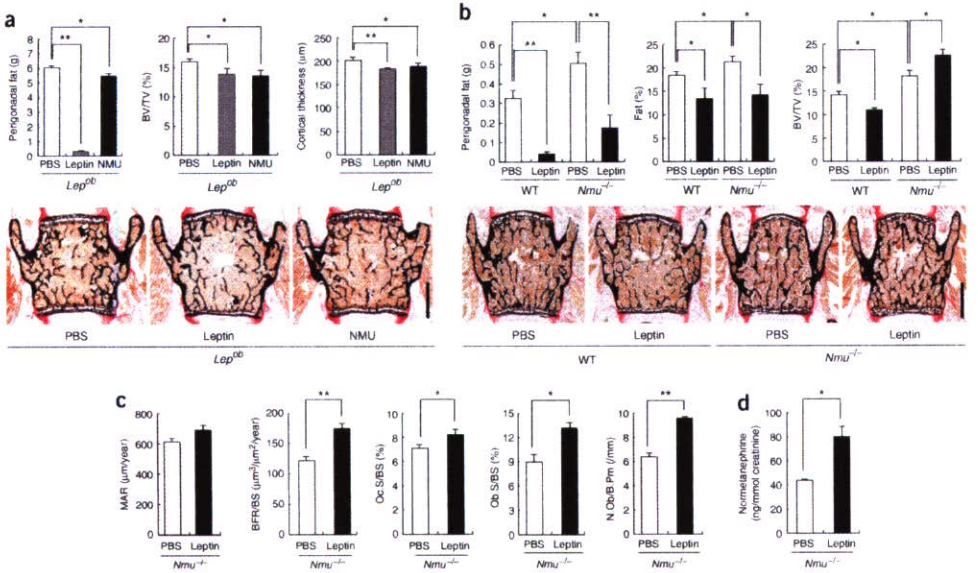

Figure 3 Leptin does not eliminate high bone mass in *Nmu*$^{-/-}$ mice. (**a**) Effect of NMU or leptin i.c.v. infusion in *Lep*^{ob} mice (3-month-old males). Fat pad weight and bone mass were determined by histology and cortical thickness by μCT analysis. (**b–d**) Effect of leptin i.c.v. infusion on *Nmu*$^{-/-}$ mice (3-month-old males). (**b**) Fat pad weight, fat mass and bone mass shown by histology. (**c**) Histomorphometric analysis. N. Ob/B.Pm indicates the number of osteoblasts per bone perimeter. (**d**) Urinary elimination of normetanephrine. Scale bars, 1 mm. **, $P < 0.01$; *, $P < 0.05$.

The SNS is a major mediator of leptin's antiosteogenic action[7]. NMUR2 is expressed in paraventricular nuclei, whose neurons directly project to the sympathetic preganglionic neurons, and NMU stimulates sympathetic outflow[9,21]. These observations, along with the fact that *Nmu*$^{-/-}$ mice have osteoblastic defects similar to the one observed in *Adrb2*-deficient mice[16], prompted us to explore whether NMU and sympathetic tone are in the same pathway regulating bone formation. Indeed, *Nmu/Adrb2* double heterozygote mice had higher bone mass than *Adrb2* single heterozygote mice (**Fig. 4a**), although *Nmu* single heterozygote mice had normal bone mass (**Fig. 1e** and **Supplementary Fig. 1**). Given that *Nmu* expression in the hypothalamus was reduced in *Nmu* single heterozygote mice (data not shown), compound heterozygosity of *Nmu* and *Adrb2* may have resulted in higher bone mass. Furthermore, this result suggests that these two pathways share a common molecule. Of note, *Nmu*$^{-/-}$ mice had a higher degree of urinary elimination of normetanephrine than WT littermates (**Fig. 4b**), which would decrease bone mass, yet they had high bone mass. This suggests that their high bone mass phenotype is not caused by decreased SNS activity, but is instead the result of resistance to the antiosteogenic activity of the SNS. This is in agreement with the observation that i.c.v. infusion of leptin, a potent stimulator of SNS activity, did not decrease bone mass in *Nmu*$^{-/-}$ mice (**Fig. 3b** and **Supplementary Fig. 3**). Furthermore, injection of isoproterenol, a sympathomimetic, reduced bone mass in WT mice[7] but not in *Nmu*$^{-/-}$ mice (**Fig. 4c** and **Supplementary Fig. 4** online). Thus, *Nmu*$^{-/-}$ mice are resistant to the antiosteogenic effects of both leptin and the SNS.

We present six experimental arguments to strongly suggest that the failure of leptin or isoproterenol to decrease bone mass in *Nmu*$^{-/-}$ mice is not due to leptin-SNS signaling defects. First, leptin infusion decreased fat pad weight equally well in WT and in *Nmu*$^{-/-}$ mice and could increase normetanephrine abundance in *Nmu*$^{-/-}$ mice (**Fig. 3b,d** and **Supplementary Fig. 3**). Second, the expression of *Adrb2* was not different in WT and *Nmu*$^{-/-}$ bones (**Fig. 4d**). Third, treatment with NMU did not affect *Adrb2* expression in osteoblasts (**Supplementary Fig. 5** online). Fourth, isoproterenol induced expression of *Tnfsf11* (encoding tumor necrosis factor superfamily, member 11) and decreased expression of *Tnfrsf11b* (encoding tumor necrosis factor superfamily, member 11b, also known as osteoprotegerin), *Runx2* (encoding runt-related transcription factor-2) and *Col1a1* (encoding collagen type I), molecular markers for the effect of SNS activation on osteoblasts, in both WT and *Nmu*$^{-/-}$ osteoblasts (**Fig. 4d**). Fifth, isoproterenol induced cAMP production equally well in WT and *Nmu*$^{-/-}$ osteoblasts (**Fig. 4e**). Sixth, and most notably, leptin increased bone resorption to a similar extent in WT and *Nmu*$^{-/-}$ mice (**Fig. 3c** and **Supplementary Fig. 3**).

The fact that the leptin-SNS pathway is intact in *Nmu*$^{-/-}$ mice, together with the paradoxical increase in osteoblast number induced by leptin i.c.v. infusion in *Nmu*$^{-/-}$ mice (**Fig. 3c**), suggests that NMU affects only the negative regulator of bone remodeling by leptin, that is, the molecular clock. Indeed, the expression of *Per1* and *Per2* (encoding period homolog-1 and -2, respectively) was downregulated in *Nmu*$^{-/-}$ bones as compared to WT bones (**Fig. 4f** and **Supplementary Fig. 6** online). Thus, NMU, acting through the central nervous system, affects the molecular clock in bone.

Because bone resorption in *Nmu*$^{-/-}$ mice was comparable to that in the wild type, despite the high SNS activity in these mice, we also

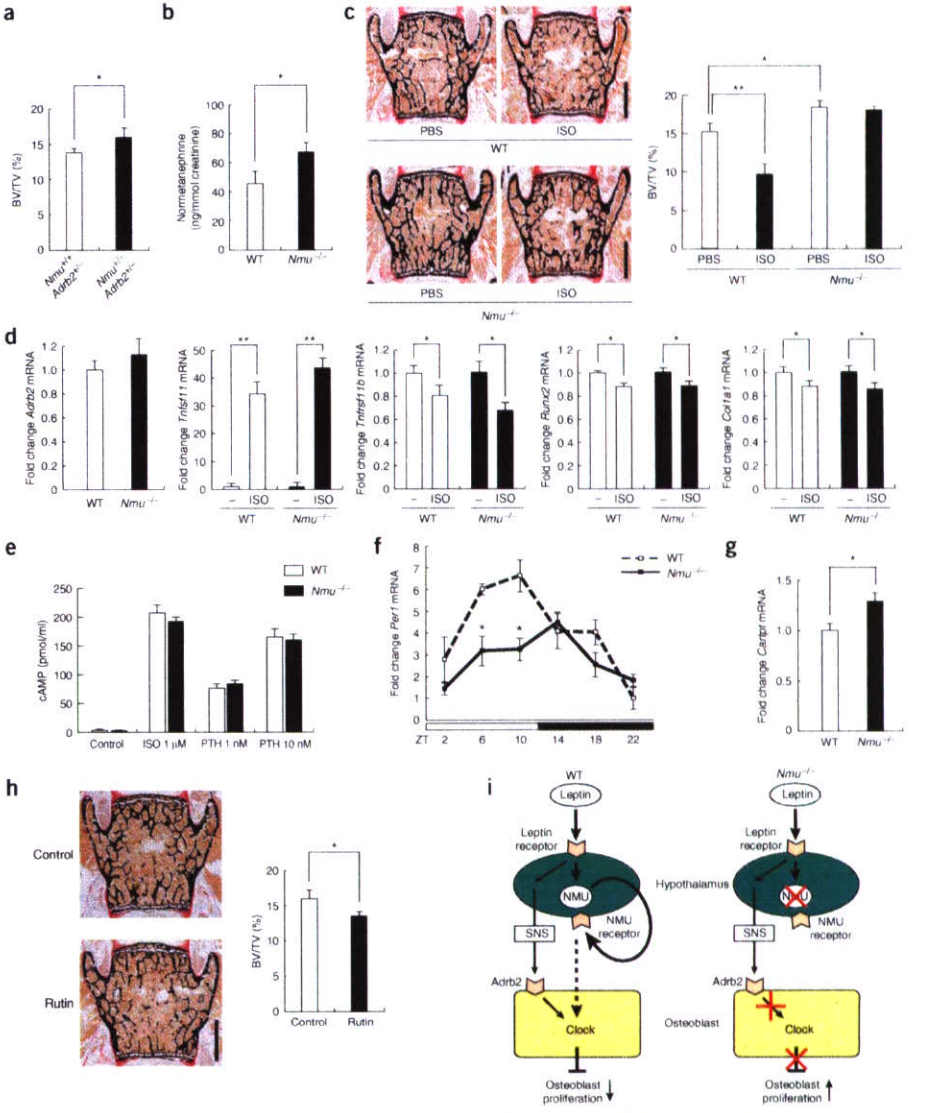

Figure 4 Sympathetic activation does not rescue high bone mass in *Nmu*$^{-/-}$ mice. (**a**) Bone mass in *Adrb2*$^{+/-}$/*Nmu*$^{+/-}$ and *Adrb2*$^{+/-}$/*Nmu*$^{+/+}$ mice as determined by histology (3-month-old males). (**b**) Increased urinary elimination of normetanephrine in *Nmu*$^{-/-}$ mice. (**c**) Effect of sympathetic activation by isoproterenol (ISO) injection in *Nmu*$^{-/-}$ mice (3-month-old males). Shown is the bone mass of vertebrae as determined by histology. (**d**) Expression of *Adrb2* in the femurs of WT and *Nmu*$^{-/-}$ mice (left). Gene expression changes induced by isoproterenol (ISO) treatment of WT and Nmu$^{-/-}$ osteoblasts (four rightmost graphs). (**e**) cAMP concentration in the culture medium of WT and *Nmu*$^{-/-}$ osteoblasts after ISO treatment. Parathyroid hormone (PTH) was used as a control. (**f**) Expression of *Per1* in the femurs of WT and *Nmu*$^{-/-}$ mice. Zeitberger time (ZT) is indicated on the *x*-axis. (**g**) Expression of *Cartpt* in the hypothalamus of WT and *Nmu*$^{-/-}$ mice. (**h**) Rutin decreases bone mass in WT mice as determined by histological analysis of vertebrae (left) and quantitative histomorphometric analysis (right) (3-month-old males). Scale bar, 1 mm. **, $P < 0.01$; *, $P < 0.05$. (**i**) Model of leptin, sympathetic nervous system (SNS) and NMU signaling for the regulation of bone formation in WT mice (left) and *Nmu*$^{-/-}$ mice (right).

tested whether the expression of *Cartpt* (encoding cocaine- and amphetamine-regulated transcript propeptide), a central mediator of leptin's action on bone resorption[16], was altered in these mice. Indeed, *Cartpt* expression was increased in *Nmu*$^{-/-}$ mice as compared to WT littermates (**Fig. 4g** and **Supplementary Fig. 7** online). These results suggest that the protective activity of Cart on bone resorption compensates for the bone-resorbing activity induced by the SNS in *Nmu*$^{-/-}$ mice. The effect of other leptin-regulated neuropeptides, such as NPY (neuropeptide Y), AgRP (agouti-related protein) and α-MSH (α-melanotropin), will be limited, because the expression of *Npy* and *Agrp* was unchanged in *Nmu*$^{-/-}$ mice[8] and melanocortin 4 receptor, a major receptor for α-MSH, has been shown to have little effect on bone remodeling by itself[22].

Lastly, we treated WT mice with rutin, a natural NMUR2 agonist found in daily foods such as buckwheat[23]. Consistent with the high bone mass phenotype of the *Nmu*$^{-/-}$ mice, rutin decreased bone mass significantly in WT mice (**Fig. 4h**). This result, together with the predominant expression of *Nmur2* in the hypothalamus (**Fig. 2a**), suggests that NMU regulates bone remodeling through NMUR2.

Collectively, these results suggest that NMU, through a central relay and via an unidentified pathway, acts as a modulator of leptin-SNS-Adrb2 regulation of bone formation (**Fig. 4i**). However, one concern still remains: because leptin affects several pathways originating in the hypothalamus and elsewhere in the brain, i.c.v. infusion of leptin may have resulted in an uncoordinated change in leptin-regulated bone remodeling that does not reflect a physiological role of leptin. To rigorously address that question, an analysis of a mouse model in which a specific nucleus of the hypothalamus is activated by leptin will be necessary. From a therapeutic point of view, given the lack of an obesity phenotype in *Nmur2*-deficient mice[24], an NMU antagonist may be a candidate for the treatment of bone-loss disorders without inducing unwanted body weight gain.

METHODS

Animals. *Nmu*$^{-/-}$ and *Adrb2*$^{-/-}$ mice were previously described[8,16]. We purchased C57BL/6J mice and C57BL/6J *Lep*^{ob} from the Jackson Laboratory. We maintained all of the mice under a 12 hr light-dark cycle with *ad libitum* access to regular food and water, unless specified. For pair-fed experiments, we caged *Nmu*$^{-/-}$ and WT mice individually for 12 weeks as described[8]. In brief, *Nmu*$^{-/-}$ mice were given access to water *ad libitum* and fed the amount of chow eaten on the previous day by a WT littermate. We determined mouse genotypes by PCR as previously described[8,16]. We injected isoproterenol (10 mg/kg, Sigma) intraperitoneally (i.p.) once daily for 4 weeks. Rutin (Sigma) was administered orally 300 mg per kg body weight per day for 4 weeks. All animal experiments were performed with the approval of the Animal Study Committee of Tokyo Medical and Dental University and conformed to relevant guidelines and laws.

Dual X-ray absorptiometry and microcomputed tomography analysis. We measured bone mineral density (BMD) of the femurs and fat pad composition by DCS-600 (Aloka). We obtained two-dimensional images of the distal femurs by microcomputed tomography (μCT, Comscan). We measured cortical thickness and cross-sectional area at the center of the femur. We examined at least eight mice for each group.

Histological and histomorphometric analysis. We injected calcein (25 mg/kg, Sigma) i.p. 5 and 2 d before sacrifice. We stained undecalcified sections of the third and fourth lumbar vertebrae and tibiae with von Kossa staining. We performed static and dynamic histomorphometric analyses using the Osteomeasure Analysis System (Osteometrics). We analyzed 8–10 mice for each group.

***In situ* hybridization analysis.** We performed *in situ* hybridization analysis according to the established protocol[25]. Antisense cRNA probe for *Cartpt* was previously described[26]. We used fragments of cDNA for *Nmu* (105 base pairs upstream to 647 base pairs downstream of the initiation codon), *Nmur1* (13–1242 base pairs downstream of the initiation codon) and *Nmur2* (16–1252 base pairs downstream of the initiation codon) to generate antisense probes. We stained sections hybridized with ^{35}S-labeled probes with Hoechst 33528 and quantitatively analyzed the expression of *Cartpt* with a phosphorimager (Bass-2500, Fuji). The atlas-level of designations corresponds to those described previously[27]. We analyzed six mice for each group.

Measurement of deoxypyridinoline cross-links and normetanephrine. We measured urinary deoxypyridinoline cross-links (DPD) and normetanephrine with the METRA DPD-EIA kit (Quidel) and the Normetanephrine-ELISA kit (ALPCO), respectively, according to the manufacturer's instructions. We used creatinine values to standardize between samples (Creatinine Assay Kit, Cayman). We examined eight samples for each group.

Cell culture. *In vitro* primary osteoblast cultures were established as previously described[6]. Briefly, we cultured primary osteoblasts from calvariae of 4-d-old mice in α-MEM (Sigma) containing ascorbic acid (0.1 mg/ml, Sigma). We added NMU to the medium twice daily. After 14 d, we measured alkaline phosphatase activity with the ALP kit (Wako). For the mineralization assay, we supplemented the medium with β-glycerophosphate (5 mM, Sigma). We assessed mineralized nodule formation by von Kossa staining. We performed the cell proliferation and cAMP assays with the Cell Proliferation Assay (Promega) and cAMP EIA kit (Cayman Chemical), respectively. *In vitro* osteoclast differentiation has been described previously[16]. Briefly, bone marrow cells of 2-month-old mice were cultured in the presence of human macrophage colony-stimulating factor (10 ng/ml, R&D Systems) for 2 d and then differentiated into osteoclasts with human RANKL (50 ng/ml, Peprotech) and human macrophage colony-stimulating factor (10 ng/ml) for 3 d. We counted tartrate-resistant acid phosphatase (TRAP)-positive multinucleated cells (more than 3 nuclei). We performed all the cell cultures in triplicate or quadruplicate wells and repeated more than 3 times.

BrdU immunohistochemistry. For BrdU labeling, we injected 100 μg BrdU i.p. into 3-d-old mice 1 h before sacrifice. We embedded calvariae in paraffin and cut coronally. We detected BrdU-incorporated osteoblasts with the BrdU Immunohistochemistry Kit (Exalpha Biologicals). We calculated the number of BrdU-positive osteoblasts over the total number of osteoblasts (osteoblast mitotic index) at three different locations (+3.0, 3.5 and 4.0 AP (0 point: bregma)) per mouse. We analyzed six mice per group.

Intracerebroventricular infusion. Intracerebroventricular infusion was performed as previously described[6]. Briefly, we exposed the calvaria of an anesthetized mouse, implanted a 28-gauge cannula (Plastics ONE) into the third ventricle and then connected the cannula to an osmotic pump (Durect) placed in the dorsal subcutaneous space of the mouse. We infused rat Neuromedin U-23 (Peptide Institute) or human leptin (Sigma) at 0.125 nmol/hr or 8 ng/hr, respectively, for 28 d.

Quantitative RT–PCR analysis. After flushing mouse bone marrow out of the bone with PBS, we extracted bone RNA with Trizol (Invitrogen) and performed reverse transcription for cDNA synthesis. We performed quantitative analysis of gene expression with the Mx3000P real-time PCR system (Stratagene). Primer sequences are available upon request. We used GAPDH expression as an internal control.

Statistical analysis. All data are represented as mean ± s.d. ($n = 8$ or more). We performed statistical analysis by Student's *t*-test. Values were considered statistically significant at $P < 0.05$. Results are representative of more than four individual experiments.

Note: Supplementary information is available on the Nature Medicine website.

ACKNOWLEDGMENTS

We thank G. Karsenty, M. Patel and P. Ducy for critical review of the manuscript and for helpful discussions; K. Nakao, M. Noda, T. Matsumoto and S. Ito for insightful suggestions; P. Barrett (Rowett Research Institute, UK) for providing a plasmid for the *Cartpt* probe; and J. Chen, M. Starbuck, S. Sunamura, H. Murayama, H. Yamato, and M. Kajiwara for technical assistance. This work was supported by grant-in-aid for scientific research from the Japan Society for the Promotion of Science, a grant for the 21st Century Center of Excellence program from the Ministry of Education, Culture, Sports, Science, and Technology of Japan, Ono Medical Research Foundation, Yamanouchi Foundation for Research on Metabolic Disorders, Kanae Foundation for the Promotion of the Medical Science and the Program for Promotion of Fundamental Studies in Health Sciences of the National Institute of Biomedical Innovation of Japan.

AUTHOR CONTRIBUTIONS

S. Sato conducted most of the experiments. K. Kangawa and M. Kojima generated *Nmu*$^{-/-}$ mice. R. Hanada and T. Ida conducted *in vitro* experiments. S. Fukumoto, Y. Takeuchi and T. Fujita contributed by conducting dual X-ray absorptiometry analyses and providing suggestions on the project. M. Iwasaki prepared the constructs. A. Kimura performed i.c.v. infusion experiments. H. Inose conducted μCT analyses. T. Matsumoto and S. Kato conducted histological analyses for brain tissue. T. Abe and M. Mieda performed *in situ* hybridization analysis. S. Takeda and K. Shinomiya designed the project. S. Takeda supervised the project and wrote most of the manuscript.

Published online at http://www.nature.com/naturemedicine
Reprints and permissions information is available online at http://npg.nature.com/reprintsandpermissions

1. Rodan, G.A. & Martin, T.J. Therapeutic approaches to bone diseases. *Science* **289**, 1508–1514 (2000).
2. Teitelbaum, S.L. & Ross, F.P. Genetic regulation of osteoclast development and function. *Nat. Rev. Genet.* **4**, 638–649 (2003).
3. Saper, C.B., Chou, T.C. & Elmquist, J.K. The need to feed: homeostatic and hedonic control of eating. *Neuron* **36**, 199–211 (2002).
4. Ahima, R.S. & Flier, J.S. Leptin. *Annu. Rev. Physiol.* **62**, 413–437 (2000).
5. Spiegelman, B.M. & Flier, J.S. Obesity and the regulation of energy balance. *Cell* **104**, 531–543 (2001).
6. Ducy, P. *et al.* Leptin inhibits bone formation through a hypothalamic relay: a central control of bone mass. *Cell* **100**, 197–207 (2000).
7. Takeda, S. *et al.* Leptin regulates bone formation via the sympathetic nervous system. *Cell* **111**, 305–317 (2002).
8. Hanada, R. *et al.* Neuromedin U has a novel anorexigenic effect independent of the leptin signaling pathway. *Nat. Med.* **10**, 1067–1073 (2004).
9. Brighton, P.J., Szekeres, P.G. & Willars, G.B. Neuromedin U and its receptors: structure, function, and physiological roles. *Pharmacol. Rev.* **56**, 231–248 (2004).
10. Fang, L., Zhang, M., Li, C., Dong, S. & Hu, Y. Chemical genetic analysis reveals the effects of NMU2R on the expression of peptide hormones. *Neurosci. Lett.* **404**, 148–153 (2006).
11. Riggs, B.L., Khosla, S. & Melton, L.J. 3rd. A unitary model for involutional osteoporosis: estrogen deficiency causes both type I and type II osteoporosis in postmenopausal women and contributes to bone loss in aging men. *J. Bone Miner. Res.* **13**, 763–773 (1998).
12. Karsenty, G. & Wagner, E.F. Reaching a genetic and molecular understanding of skeletal development. *Dev. Cell* **2**, 389–406 (2002).
13. Harada, S. & Rodan, G.A. Control of osteoblast function and regulation of bone mass. *Nature* **423**, 349–355 (2003).
14. Idris, A.I. *et al.* Regulation of bone mass, bone loss and osteoclast activity by cannabinoid receptors. *Nat. Med.* **11**, 774–779 (2005).
15. Abe, E. *et al.* TSH is a negative regulator of skeletal remodeling. *Cell* **115**, 151–162 (2003).
16. Elefteriou, F. *et al.* Leptin regulation of bone resorption by the sympathetic nervous system and CART. *Nature* **434**, 514–520 (2005).
17. Fu, L., Patel, M.S., Bradley, A., Wagner, E.F. & Karsenty, G. The molecular clock mediates leptin-regulated bone formation. *Cell* **122**, 803–815 (2005).
18. Howard, A.D. *et al.* Identification of receptors for neuromedin U and its role in feeding. *Nature* **406**, 70–74 (2000).
19. Wren, A.M. *et al.* Hypothalamic actions of neuromedin U. *Endocrinology* **143**, 4227–4234 (2002).
20. Parfitt, A.M. The physiological and clinical significance of bone histomorphometric data. in *Bone Histomorphometry* (ed. Recker, R.R.) 143–223 (CRC Press, Boca Raton, FL, 1983).
21. Chu, C. *et al.* Cardiovascular actions of central neuromedin U in conscious rats. *Regul. Pept.* **105**, 29–34 (2002).
22. Ahn, J.D., Dubern, B., Lubrano-Berthelier, C., Clement, K. & Karsenty, G. Cart overexpression is the only identifiable cause of high bone mass in melanocortin 4 receptor deficiency. *Endocrinology* **147**, 3196–3202 (2006).
23. Kalinova, J., Triska, J. & Vrchotova, N. Distribution of vitamin E, squalene, epicatechin, and rutin in common buckwheat plants (*Fagopyrum esculentum* Moench). *J. Agric. Food Chem.* **54**, 5330–5335 (2006).
24. Zeng, H. *et al.* Neuromedin U receptor 2-deficient mice display differential responses in sensory perception, stress, and feeding. *Mol. Cell. Biol.* **26**, 9352–9363 (2006).
25. Elias, C.F. *et al.* Leptin differentially regulates NPY and POMC neurons projecting to the lateral hypothalamic area. *Neuron* **23**, 775–786 (1999).
26. Graham, E.S. *et al.* Neuromedin U and Neuromedin U receptor-2 expression in the mouse and rat hypothalamus: effects of nutritional status. *J. Neurochem.* **87**, 1165–1173 (2003).
27. Paxinos, G. & Franklin, K. *The Mouse Brain in Stereotaxic Coordinates* 2nd edn. (Academic Press, San Diego, 2001).

Available online at www.sciencedirect.com
ScienceDirect
Journal of Steroid Biochemistry & Molecular Biology 103 (2007) 372–380
The Journal of Steroid Biochemistry & Molecular Biology
www.elsevier.com/locate/jsbmb

Ligand-induced transrepressive function of VDR requires a chromatin remodeling complex, WINAC

Shigeaki Kato [a,b,*], Ryoji Fujiki [a], Mi-Sun Kim [a], Hirochika Kitagawa [a]

[a] *The Institute of Molecular and Cellular Biosciences, The University of Tokyo, 1-1-1 Yayoi, Bunkyo-ku, Tokyo 113-0032, Japan*
[b] *ERATO, Japan Science and Technology Agency, Kawaguchi, Saitama 332-0012, Japan*

Received 30 November 2006

Abstract

We have previously shown that the novel ATP-dependent chromatin remodeling complex WINAC is required for the ligand-bound Vitamin D receptor (VDR)-mediated transrepression of the 25(OH)D_3 1α-hydroxylase [1α(OH)ase] gene. However, the molecular basis for VDR promoter association, which does not involve its binding to specific DNA sequences, remains unclear. To address this issue, we investigated the function of WSTF in terms of the association between WINAC and chromatin for ligand-induced transrepression by VDR. Results of *in vitro* experiments using chromatin templates showed that the association of unliganded VDR with the promoter required physical interactions between WSTF and both VDR and acetylated histones prior to VDR association with chromatin. The acetylated histone-interacting region of WSTF was mapped to the bromodomain, and a WSTF mutant lacking the bromodomain served as a dominant-negative mutant in terms of ligand-induced transrepression of the 1α(OH)ase gene. Thus, our findings indicate that WINAC associates with chromatin through a physical interaction between the WSTF bromodomain and acetylated histones, that appears to be indispensable for VDR/promoter association for ligand-induced transrepression of 1α(OH)ase gene expression.

Keywords: Acetylated histone; Transrepression; VDIR; VDR; WSTF

1. Introduction

Lipophilic ligands, such as fat-soluble Vitamins A and D, as well as thyroid/steroid hormones, are thought to exert their physiological effects through transcriptional control of target genes via cognate nuclear receptors (NRs) [1]. NRs form a gene superfamily, and they act as ligand-inducible activators. A number of co-regulator complexes that support ligand-dependent transcription control have been identified, and these complexes can be classified into three categories according to function [2]. The first co-regulator complex class regulates transcriptional control directly, through a physical interaction with general transcription factors and RNA polymerase II [3,4]. Members of the second co-regulator complex class modify histone tails covalently, for example by acetylation, in promoter nucleosomal arrays [5–8]. The major function of the last class of complexes is chromatin remodeling, which involves the ATP-dependent dynamic remodeling of chromatin structure [9–13]. Chromatin remodeling complexes utilize energy from ATP hydrolysis to rearrange nucleosomal arrays in a non-covalent manner. As chromosomal DNA is generally packed as nucleosomal arrays, chromatin remodeling complexes are thought to render specific promoter regions accessible to other co-regulator complex classes and sequence-specific regulators.

Recently, we identified a novel, multifunctional, ATP-dependent chromatin remodeling complex, designated WINAC, which consists of 13 subunits [11]. It contains SWI/SNF chromatin remodeling complex components and DNA replication-related factors. VDR interacts with WINAC in a ligand-independent manner through the Williams syndrome transcription factor (WSTF). WSTF contains a bromodomain that is adjacent to a zinc-finger motif of the (BAZ) protein family. Members of this family harbor both a PHD finger and a bromodomain in their C-terminal domain [14]. As bromodomains have been recently shown to bind acetylated histones, it is possible that WSTF serves as an adaptor protein for acetylated histones, facilitating the association between WINAC and chromatin [15–18].

* Corresponding author at: The Institute of Molecular and Cellular Biosciences, The University of Tokyo, 1-1-1 Yayoi, Bunkyo-ku, Tokyo 113-0032, Japan. Tel.: +81 3 5841 8478; fax: +81 3 5841 8477.
E-mail address: uskato@mail.ecc.u-tokyo.ac.jp (S. Kato).

0960-0760/$ – see front matter © 2006 Elsevier Ltd. All rights reserved.
doi:10.1016/j.jsbmb.2006.12.038

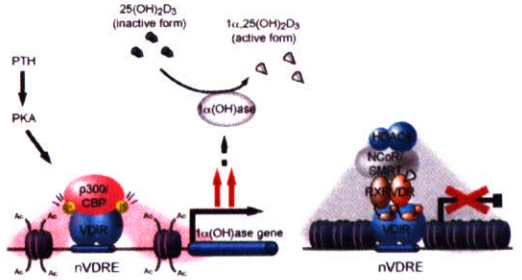

Fig. 1. Schematic view of ligand-induced transrepression by VDR in the human 1α(OH)ase gene promoter. A bHLH-type activator, VDIR, binds to the 1αnVDRE, and activates transcription. PKA signaling downstream of PTH/PTHrP phosphorylates VDIR, leading association of VDIR with HAT co-activator p300/CBP. Upon 1α,25(OH)$_2$D$_3$ binding, VDR associates with VDIR, inducing dissociation of the HAT co-activator, and recruitment of HDAC co-repressor for ligand-induced transrepression.

2. Vitamin D negatively regulates expression of the 25(OH)D_3 1α-hydroxylase gene

Expression of the 25(OH)D_3 1α-hydroxylase [1α(OH)ase] gene a key enzyme in Vitamin D biosynthesis, is negatively regulated by Vitamin D [19–21].

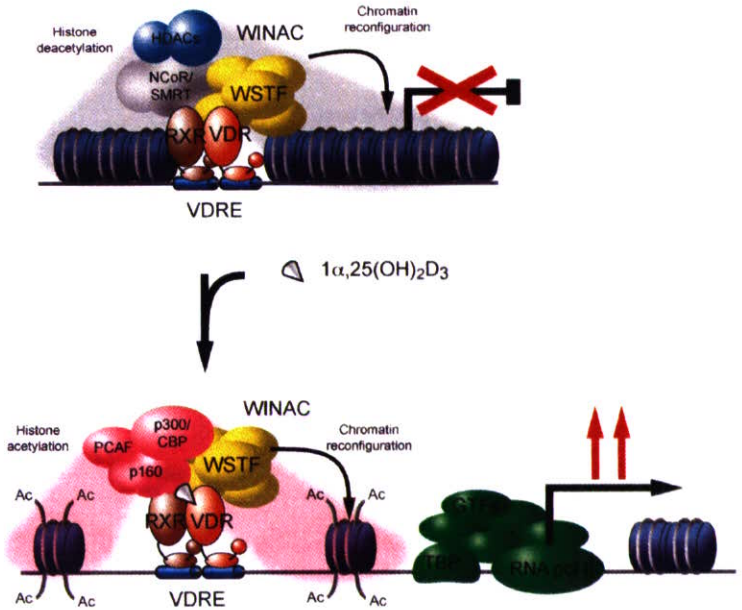

Fig. 2. WINAC supports ligand-induced transactivation by VDR. A WSTF-containing chromatin remodeling complex, WINAC, associates with VDR in a ligand-independent manner, and aids VDR to stably bind to the VDRE for ligand-induced transactivation.

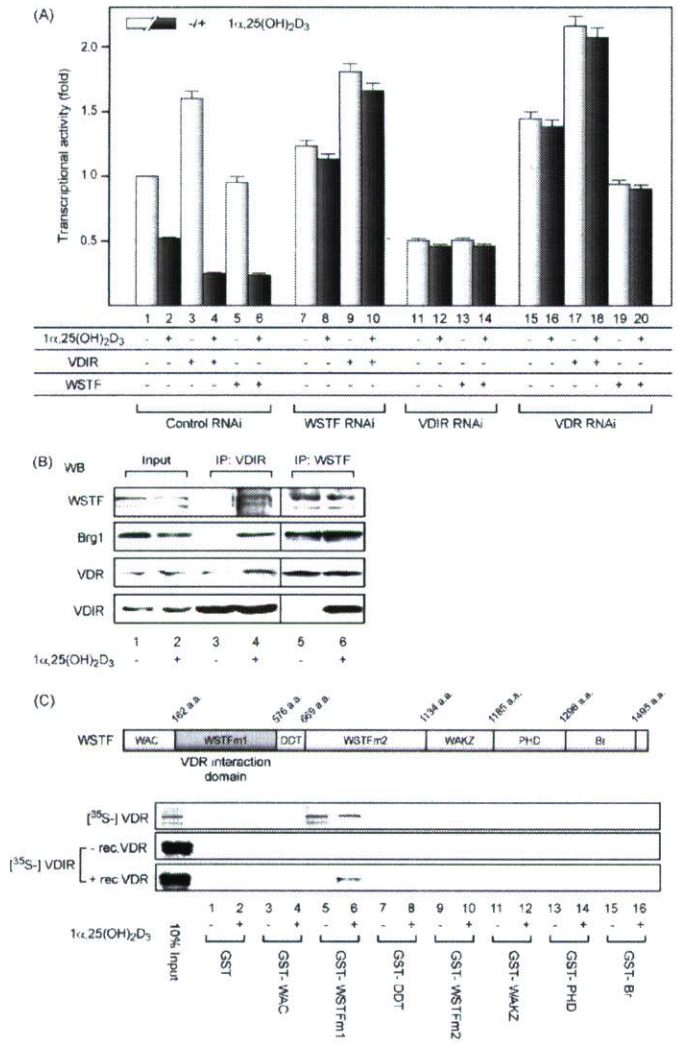

Fig. 3. WSTF enhances VDIR-mediated transrepression of 1α(OH)ase gene expression. (A) The effect of gene-specific knockdown of endogenous factors, WSTF, VDIR and VDR on 1α(OH)ase gene expression in a luciferase reporter assay. Gene-specific knockdown of the factors by RNAi was confirmed by Western blots using the relative antibodies (data not shown). MCF7 cells were transfected with 0.3 μg of the indicated siRNAs, 48 h after the transfection luciferase reporter gene containing 1α(OH)ase native promoter was transfected again into the cells. Luciferase activity was assessed after 12 h culture in the presence or absence of $1\alpha,25(OH)_2D_3$ (10^{-8} M). (B) $1\alpha,25(OH)_2D_3$-dependent interaction between endogenous WSTF and VDIR *in vivo*. MCF7 cells cultured with or without with $1\alpha,25(OH)_2D_3$ for 12 h were subjected to immunoprecipitation with anti-WSTF or anti-VDIR antibodies. Immunoprecipitates were Western blotted with specific antibodies as shown on the left. (C) SDS-PAGE gels of a series of GST-fused WSTF deletion mutants was visualized by CBB staining. Recombinant proteins were expressed in *E. coli* and purified by affinity chromatography. (D) GST pull-down assay. Schematic diagrams of the WSTF deletion mutants used are illustrated. [^{35}S]-labeled VDR translated *in vitro* was incubated with deletion mutants immobilized onto glutathione–sepharose beads in the presence or absence of $1\alpha,25(OH)_2D_3$ (10^{-6} M). Bound proteins were resolved by SDS-PAGE followed by autoradiography (upper panel). Autoradiographs show [^{35}S]-labeled VDIR, preincubated with (lower panel) or without (middle panel) cold recombinant VDR, bound to the GST-fused mutants immobilized on beads [22].

We recently reported that a bHLH-type activator, VDR-interacting repressor (VDIR), directly binds to the negative Vitamin D response element (1αnVDRE) in the human 1α(OH)ase gene promoter, thus activating transcription (Fig. 1) [22]. However, ligand-induced association between VDR and VDIR results in ligand-induced transrepression of 1α(OH)ase gene expression. This occurs through the switching of co-regulator complexes from histone acetyltransferase (HAT) co-activator complexes to histone deacetylase (HDAC) co-repressors upon VDIR binding to 1αnVDRE [22].

3. WSTF potentiates the ligand-induced transrepression by VDR in the human 1α(OH)ase gene promoter

We have previously shown that WINAC supports ligand-induced transactivation through chromatin remodeling [11] (see Fig. 2). However, it remained unclear if ligand-induced transrepression by VDR requires WINAC. To test this idea, the function of WSTF, with respect to ligand-induced VDR/VDIR transrepression, was studied by a transient expression assay using MCF7 cells, which express the 1α(OH)ase gene endogenously. A luciferase reporter gene plasmid containing two consensus 1αnVDRE sequences recognized by VDIR, that confer negative responsiveness to $1\alpha,25(OH)_2D_3$ in gene repression.

We found that endogenous VDR, VDIR and WSTF were responsible for ligand-induced negative responsiveness of the 1α(OH)ase gene, by their overexpression assay and RNAi approach (Fig. 3A). It is likely that WSTF mediates the ligand-induced transrepression of the 1α(OH)ase gene, together with VDR and VDIR.

We then examined the complex formed by these three factors in MCF-7 cells using an immunoprecipitation assay. As unliganded VDR was reported to associate with NCoR co-repressor complex [2], the co-repressor dissociation of exogenous VDR was observed in respond to ligand binding. As previously reported [11,22,23], while VDR associated with WSTF irrespective of $1\alpha,25(OH)_2D_3$ binding, $1\alpha,25(OH)_2D_3$ binding enhanced the interaction between VDR and VDIR (Fig. 3B).

By *in vitro* GST pull-down assay on a series of bacterially-expressed GST-fused WSTF mutants (Fig. 3C). The WSTF m1 domain (a.a. 163–576, illustrated as a shaded box above the panel) was found to interact with *in vitro* translated VDR, irrespective of $1\alpha,25(OH)_2D_3$ binding. While none of the WSTF regions exhibited physical interaction with VDIR, in the presence of $1\alpha,25(OH)_2D_3$-bound VDR, an association between WSTF and VDIR was detected (Fig. 3D, middle and lower panel). Together, these findings suggest that while WSTF interacts with VDR, VDIR is stably recruited only when VDR is liganded.

4. WSTF aids recruitment of ligand-unbound VDR to the 1α(OH)ase gene promoter

To test whether WSTF was recruited to VDIR via liganded VDR in the nuclei of living cells, we performed a ChIP assay using endogenous proteins and the native 1α(OH)ase gene promoter. In agreement with previous reports [11,22], VDIR was constitutively bound to 1αnVDRE (Fig. 4). As WSTF RNAi remarkably attenuated the promoter occupancy of VDR in the absence of ligand, WSTF appeared to facilitate the binding of ligand-unbound VDR to the 1αnVDRE region (Fig. 4).

To clarify the mechanism by which WSTF targets unliganded VDR to the promoter *in vitro*, we addressed which factors are indispensable for the promoter targeting of unliganded VDR by employing an immobilized DNA/chromatin template recruitment assay. DNA fragments containing either 1αnVDRE (−60 to −615) or the 1α(OH)ase distal region (−3632 to −3032) were end-biotinylated to allow their immobilization onto streptavidin beads. Using these factors, the end-biotinylated DNA fragments were correctly reconstituted into nucleosome arrays according to the MNase digestion assay (Fig. 5A). Whole cell extracts from MCF-7 cells that stably expressed FLAG-tagged WSTF treated

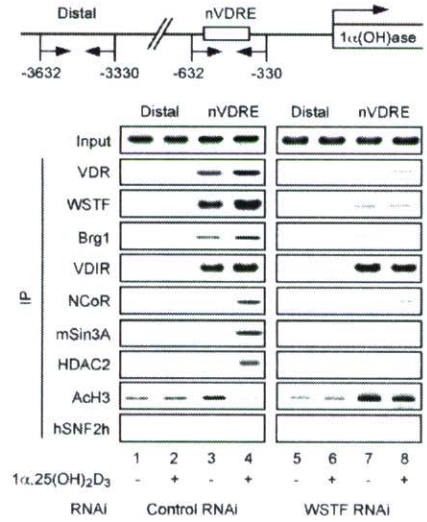

Fig. 4. WSTF is indispensable for ligand-induced promoter assembly of the VDR and HDAC co-repressor complex. Recruitment of VDR, WSTF, VDIR, and other co-regulators to the 1α(OH)ase gene promoter *in vivo*, as shown by ChIP analysis. Soluble chromatin was prepared from MCF7 cells treated with $1\alpha,25(OH)_2D_3$ (10^{-8} M) for 45 min and immunoprecipitated with the indicated antibodies. Extracted DNA samples were amplified using primer pairs that covered the 1α(OH)ase negative VDRE region (1αnVDRE) [11,22] or a distal region (3 kb upstream from 1αnVDRE) as a control.

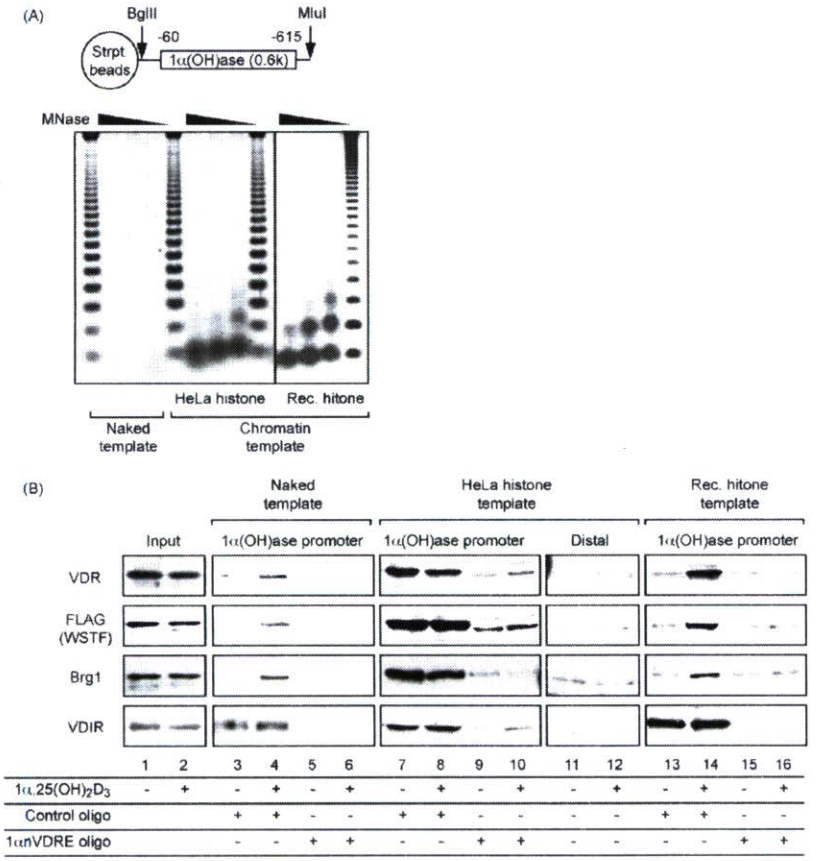

Fig. 5. Chromatin structures are required to target unliganded VDR to the 1α(OH)ase promoter. (A) Chromatin template containing the 1α(OH)ase gene promoter immobilized to streptavidin beads. Schematic representation of the DNA template containing the 1α(OH)ase gene promoter is illustrated above. Chromatinized template reconstituted *in vitro* was confirmed using the standard *Micrococcal* nuclease (MNase) digestion assay. The 123 bp ladder DNA was used as a size marker. (B) Stabilization of the ligand-free VDR/WSTF complex on the 1α(OH)ase promoter required chromatin structure *in vitro*. Whole cell extracts from MCF7 cells stably expressing FLAG-WSTF treated with or without $1\alpha,25(OH)_2D_3$ (10^{-8} M) were mixed with immobilized templates. The template beads were then concentrated using a magnet and analyzed by Western blotting using the indicated antibodies.

with or without $1\alpha,25(OH)_2D_3$ were incubated with either naked or chromatin DNA templates containing 1αnVDRE. Proteins bound to the DNA templates were then analyzed by immunoblotting (Fig. 5B). WSTF and VDR bound to naked DNA templates only in the presence of ligand, while VDIR stably associated with naked DNA templates even in the absence of ligand (Fig. 5B). The specific recruitment of WSTF, together with VDR and VDIR, to 1αnVDRE was confirmed by the finding that addition of excessive synthetic 1αnVDRE–oligonucleotides blocked recruitment (Fig. 5B). In contrast, for the chromatin templates with HeLa histone octamers, recruitment of WSTF and VDR was ligand-independent (Fig. 5B). However, WSTF and VDR were removed to significant extents from chromatinized templates by the addition of excess 1αnVDRE–oligonucleotides (Fig. 5B), indicating a role for DNA-bound VDIR in the stable association of VDR/WSTF with chromatin. This supported the significance of WSTF function in unliganded VDR recruitment to the native 1α(OH)ase promoter.

5. WSTF associates with acetylated histones for ligand-induced transrepression by VDR

We next examined the role of WSTF in binding to acetylated histones during VDR-mediated gene repression. A WSTFΔC construct was first assessed in MCF7 cells by immunoprecipitation using anti-FLAG antibodies and Western blotting with anti-acetylated lysine 14 of histone H3 (AcH3K14), anti-acetylated histone H3 (AcH3), anti-Brg1 and anti-VDR antibodies. Both wild-type WSTF and the

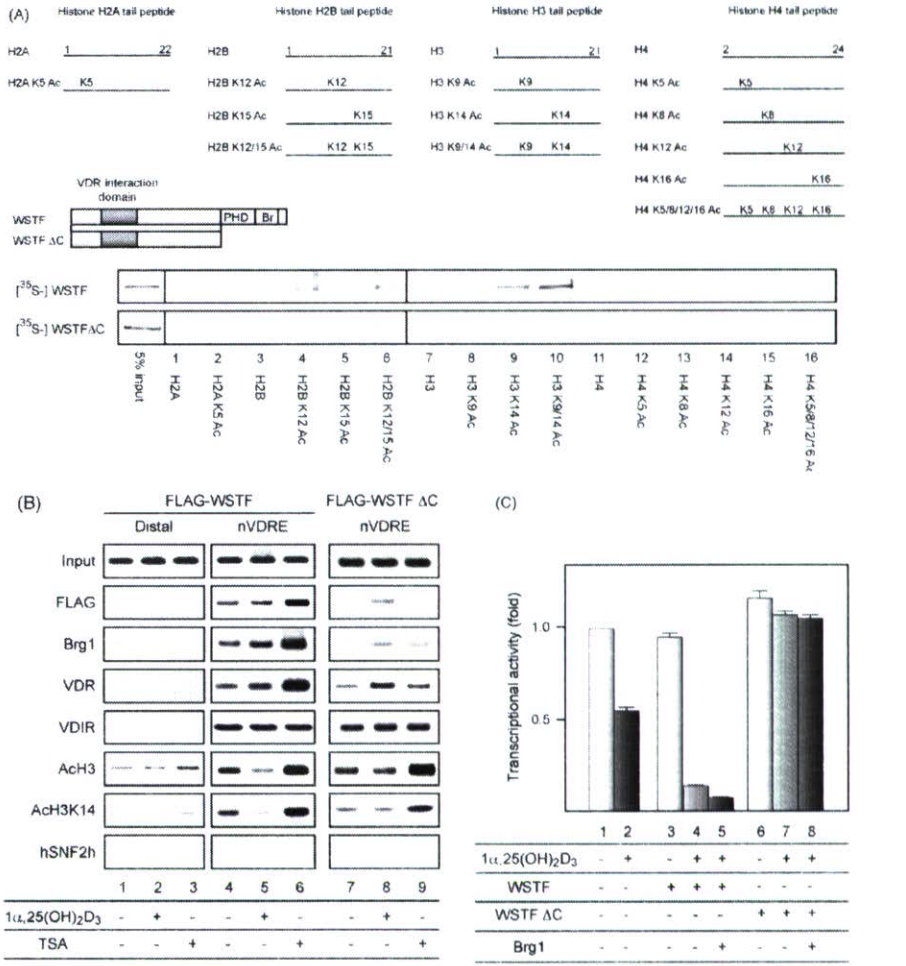

Fig. 6. The WSTF C-terminal region is indispensable for the promoter targeting of ligand-unbound VDR and for VDR-mediated transrepression of the 1α(OH)ase gene. (A) Site-specific recognition between the WSTF bromodomain and histones with tail modification. Schematic diagrams of the WSTF deletion mutants used are illustrated (upper panel). [^{35}S]-labeled WSTF and a WSTFΔC mutant translated *in vitro* were incubated with a series of acetylated N-terminal histone tails immobilized onto streptavidin beads. Histone tail peptides were tested for WSTF binding (middle panel). Bound WSTF were resolved by SDS-PAGE, followed by autoradiography (lower panel). (B) Histone acetylation-dependent recruitment of WSTF to the 1αnVDRE region. MCF7 cells transfected with FLAG-tagged WSTF or FLAG-tagged WSTFΔC were treated with either $1\alpha,25(OH)_2D_3$ (10^{-8} M) for 45 min, or TSA (10^{-7} M) for 120 min, and then subjected to ChIP analysis. (C) A WSTF mutant with a deleted C-terminal bromodomain and PHD finger (WSTFΔC) exerted a partial dominant-negative effect on the ligand-induced transrepression function of VDR. The amounts of each transfected plasmid are described in Fig. 1A.

WSTFΔC mutant appeared to associate with VDR and Brg1, that is an ATPase subunit of WINAC, as well as the other SWI/SNF chromatin remodeling complex subtypes. However, the WSTFΔC mutant exhibited no clear association with AcH3 and AcH3K14 (Fig. 6A). These findings imply that the highly acetylated state of histones induces a stable association between WSTF and chromatin *in vivo*. The WSTFΔC mutant was again unable to associate with the 1αnVDRE region, regardless of the hyperacetylated state of histone H3 (right panel, Fig. 6B). A reporter assay using the luciferase gene driven by the 1α(OH)ase promoter showed that WSTF expression potentiated the $1\alpha,25(OH)_2D_3$-induced transrepression along with Brg1 (Fig. 6C), whereas the WSTFΔC mutant acted as a dominant-negative factor in terms of the ligand-induced transrepression (Fig. 6C, black bars). Thus, it appears that WSTF interacts with acetylated histones via the bromodomain *in vivo*, and that this interaction is indispensable for VDR-mediated transrepression through the 1αnVDR.

6. Discussion

6.1. WINAC supports ligand-induced transrepression by VDR on the human 1α(OH)ase gene promoter region

A large number of co-regulator complexes appear to support transcription control by NRs at multiple but sequential steps [2,24,25]. ATP-dependent chromatin remodeling complexes are considered to facilitate the promoter-specific recruitment of other co-regulator complexes [13,26]. We have previously reported that the WINAC disfunction resulted in a failure of proper transcriptional regulation by VDR, possibly because of impairment of co-regulator recruitment to VDR-target gene promoter [11]. These findings strongly suggested that ATP-dependent chromatin remodeling activity is indispensable for subsequent co-regulator recruitment in responding to ligand binding.

In the present study, we have challenged to define the function of WSTF in the ligand-induced transrepression by VDR. From our previous findings [22], it has been considered that ligand-unbound VDR/RXR on the VDRE mainly associates with HDAC complex to actively repress target genes. Reflecting this model, ligand binding led to co-repressor dissociation from VDR, and WINAC assisted promoter recruitment of HDAC co-repressor complex in VDIR-mediated transrepression on a negative VDRE. These results imply a difference in the set of associating factors/complexes with unliganded VDR on negative VDREs from positive VDREs on the VDR target gene promoters. Indeed, ligand binding significantly increased the interaction of VDR/WINAC with HDAC complex (Fig. 4). Hence, in addition to ligand-induced transactivation by VDR, WINAC has also important role of VDR-mediated transrepression mechanism. The proposed mechanism of the ligand-induced

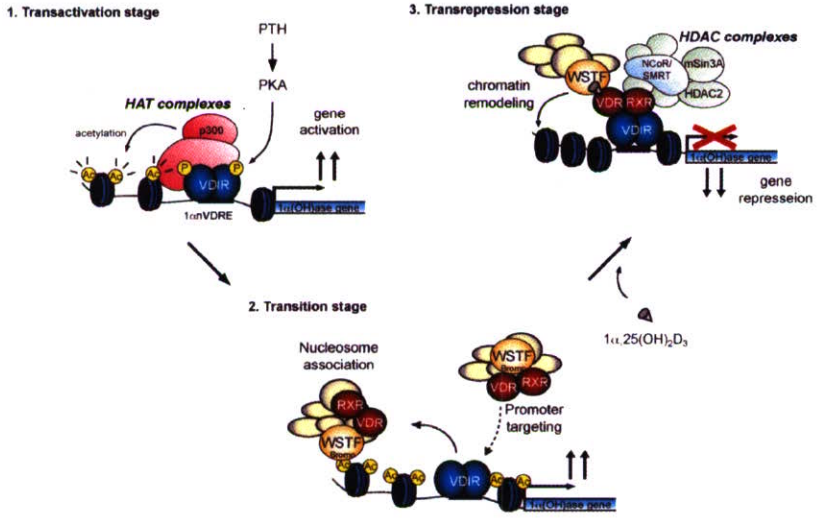

Fig. 7. Model demonstrating the role of WINAC in the ligand-induced transrepression function of VDR at the 1α(OH)ase gene promoter. p300 is recruited to VDIR, which was phosphorylated via PKA signaling, and it acetylates the nucleosomes around the 1α(OH)ase gene promoter region (transactivation stage). WINAC, along with VDR, sequentially targets VDIR through interaction between unliganded VDR and VDIR, and is retained on the acetylated promoter via the WSTF bromodomain. VDR becomes receptive to $1\alpha,25(OH)_2D_3$ binding (transition stage). Upon $1\alpha,25(OH)_2D_3$ binding, HDAC co-repressor complexes are recruited to the ligand-bound VDR/VDIR complex, and they then deacetylate the nucleosomes. WINAC then exerts its ATP-dependent chromatin remodeling activity (transrepression stage).

transrepression by VDR in the present study appears to be dependent on the promoter-content, since it is unlikely that all of the VDR target gene promoters for Vitamin D-induced transrepression harbor VDIR binding sites. The other mode and mechanism of ligand-induced transrepression might be unrevealed in the other promoters for VDR and the other NRs, like recently reported in the transrepressive function of PPARγ [27].

6.2. WSTF associates with acetylated histones to anchor VDR/WINAC complex upon VDIR on the 1α(OH)ase gene promoter region

Physical interaction of acetylated histones with the ATP-dependent chromatin remodeling complex components is a critical step in activation of chromatin, modulating its architecture by rearrangement of nucleosome arrays [14,18]. Hassan et al. found that both the SAGA and SWI/SNF complexes are capable of anchoring to promoter nucleosomes through direct contact of acetylated histones with the bromodomains [16]. However, it remained unclear how these chromatin remodeling complexes selectively discriminate their target chromosomal areas from others through their chromatin recognition modules. To address this point, we have examined two aspects of WINAC promoter targeting. One is the mechanism by which specific chromatin areas are recognized by WSTF through association with sequence-specific regulators, and the other is the preference of WSTF for a specific chromatin condition.

Thus, considering all of these results, we conclude that WINAC facilitates VDR-mediated transrepression of the 1α(OH)ase gene through a physical interaction between the WSTF bromodomain and an acetylated nucleosomal array (Fig. 7).

References

[1] D.J. Mangelsdorf, C. Thummel, M. Beato, P. Herrlich, G. Schutz, K. Umesono, B. Blumberg, P. Kastner, M. Mark, P. Chambon, R.M. Evans, The nuclear receptor superfamily: the second decade, Cell 83 (1995) 835–839.
[2] C.K. Glass, M.G. Rosenfeld, The co-regulator exchange in transcriptional functions of nuclear receptors, Genes Dev. 14 (2000) 121–141.
[3] W. Gu, S. Malik, M. Ito, C.X. Yuan, J.D. Fondell, X. Zhang, E. Martinez, J. Qin, R.G. Roeder, A novel human SRB/MED-containing cofactor complex, SMCC, involved in transcription regulation, Mol. Cell 3 (1999) 97–108.
[4] C. Rachez, Z. Suldan, J. Ward, C.P. Chang, D. Burakov, H. Erdjument-Bromage, P. Tempst, L.P. Freedman, A novel protein complex that interacts with the Vitamin D3 receptor in a ligand-dependent manner and enhances VDR transactivation in a cell-free system, Genes Dev. 12 (1998) 1787–1800.
[5] T. Heinzel, R.M. Lavinsky, T.M. Mullen, M. Soderstrom, C.D. Laherty, J. Torchia, W.M. Yang, G. Brard, S.D. Ngo, J.R. Davie, E. Seto, R.N. Eisenman, D.W. Rose, C.K. Glass, M.G. Rosenfeld, A complex containing N-CoR, mSin3 and histone deacetylase mediates transcriptional repression, Nature 387 (1997) 43–48.
[6] Y. Kamei, L. Xu, T. Heinzel, J. Torchia, R. Kurokawa, B. Gloss, S.C. Lin, R.A. Heyman, D.W. Rose, C.K. Glass, M.G. Rosenfeld, A CBP integrator complex mediates transcriptional activation and AP-1 inhibition by nuclear receptors, Cell 85 (1996) 403–414.
[7] S.A. Onate, S.Y. Tsai, M.J. Tsai, B.W. O'Malley, Sequence and characterization of a co-activator for the steroid hormone receptor superfamily, Science 270 (1995) 1354–1357.
[8] J. Yanagisawa, H. Kitagawa, M. Yanagida, O. Wada, S. Ogawa, M. Nakagomi, H. Oishi, Y. Yamamoto, H. Nagasawa, S.B. McMahon, M.D. Cole, L. Tora, N. Takahashi, S. Kato, Nuclear receptor function requires a TFTC-type histone acetyl transferase complex, Mol. Cell 9 (2002) 553–562.
[9] D.V. Fyodorov, J.T. Kadonaga, The many faces of chromatin remodeling: switching beyond transcription, Cell 106 (2001) 523–525.
[10] T. Ito, M. Bulger, M.J. Pazin, R. Kobayashi, J.T. Kadonaga, ACF, an ISWI-containing and ATP-utilizing chromatin assembly and remodeling factor, Cell 90 (1997) 145–155.
[11] H. Kitagawa, R. Fujiki, K. Yoshimura, Y. Mezaki, Y. Uematsu, D. Matsui, S. Ogawa, K. Unno, M. Okubo, A. Tokita, T. Nakagawa, T. Ito, Y. Ishimi, H. Nagasawa, T. Matsumoto, J. Yanagisawa, S. Kato, The chromatin remodeling complex WINAC targets a nuclear receptor to promoters and is impaired in Williams syndrome, Cell 113 (2003) 905–917.
[12] B. Lemon, C. Inouye, D.S. King, R. Tjian, Selectivity of chromatin-remodelling cofactors for ligand-activated transcription, Nature 414 (2001) 924–928.
[13] G.J. Narlikar, H.Y. Fan, R.E. Kingston, Cooperation between complexes that regulate chromatin structure and transcription, Cell 108 (2002) 475–487.
[14] M.H. Jones, N. Hamana, J. Nezu, M. Shimane, A novel family of bromodomain genes, Genomics 63 (2000) 40–45.
[15] C. Dhalluin, J.E. Carlson, L. Zeng, C. He, A.K. Aggarwal, M.M. Zhou, Structure and ligand of a histone acetyltransferase bromodomain, Nature 399 (1999) 491–496.
[16] A.H. Hassan, P. Prochasson, K.E. Neely, S.C. Galasinski, M. Chandy, M.J. Carrozza, J.L. Workman, Function and selectivity of bromodomains in anchoring chromatin-modifying complexes to promoter nucleosomes, Cell 111 (2002) 369–379.
[17] R.H. Jacobson, A.G. Ladurner, D.S. King, R. Tjian, Structure and function of a human TAFII250 double bromodomain module, Science 288 (2000) 1422–1425.
[18] F. Winston, C.D. Allis, The bromodomain: a chromatin-targeting module? Nat. Struct. Biol. 6 (1999) 601–604.
[19] A. Murayama, K. Takeyama, S. Kitanaka, Y. Kodera, T. Hosoya, S. Kato, The promoter of the human 25-hydroxyvitamin D3 1-alpha-hydroxylase gene confers positive and negative responsiveness to PTH, calcitonin, and 1-alpha,$25(OH)_2D_3$, Biochem. Biophys. Res. Commun. 249 (1998) 11–16.
[20] K. Takeyama, S. Kitanaka, T. Sato, M. Kobori, J. Yanagisawa, S. Kato, 25-Hydroxyvitamin D3 1-alpha-hydroxylase and Vitamin D synthesis, Science 277 (1997) 1827–1830.
[21] T. Yoshizawa, Y. Handa, Y. Uematsu, S. Takeda, K. Sekine, Y. Yoshihara, T. Kawakami, K. Arioka, H. Sato, Y. Uchiyama, S. Masushige, A. Fukamizu, T. Matsumoto, S. Kato, Mice lacking the Vitamin D receptor exhibit impaired bone formation, uterine hypoplasia and growth retardation after weaning, Nat. Genet. 16 (1997) 391–396.
[22] A. Murayama, M.S. Kim, J. Yanagisawa, K.I. Takeyama, S. Kato, Transrepression by a liganded nuclear receptor via a bHLH activator through co-regulator switching, EMBO J. 23 (2004) 1598–1608.
[23] S. Kato, R. Fujiki, H. Kitagawa, Vitamin D receptor (VDR) promoter targeting through a novel chromatin remodeling complex, J. Steroid Biochem. Mol. Biol. 89/90 (2004) 173–178.
[24] N.J. McKenna, B.W. O'Malley, Combinatorial control of gene expression by nuclear receptors and coregulators, Cell 108 (2002) 465–474.

[25] V. Perissi, M.G. Rosenfeld, Controlling nuclear receptors: the circular logic of cofactor cycles, Nat. Rev. Mol. Cell. Biol. 6 (2005) 542–554.
[26] B.M. Emerson, Specificity of gene regulation, Cell 109 (2002) 267–270.
[27] G. Pascual, A.L. Fong, S. Ogawa, A. Gamliel, A.C. Li, V. Perissi, D.W. Rose, T.M. Willson, M.G. Rosenfeld, C.K. Glass, A SUMOylation-dependent pathway mediates transrepression of inflammatory response genes by PPAR-gamma, Nature 437 (2005) 759–763.

Available online at www.sciencedirect.com
ScienceDirect
Journal of Steroid Biochemistry & Molecular Biology 103 (2007) 269–276
The Journal of Steroid Biochemistry & Molecular Biology
www.elsevier.com/locate/jsbmb

Creative synthesis of novel vitamin D analogs for health and disease

Atsushi Kittaka [a,*], Nozomi Saito [a], Shinobu Honzawa [a], Kazuya Takenouchi [b], Seiichi Ishizuka [b], Tai C. Chen [c], Sara Peleg [d], Shigeaki Kato [e], Midori A. Arai [a]

[a] Faculty of Pharmaceutical Sciences, Teikyo University, Sagamiko, Sagamihara, Kanagawa 199-0195, Japan
[b] Teijin Pharma Ltd., Tokyo 191-8512, Japan
[c] Boston University School of Medicine, Boston, MA 02118, USA
[d] The University of Texas, Houston, TX 77030, USA
[e] The University of Tokyo, Tokyo 113-0032, Japan

Abstract

We report new analogs of 1α,25-dihydroxyvitamin D_3 (**1**) in three categories. First, design and synthesis of ligands for a mutant vitamin D receptor (VDR)(Arg274Leu), which possess proper functional groups at both C1α and C2α positions of **1** to study the biological activity of the mutant VDR. Among our synthetic analogs, 1α-methyl-2α-(3-hydroxypropyl)-25-hydroxyvitamin D_3 (**8**) showed 7.3-fold greater transcriptional activity for the VDR(Arg274Leu) than that of **1**. Next, we examined the antiproliferative activity of 2-substituted 19-norvitamin D_3 analogs on an immortalized normal prostate cell line, PZ-HPV-7, and we found MART 10 (**14**) showed the activity even at very low concentration of 10^{-10} to 10^{-11} M. We also synthesized 25-hydroxy-19-norvitamin D_3 (**13**) using Julia-type olefination to connect between the C5 and C6 positions, effectively, to test it as a prohormone type agent for antiprostate diseases. Synthesized compound **13** showed potent antiproliferative activity in PZ-HPV-7, which has high 1α-hydroxylase activity. Finally, we describe design and synthesis of a new TEI-9647 analog, 2α-(3-hydroxypropoxy)-24-propyl-25-dehydro-1α-hydroxyvitamin D_3-26,23-lactone (**17**), which showed the strongest VDR antagonism. Its IC_{50} value is 7.4 pM to inhibit differentiation of HL-60 cells induced by 10 nM of **1**.

Keywords: Vitamin D analogs; Chemical synthesis; Structure–activity relationships; Vitamin D receptor; Antagonist

1. Introduction

1α,25-Dihydroxyvitamin D_3 (1α,25$(OH)_2D_3$, **1**), the physiologically active hormonal form of vitamin D_3, regulates cellular proliferation and differentiation in addition to its classical role in calcium and phosphorus homeostasis and bone mineralization [1–4]. The cellular and physiological actions of 1α,25$(OH)_2D_3$ are mediated primarily through the specific receptor, vitamin D receptor (VDR), which belongs to the nuclear receptor superfamily acting as a ligand-dependant transcription factor [5,6]. The VDR–[1α,25$(OH)_2D_3$] signaling works to stimulate intestinal calcium and phosphate absorption to prevent rickets, enhance of bone remodeling, differentiation of skin cells, potential anticancer actions, and so on. Therefore, 1α,25$(OH)_2D_3$ (**1**) and some synthetic analogs of **1** are clinically used in the treatment of bone diseases, secondary hyperparathyroidism, and psoriasis [1].

In order to investigate the structure–activity relationships of the natural hormone, we systematically synthesized the A-ring modified analogs, such as 2α-alkyl-, and 2α-(ω-hydroxyalkyl)-1α,25$(OH)_2D_3$ (Fig. 1) [7–11]. Elongation of the 2α-alkyl chain as in **2b–d**, however, decreased the binding affinity and agonistic activity for the VDR [9]. On the other hand, in regard to modification with the 2α-(ω-hydroxyalkyl) group, it was found that **3c** with the 2α-(3-hydroxypropyl) group on **1** had a three-fold higher binding activity for the VDR than **1** [9,10]. We also synthesized 2α-(ω-hydroxyalkoxy)-1α,25$(OH)_2D_3$ (**4a–c**), and **4b** showed 1.8-fold stronger binding affinity for the VDR than **1** [11–13]. Posner and Johnson also synthesized ED-71 [14] related analogs starting with the [4 + 2] cycloaddition of pyrone derivatives [15]. We report here the design and synthesis of the new analogs of **1** based on our accumulated knowledge of the 2α-functional group in three categories: for

* Corresponding author. Tel.: +81 42 685 3713; fax: +81 42 685 3713.
E-mail address: akittaka@pharm.teikyo-u.ac.jp (A. Kittaka).

0960-0760/$ – see front matter © 2006 Elsevier Ltd. All rights reserved.
doi:10.1016/j.jsbmb.2006.12.002

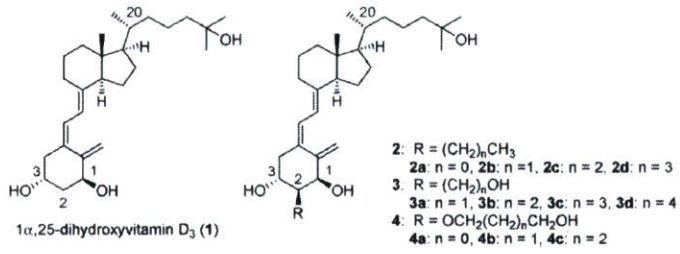

Fig. 1. Structures of 1α,25-dihydroxyvitamin D_3 (**1**) and its 2α-substituted analogs **2**–**4** [7–13].

hereditary vitamin D-resistant rickets (HVDRR), for prostate cancer, and for Paget's disease.

2. Material and methods

2.1. Preparation of vitamin D analogs

All vitamin D analogs in this report were synthesized at the Faculty of Pharmaceutical Sciences, Teikyo University according to the representative synthetic route presented in Scheme 1. Construction of the vitamin D_3 triene skeleton, for example, compounds **8** and **17**, was accomplished by Pd-catalyzed alkenylative cyclization of enyne as the A-ring precursor with the CD-ring bromoolefin [16]. To connect the C5–C6 double bond of 19-norvitamin D_3 analogs, for example, compound **13**, Julia-type olefination was utilized. Full synthetic details and physiological data of the synthetic compounds will be reported elsewhere.

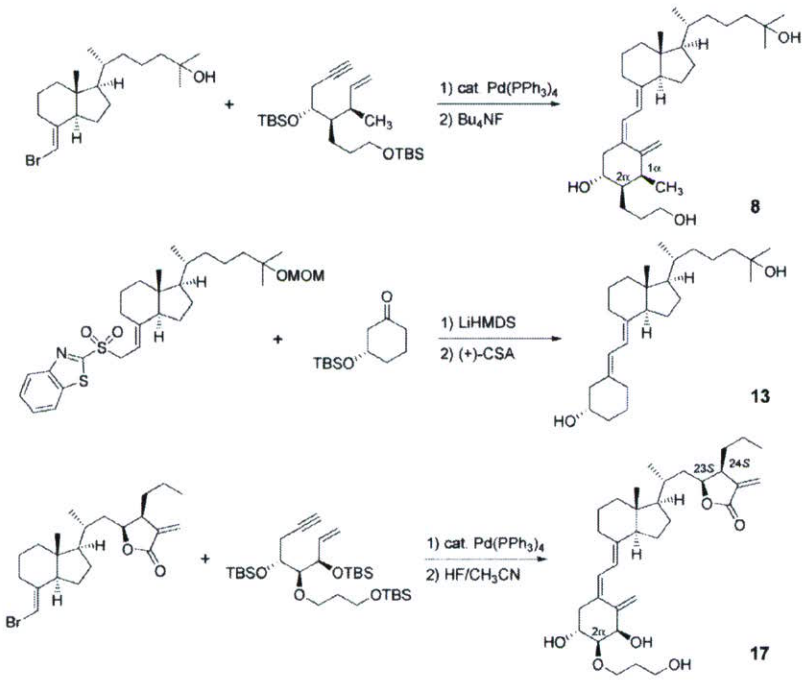

Scheme 1. Synthesis of 1α-alkyl vitamin D_3 analog **8**, 19-norvitamin D_3 analog **13**, and TEI-9647 analog **17**.

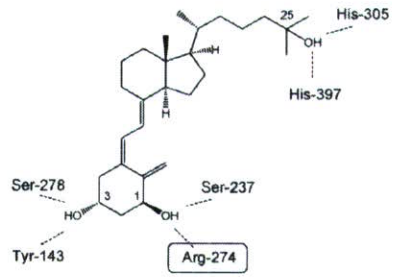

Fig. 2. Amino acid residues forming hydrogen bonds with the hydroxyl groups of **1**.

3. Results and discussion

3.1. Designed ligands for HVDRR

Hydrogen bonds between three hydroxyl groups of **1** and hydrophilic amino acid residues in the ligand-binding domain (LBD) of VDR are essential for its actions. For example, Arg-274 is well known to form a hydrogen bond with 1α-OH of **1** [17], and its mutation would lead to loss of the affinity for **1** and its actions (Fig. 2) [18].

In fact, substitution of the amino acid to a hydrophobic leucine is shown to cause hereditary Vitamin D-resistant rickets, a rare genetic disease caused by a generalized resistance to **1** [19]. The mutation causes a 1000-fold decrease in the affinity for **1**, thus the vitamin D action is disrupted. Vitamin D derivatives that bind specifically to a mutated VDR of this type would be a candidate for therapeutic agent against HVDRR [20]. A few research groups have reported such ligand designs for the mutant VDR. Posner and co-workers reported that 1α-hydroxymethyl-16-ene-26a,27a-bishomo-25-hydroxyvitamin D_3 was an effective ligand for the mutant VDR [20]. Koh and co-workers developed derivatives whose 1α-hydroxy group is protected by a substituted benzyl group [21,22]. On the other hand, we have approached the issue by using 2α-hydroxypropylated **1** (**5**) [23]. In this case, we have shown that **5** would form a hydrogen bond with the Asp-144 of the mutant VDR through the terminal hydroxy group of the 2α-substituent, thus could restore its complex formation ability with the mutant VDR. We were interested in whether these motifs could increase biological activity of Posner and co-workers 1-hydroxymethylated analogs, and we decided to synthesize the analog (**7**), which possesses the 2α-(3-hydroxypropyl) group on the A-ring (Fig. 3). Furthermore, introduction of a methyl group at 1α-position of 25(OH)D_3 would be also expected to recover the affinity for the mutant VDR by interacting with the hydrophobic pocket formed by the mutation. We designed and synthesized the analog of 1α-methyl-2α-(3-hydroxypropyl)-25(OH)D_3 (**8**) as the new ligand for the mutant VDR. It was found that the transcriptional activity of **5**–**8**, in which compound **6** was also synthesized as the standard compound for the mutant VDR(Arg274Leu), was 5.6–7.3-times greater than that of the natural hormone **1**, when tested by Dual-Luciferase® reporter assay [24].

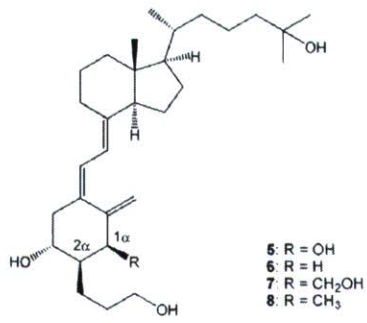

Fig. 3. Structures of 2α-(3-hydroxypropyl)-1α-modified 25(OH)D_3 analogs (**5**–**8**).

Originally, we considered that the affinity of the 2α-methyl analog (**2a**) for the normal VDR would be greater because of hydrophobic interaction between 2α-methyl group and the hydrophobic pocket of the LBD [11]. We examined the hypothesis that the affinity for VDR would be greater if a larger hydrophobic group, for example, the phenyl group, could interact with the hydrophobic pocket of the mutant VDR(Arg274Leu) and restore ligand-mediated VDR action. In order to test this hypothesis, we synthesized novel analogs that have aromatic groups at the 2α-position. That is, we synthesized 2α-phenyl- (**9**), 2α-benzyl- (**10**), and 2α-phenethyl-1α,25-$(OH)_2D_3$ (**11**) (Fig. 4).

Contrary to our expectation, these analogs showed a poor ability to stabilize the conformation of the mutant VDR as shown by protease sensitivity assay [20], and only the 2α-benzyl analog induced detectable stabilization of the mutant VDR at the almost same level as the natural hormone **1** [25].

On the other hand, in all cases where biological activities via the normal VDR were assayed, the 2α-benzyl analog (**10**) was the most potent in the aromatic analog series. Data from biological assays showed that these analogs induce HL-60 cell differentiation and transcriptional activities as potently as **1**, whereas the affinity for the normal VDR was less than 10% relative to the natural hormone [25]. Further studies are now on the way to elucidate the discrepancies between binding affinity of the analogs for VDR in vitro and their potencies in the cellular assays, including studies on metabolism by CYP27A1 and CYP24A1 [26].

3.2. Designed ligands for prostate cancer

It has been shown that prostate cells possess 1α-hydroxylase (1α(OH)ase), and can convert 25-hydroxyvitamin D_3, 25(OH)D_3 (**12**), to **1** intracellularly to inhibit their prolifera-

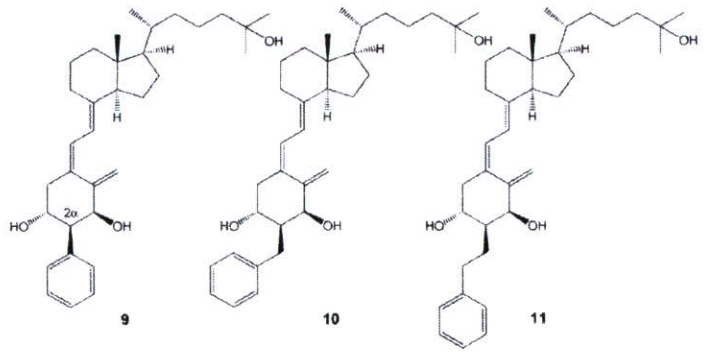

Fig. 4. Structures of 2α-phenyl-, 2α-benzyl-, and 2α-phenethyl-1α,25(OH)$_2$D$_3$ (**9**–**11**).

tion [27]. It is also known that a 19-demethylenated analog of **1**, i.e., 1α,25-dihydroxy-19-norvitamin D$_2$, possesses pro-differentiation and antiproliferative activities similar to **1** [28]. Since 19-norvitamin D derivatives are known to be less calcemic than **1** when administered systemically [29], we are interested in knowing whether 25-hydroxy-19-norvitamin D$_3$, 25(OH)-19-norD$_3$ (**13**) (Fig. 5), can exert potent antiproliferative activity toward prostate cells which possess 1α(OH)ase activity and therefore can be used as chemopreventive agents without causing hypercalcemic side

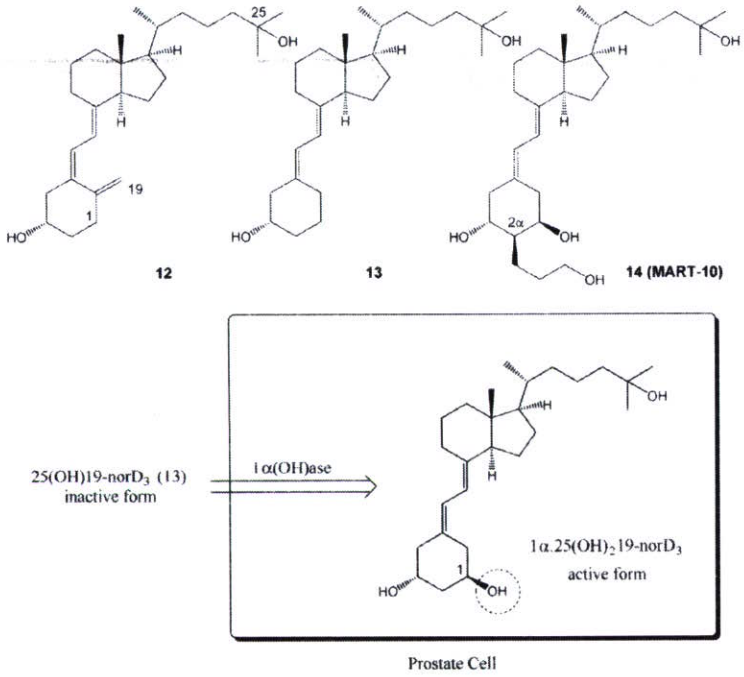

Fig. 5. Structures of **12** and 19-norvitamin D$_3$ analogs (**13**,**14**), and concept of antiagent for prostate disease on 25-hydroxy-19-norvitamin D$_3$ (**13**) as a prohormone analog.

effects. We synthesized **13** by using Julia-type olefination [30] to test its antiproliferative activity in PZ-HPV-7 normal prostate cells [31].

25-Hydroxy-19-norvitamin D$_3$ (**13**) showed high antiproliferative activity in PZ-HPV-7 cells, almost at the same level as that of the natural hormone (**1**) [31]. When the cells were treated with both **13** and the natural hormone (**1**), synergistic effect was observed. It is interesting that **13** showed such high antiproliferative activity, even though the binding affinity of **13** for the vitamin D receptor is low [32]. To evaluate a more precise molecular mechanism, we also studied the metabolism of **13** by 1α(OH)ase (CYP27B1) in an in vitro system. After incubating **13** with the *E. coli* extract containing the recombinant 1α(OH)ase (CYP27B1), the resulted mixture was analyzed by HPLC. It was shown that **13** was hydroxylated at the 1α-position to form 1α,25(OH)$_2$-19-norvitamin D$_3$, which is known to be active [31]. It seems that the antiproliferative activity of **13** in prostate cells is primarily the result of its hydroxylation by endogenous 1α(OH)ase (CYP27B1) at the 1α-position leading to the formation of the active 1α,25(OH)$_2$-19-norvitamin D$_3$ compound [31].

We also synthesized 2α-(3-hydroxypropyl)-1α,25-dihydroxy-19-norvitamin D$_3$ (MART 10, **14**), which showed strong HL-60 cell differentiation inducing effect [30], and tested antiproliferative activity in the prostate cells, PZ-HPV-7. The results are summarized in Fig. 6.

We can see the highly potent antiproliferative activity of MART 10 (**14**), which showed the activity in very low concentration, even from 10^{-10} to 10^{-11} M (Fig. 6). The cancer cell antiinvasion activity of MART 10 has also been examined and will be reported elsewhere.

3.3. Designed ligands for Paget's disease

Paget's disease [33–35], which is known as the most flagrant example of disordered bone remodeling and the second most common bone disease after osteoporosis in Anglo-Saxons [35]. Recent studies on Paget's disease suggested a specific increase in osteoclast sensitivity to the differentiation activity of **1** as the principal mechanism for abnormal bone formation [33–35]. The VDR antagonists are expected to be potent therapeutic agents for some diseases caused by hypersensitivity to 1α,25-dihydroxyvitamin D$_3$, such as Paget's disease.

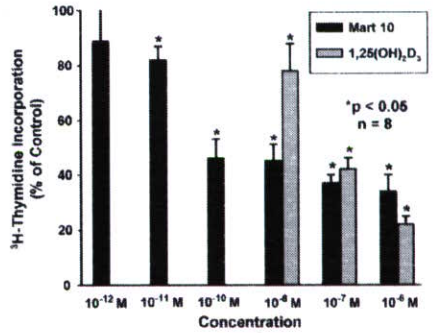

Fig. 6. Antiproliferative activity of MART 10 (**14**) on immortalized normal prostate cells (PZ-HPV-7).

In 1999, studies on the modification of the side-chain structure based on the 1α,25-dihydroxyvitamin D$_3$-26,23-lactone metabolite derived from **1** led to the discovery of the TEI-9647 (**15**) and TEI-9648 (**16**) (Fig. 7) [36,37]. Both vitamin D$_3$ analogs **15** and **16**, which have an α-methylene-γ-butyrolactone part on the side-chain, are the first specific antagonists of VDR-mediated genomic action of **1**, and **15** with 23*S*-configration has stronger antagonism (IC$_{50}$ 9.4 nM) than **16** with 23*R*-configration (IC$_{50}$ 134.3 nM). After our synthetic studies on the C2α and C24-double functionalization of **15** and **16** to investigate the structure–activity relationships, we found that 2α-(3-hydroxypropoxy)-24-propyl-25-dehydro-1α-hydroxyvitamin D$_3$-26,23-lactone (**17**) showed the strongest VDR antagonism, as far as we know, and its IC$_{50}$ value was 7.4 pM to inhibit differentiation of human leukemia cells (HL-60 cells) induced by 10 nM of **1** [51].

Structures of representative C2α and C24 modified TEI-9647 analogs and biological activities are shown in Fig. 8 and Table 1 [38–42].

When the VDR antagonist TEI-9647 (**15**) binds to the ligand-binding domain of VDR, the complex may change into an unusual transcriptionally inactive form. We speculate that some amino acid residues in the LBD, which participate in the conformational change of the VDR, react with the *exo*-methylene moiety on the lactone ring of **15**. Namely, there are two cysteine residues, Cys-403 on helix 11 and Cys-410 in the hinge region between helices 11 and 12, in the LBD of the human VDR. Recently, it was revealed that the two cysteines, Cys-403 and Cys-410, play an important role in the VDR antagonism of TEI-9647 (**15**) [46]. Furthermore, the *exo*-methylene lactone structure is indispensable for the antagonistic action of the vitamin D$_3$ lactones [47]. Based on these results, we consider that the nucleophilic thiol groups of the cysteines could attack the α-methylene-γ-lactone of TEI-analogs via 1,4-addition to give the corresponding cysteine adduct [48]. Such interaction between the ligand

Table 1
Biological activity of C2α and C24 modified TEI-9647 analogs **17**–**21**

Compound	Binding affinity for VDR[a]	Antagonistic activity (IC$_{50}$, nM)[b]	Reference
TEI-9647 (**15**)	12	9.4	
17	37	0.0074	[51]
18	23	0.13	[39]
19	34	0.23	[40]
20	67	0.093	[41]
21	111	0.49	[42]

[a] Chick intestinal VDR [43,44]. The potency of **1** is normalized to 100.
[b] Antagonistic activity was assessed in terms of IC$_{50}$ for the differentiation of HL-60 cells induced by 10 nM of **1** [45].

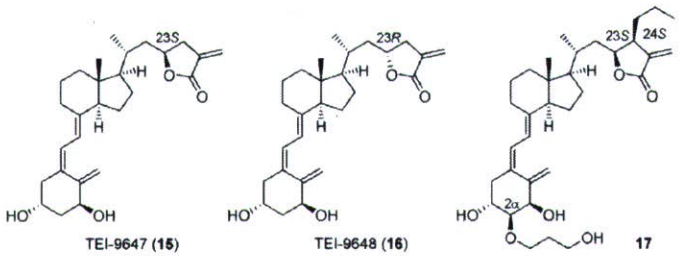

Fig. 7. Structures of TEI-9647 (**15**), TEI-9648 (**16**), and 2α-(3-hydroxypropoxy)-24-propyl-TEI-9647 (**17**).

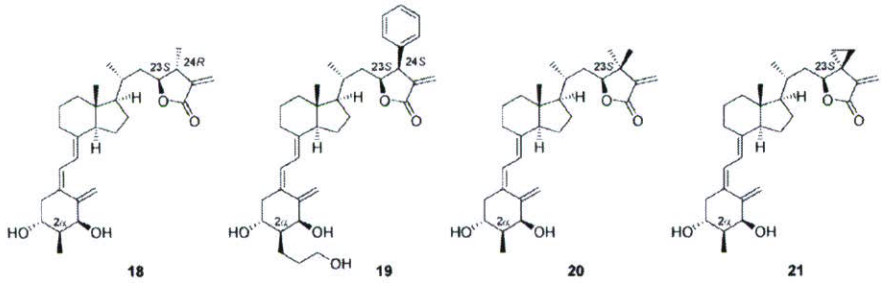

Fig. 8. Structures of C2α and C24 modified TEI-9647 analogs **18**–**21**.

and the LBD might prevent correct positioning of helix 12 to activate the target genes. Therefore, it is conceivable that the VDR antagonists, whose *exo*-methylene moiety is located at a more favorable position to react with Cys-403 and/or Cys-410 after binding, show stronger VDR antagonistic activity. The novel vitamin D_3 lactones we synthesized, which showed more potent antagonistic activity, might be situated in a preferable position of the *exo*-methylene group toward the cysteine residues after binding to the LBD of the VDR, and vice versa. The other VDR antagonists ZK-159222 [49] and DLAMs [50] would have presumably different mechanism as antagonists on VDR from TEI-lactone analogs.

4. Conclusions

We synthesized A-ring modified analogs of the natural hormone, which have hydrophobic group at the 1α-position and the 3-hydroxypropyl group at the 2α-position, as the new ligand for the mutant VDR(Arg274Leu). We found that 1α-methyl-2α-(3-hydroxypropyl)-25(OH)D_3 (**8**) showed 7.3-fold greater transcriptional activity through the mutant VDR than **1**. Next, we synthesized 25-hydroxy-19-norvitamin D_3 (**13**) and MART-10 (**14**) by using Julia-type olefination, which we have reported as the new coupling method for the synthesis of 19-norvitamin D derivatives [30]. Both compounds exhibited high antiproliferative activity in the immortalized normal prostate cells. Finally, we synthesized 2α-substituted 24-alkyl-TEI-lactone analogs, such as **17** to investigate structure–activity relationships of VDR antagonists. It was found that antagonistic activity of 2α-(3-hydroxypropoxy)-24-propyl-TEI-9647 (**17**) increased about three orders over the original TEI-9647. We expect that these highly potent vitamin D_3 analogs would contribute to understanding the mechanisms involved in the expression of agonistic and antagonistic activity on VDR, for example, based on X-ray crystallography data if available, as well as to finding the seeds of new medicines for treating VDR related diseases [52].

Acknowledgements

We thank Ms. Junko Shimode and Ms. Akiko Tonoki (Teikyo University) for spectroscopic measurements. This study has been supported in part by Grants-in-Aid from the Ministry of Education, Culture, Sports, Science and Technology, Japan (#15790015 and 17790019 to N.S., #17790095 to S.H., and #16790027 to M.A.A.), and by Grants-in-Aid from Japan Society for the Promotion of Science (#15590021 and 17590012 to A.K.). N.S. deeply thanks Takeda Science Foundation, and A.K. gratefully acknowledges Uehara Memorial Foundation.

References

[1] D. Feldman, J.W. Pike, F.H. Glorieux (Eds.), Vitamin D, second ed., Elsevier Academic Press, New York, 2005.
[2] R. Bouillon, W.H. Okamura, A.W. Norman, Structure–function relationships in the vitamin D endocrine system, Endocrinol. Rev. 16 (2) (1995) 200–257.
[3] G.D. Zhu, W.H. Okamura, Synthesis of vitamin D (calciferol), Chem. Rev. 95 (6) (1995) 1877–1952.
[4] R.A. Ettinger, H.F. DeLuca, The vitamin D endocrine system and its therapeutic potential, Adv. Drug Res. 28 (1996) 269–312.
[5] R.M. Evans, The steroid and thyroid hormone receptor superfamily, Science 240 (4854) (1988) 889–895.
[6] P. Chambon, The nuclear receptor superfamily: a personal retrospect on the first two decades, Mol. Endocrinol. 19 (6) (2005) 1418–1428.
[7] K. Konno, T. Fujishima, S. Maki, Z.-P. Liu, D. Miura, M. Chokki, S. Ishizuka, K. Yamaguchi, Y. Kan, M. Kurihara, N. Miyata, C. Smith, H.F. DeLuca, H. Takayama, Synthesis, biological evaluation, and conformational analysis of A-ring diastereomers of 2-methyl-1,25-dihydroxyvitamin D_3 and their 20-epimers: unique activity profiles depending on the stereochemistry of the A-ring and at C-20, J. Med. Chem. 43 (22) (2000) 4247–4265.
[8] K. Konno, S. Maki, T. Fujishima, Z.-P. Liu, D. Miura, M. Chokki, H. Takayama, A novel and practical route to A-ring enyne synthon for 1α,25-dihydroxyvitamin D_3 analogs: synthesis of A-ring diastereomers of 1α,25-dihydroxyvitamin D_3 and 2-methyl-1,25-dihydroxyvitamin D_3, Bioorg. Med. Chem. Lett. 8 (2) (1998) 151–156.
[9] Y. Suhara, K. Nihei, H. Tanigawa, T. Fujishima, K. Konno, K. Nakagawa, T. Okano, H. Takayama, Syntheses and biological evaluation of novel 2α-substituted 1α,25-dihydroxyvitamin D_3 analogues, Bioorg. Med. Chem. Lett. 10 (10) (2000) 1129–1132.
[10] Y. Suhara, K. Nihei, M. Kurihara, A. Kittaka, K. Yamaguchi, T. Fujishima, K. Konno, N. Miyata, H. Takayama, Efficient and versatile synthesis of novel 2α-substituted 1α,25-dihydroxyvitamin D_3 analogues and their docking to vitamin D receptors, J. Org. Chem. 66 (26) (2001) 8760–8771.
[11] For our review article of 2-substituted 1, 25-dihydroxyvitamin D_3, see: H. Takayama, A. Kittaka, T. Fujishima, Y. Suhara, Design, synthesis, and biological studies of the A-ring-modified 1,25-dihydroxyvitamin D_3 analogs, in: J. Reichrath, M. Friedrich, W. Tilgen (Eds.), Vitamin D Analogs in Cancer Prevention and Therapy, Recent Results in Cancer Research, vol. 164, Springer-Verlag, Berlin Heidelberg, 2003, pp. 289–317.
[12] A. Kittaka, Y. Suhara, H. Takayanagi, T. Fujishima, M. Kurihara, H. Takayama, A concise and efficient route to 2α-(ω-hydroxyalkoxy)-1α,25-dihydroxyvitamin D_3: remarkably high affinity to vitamin D receptor, Org. Lett. 2 (17) (2000) 2619–2622.
[13] N. Saito, Y. Suhara, M. Kurihara, T. Fujishima, S. Honzawa, H. Takayanagi, T. Kozono, M. Matsumoto, M. Ohmori, N. Miyata, H. Takayama, A. Kittaka, Design and efficient synthesis of 2α-(ω-hydroxyalkoxy)-1α,25-dihydroxyvitamin D_3 including 2-*epi*-ED-71 and its 20-epimers with HL-60 cell differentiation activity, J. Org. Chem. 69 (22) (2004) 7463–7471.
[14] K. Miyamoto, E. Murayama, K. Ochi, H. Watanabe, N. Kubodera, Synthetic studies of vitamin D analogs. XIV. Synthesis and calcium regulating activity of vitamin D_3 analogs bearing a hydroxyalkyl group at the 2β-position, Chem. Pharm. Bull. 41 (6) (1993) 1111–1113.
[15] G.H. Posner, N. Johnson, Stereocontrolled total synthesis of calcitriol derivatives: 1,25-dihydroxy-2-(4′-hydroxybutyl)vitamin D_3 analogs of an osteoporosis drug, J. Org. Chem. 59 (25) (1994) 7855–7861.
[16] B.M. Trost, J. Dumas, M. Villa, New strategies for the synthesis of vitamin D metabolites via palladium-catalyzed reactions, J. Am. Chem. Soc. 114 (25) (1992) 9836–9845.
[17] N. Rochel, J.M. Wurtz, A. Mitschler, B. Klaholz, D. Moras, The crystal structure of the nuclear receptor for vitamin D bound to its natural ligand, Mol. Cell 5 (1) (2000) 173–179.
[18] K. Kristjansson, A.R. Rut, M. Hewison, J.L. O'Riordan, M.R. Hughes, Two mutations in the hormone binding domain of the vitamin D receptor cause tissue resistance to 1,25-dihydroxyvitamin D_3, J. Clin. Invest. 92 (1) (1993) 12–16.
[19] J.P. Malloy, J.W. Pike, D. Feldman, The vitamin D receptor and the syndrome of hereditary 1,25-dihydroxyvitamin D-resistant rickets, Endocrinol. Rev. 20 (2) (1999) 156–188.
[20] S.A. Gardezi, C. Nguyen, J.P. Malloy, G.H. Posner, D. Feldman, S. Peleg, A rationale for treatment of hereditary vitamin D-resistant rickets with analogs of 1α,25-dihydroxyvitamin D_3, J. Biol. Chem. 276 (31) (2001) 29148–29156 (A-ring stereochemistry of (1α,3β): M.A. Hatcher, S. Peleg, P. Dolan, T.W. Kensler, A. Sarjeant, G.H. Posner, A-ring hydroxymethyl 19-nor analogs of the natural hormone 1α,25-dihydroxyvitamin D_3: synthesis and preliminary biological evaluation, Bioorg. Med. Chem. 13 (12) (2005) 3964–3976).
[21] S.L. Swann, J.J. Bergh, M.C. Farach-Carson, J.T. Koh, Rational design of vitamin D_3 analogues which selectively restore activity to a vitamin D receptor mutant associated with rickets, Org. Lett. 4 (22) (2002) 3863–3866.
[22] S.L. Swann, J.J. Bergh, M.C. Farach-Carson, C.A. Ocasio, J.T. Koh, Structure-based design of selective agonists for a rickets-associated mutant of the vitamin D receptor, J. Am. Chem. Soc. 124 (46) (2002) 13795–13805.
[23] A. Kittaka, M. Kurihara, S. Peleg, Y. Suhara, H. Takayama, 2α-(3-Hydroxypropyl)- and 2α-(3-hydroxypropoxy)-1α,25-dihydroxyvitamin D_3 accessible to vitamin D receptor mutant related to hereditary vitamin D-resistant rickets, Chem. Pharm. Bull. 51 (3) (2003) 357–358.
[24] N. Takahashi, Design for mutant receptor: synthesis of 1-methylvitamin D_3 derivatives, dissertation, Teikyo University, 2005 (in Japanese).
[25] S. Honzawa, K. Hirasaka, Y. Yamamoto, S. Peleg, T. Fujishima, M. Kurihara, N. Saito, S. Kishimoto, T. Sugiura, K. Waku, H. Takayama, A. Kittaka, Design, synthesis and biological evaluation of novel 1α,25-dihydroxyvitamin D_3 analogues possessing aromatic ring on 2α-position, Tetrahedron 61 (47) (2005) 11253–11263.
[26] D. Abe, T. Sakaki, T. Kusudo, A. Kittaka, N. Saito, Y. Suhara, T. Fujishima, H. Takayama, H. Hamamoto, M. Kamakura, M. Ohta, K. Inouye, Drug Metab. Dispos. 33 (6) (2005) 778–784.
[27] G.G. Schwartz, T.C. Chen, Vitamin D, sunlight, and the natural history of prostate cancer, in: D. Feldman, J.W. Pike, F.H. Glorieux (Eds.), Vitamin D, Elsevier Academic Press, New York, 2005, pp. 1599–1615.
[28] T.C. Chen, G.G. Schwartz, K.L. Burnstein, B.L. Lokeshwar, M.F. Holick, The in vitro evaluation of 25-hydroxyvitamin D_3 and 19-nor-1α,25-dihydroxyvitamin D_2 as therapeutic agents for prostate cancer, Clin. Cancer Res. 6 (3) (2000) 901–908.
[29] R.R. Sicinski, P. Rotkiewics, A. Kolinski, W. Sicinska, J.M. Prahl, C.M. Smith, H.F. DeLuca, 2-Ethyl and 2-ethylidene analogues of 1α,25-dihydroxy-19-norvitamin D_3: synthesis, conformational analysis, biological activities, and docking to the modeled rVDR ligand binding domain, J. Med. Chem. 45 (16) (2002) 3366–3380.
[30] K. Ono, A. Yoshida, N. Saito, T. Fujishima, S. Honzawa, Y. Suhara, S. Kishimoto, T. Sugiura, K. Waku, H. Takayama, A. Kittaka, Efficient synthesis of 2-modified 1α,25-dihydroxy-19-norvitamin D_3 with Julia olefination: high potency in induction of differentiation on HL-60 cells, J. Org. Chem. 83 (19) (2003) 7407–7415.
[31] M.A. Arai, R. Tsutsumi, H. Hara, T.C. Chen, T. Sakaki, N. Urushino, K. Inouye, A. Kittaka, Synthesis of 25-hydroxy-19-norvitamin D_3 analogs and their antiproliferative activities on prostate cells, Heterocycles 66 (2005) 469–479.
[32] T. Okano, K. Nakagawa, N. Kubodera, K. Ozono, A. Isaka, A. Osawa, M. Terada, K. Mikami, Catalytic asymmetric syntheses and biological activities of singly dehydroxylated 19-nor-1α,25-dihydroxyvitamin D_3 A-ring analogs in cancer cell differentiation and apoptosis, Chem. Biol. 7 (3) (2000) 173–184.
[33] Recent reviews on Paget's disease, see: S.V. Reddy, Etiology of Paget's disease and osteoclast abnormalities, J. Cell Biochem. 93 (4) (2004) 688–696.

[34] G.D. Roodman, J.J. Windle, Paget disease of bone, J. Clin. Invest. 115 (2) (2005) 200–208.
[35] S.V. Reddy, N. Kurihara, C. Menaa, G.D. Roodman, Paget's disease of bone: a disease of the osteoclast, Rev. Endocrinol. Metab. Disord. 2 (2) (2001) 195–201.
[36] D. Miura, K. Manabe, K. Ozono, M. Saito, Q. Gao, A.W. Norman, S. Ishizuka, Antagonistic action of novel 1α,25-dihydroxyvitamin D_3-26,23-lctone analogs on differentiation of human leukemia cells (HL-60) induced by 1α,25-dihydroxyvitamin D_3, J. Biol. Chem. 274 (23) (1999) 16392–16399.
[37] K. Ozono, M. Saito, D. Miura, T. Michigami, S. Nakajima, S. Ishizuka, Analysis of the molecular mechanism for the antagonistic action of a novel 1α,25-dihydroxyvitamin D_3 analogue toward vitamin D receptor function, J. Biol. Chem. 274 (45) (1999) 32376–32381.
[38] N. Saito, T. Matsunaga, T. Fujishima, M. Anzai, H. Saito, K. Takenouchi, D. Miura, S. Ishizuka, H. Takayama, A. Kittaka, Remarkable effect of 2α-modification on the VDR antagonistic activity of 1α-hydroxyvitamin D_3-26,23-lactones, Org. Biomol. Chem. 1 (24) (2003) 4396–4402.
[39] N. Saito, H. Saito, M. Anzai, A. Yoshida, T. Fujishima, K. Takenouchi, D. Miura, S. Ishizuka, H. Takayama, A. Kittaka, Dramatic enhancement of antagonistic activity on vitamin D receptor: a double functionalization of 1α-hydroxyvitamin D_3-26,23-lactones, Org. Lett. 5 (25) (2003) 4859–4862.
[40] N. Saito, T. Matsunaga, H. Saito, M. Anzai, K. Takenouchi, D. Miura, S. Ishizuka, H. Takayama, A. Kittaka, Synthesis and 2α-modification of 24-phenylvitamin D_3 lactones: effects on VDR antagonistic activity, Heterocycles 67 (1) (2006) 311–336.
[41] N. Saito, M. Masuda, M. Matsunaga, H. Saito, M. Anzai, K. Takenouchi, D. Miura, S. Ishizuka, M. Takimoto-Kamimura, A. Kittaka, 24,24-Dimethylvitamin D_3-26,23-lactones and their 2α-functionalized analogues as highly potent VDR antagonists, Tetrahedron 60 (36) (2004) 7951–7961.
[42] N. Saito, M. Masuda, H. Saito, K. Takenouchi, S. Ishizuka, J.-I. Namekawa, M. Takimoto-Kamimura, A. Kittaka, Synthesis of 24,24-ethanovitamin D_3 lactones using ruthenium-catalyzed intermolecular enyne metathesis: potent vitamin D receptor antagonists, Synthesis 15 (2005) 2533–2543.
[43] J.A. Eisman, A.J. Hamstra, B.E. Kream, H.F. DeLuca, A sensitive, precise, and convenient method for determination of 1,25-dihydroxyvitamin D in human plasma, Arch. Biochem. Biophys. 176 (1) (1976) 235–243.
[44] M. Inaba, H.F. DeLuca, Stabilization of 1,25-dihydroxyvitamin D_3 receptor in the human leukemia cell line, HL-60, with diisopropylfluorophosphate. Biochim. Biophys. Acta 1010 (1) (1989) 20–27.
[45] S.J. Collins, F.W. Ruscetti, R.E. Gallagher, R.C. Gallo, Normal functional characteristics of cultured human promyelocytic leukemia cells (HL-60) after induction of differentiation by dimethylsulfoxide, J. Exp. Med. 149 (4) (1979) 969–974.
[46] E. Ochiai, D. Miura, H. Eguchi, S. Ohara, K. Takenouchi, Y. Harada, Y. Azuma, T. Kamimura, A.W. Norman, S. Ishizuka, Molecular mechanism of the vitamin D antagonistic actions of (23S)-25-dehydro-1α-hydroxyvitamin D_3-26,23-lactone depends on the primary structure of the carboxyl-terminal region of the vitamin D receptor, Mol. Endocrinol. 19 (5) (2005) 1147–1157.
[47] K. Takenouchi, R. Sogawa, K. Manabe, H. Saitoh, Q. Gao, D. Miura, S. Ishizuka, Synthesis and structure–activity relationships of TEI-9647 derivatives as vitamin D_3 antagonists, J. Steroid Biochem. Mol. Biol. 89–90 (1–5) (2004) 31–34.
[48] Some biologically active natural products having an α-methylene-γ-lactone structure react with the thiol group of cysteine to give the corresponding cysteine adduct S.M. Kupchan, D.C. Fessler, M.A. Eakin, T.J. Giacobbe, Reactions of alpha methylene lactone tumor inhibitors with model biological nucloephile, Science 168 (929) (1970) 376–377.
[49] S. Väisänen, M. Peräkylä, J.I. Kärkkäinen, A. Steinmeyer, C. Carlberg, Critical role of helix 12 of the vitamin D_3 receptor for the partial agonism of the carboxylic ester antagonists, J. Mol. Biol. 315 (2) (2002) 229–238.
[50] Y. Kato, Y. Nakano, H. Sano, A. Tanatani, H. Kobayashi, R. Shimazawa, H. Koshino, Y. Hashimoto, K. Nagasawa, Synthesis of 1α,25-dihydroxyvitamin D_3-26,23-lactams (DLAMs), a novel series of 1α,25-dihydroxyvitamin D_3 antagonist, Bioorg. Med. Chem. Lett. 14 (10) (2004) 2579–2583.
[51] N. Saito, T. Matsunaga, H. Saito, M. Anzai, K. Takenouchi, D. Miura, J.-i. Namekawa, S. Ishizuka, A. Kittaka, Further synthetic and biological studies on vitamin D hormone antagonists based on C24-alkylation and C2α-functionalization of 25-dehydro-1α-hydroxyvitamin D_3-26,23-lactones, J. Med. Chem. 49 (24) (2006) 7063–7075.
[52] S. Hourai, T. Fujishima, A. Kittaka, Y. Suhara, H. Takayama, N. Rochel, D. Moras, Probing a water channel near the A-ring of receptor-bound 1α,25-dihydroxyvitamin D_3 with selected 2α-substituted analogues, J. Med. Chem. 49 (17) (2006) 5199–5205.

8. K. Berns *et al.*, *Nature* **428**, 431 (2004).
9. T. R. Brummelkamp *et al.*, *Nat. Chem. Biol.* **2**, 202 (2006).
10. T. Sjoblom *et al.*, *Science* **314**, 268 (2006).
11. L. D. Wood *et al.*, *Science* **318**, 1108 (2007).
12. R. A. Dickins *et al.*, *Nat. Genet.* **37**, 1289 (2005).
13. G. K. Smyth, T. Speed, *Methods* **31**, 265 (2003).
14. V. M. Draviam *et al.*, *Nat. Cell Biol.* **9**, 556 (2007).
15. M. Ito, T. Nakano, F. Erdodi, D. J. Hartshorne, *Mol. Cell. Biochem.* **259**, 197 (2004).
16. H. Jin, T. Sperka, P. Herrlich, H. Morrison, *Nature* **442**, 576 (2006).
17. L. T. Vassilev *et al.*, *Science* **303**, 844 (2004).
18. N. L. Solimini, J. Luo, S. J. Elledge, *Cell* **130**, 986 (2007).
19. J. M. Silva *et al.*, *Science* **319**, 617 (2008).
20. We thank A. L. Brass for the pMSCV-PM, pMSCV-PM-FF, and pMSCV-PM-mir30 vectors and for scientific advice; M. J. Solimini for help with data analysis; E. R. McDonald for scientific advice; T. Waldman and B. Vogelstein for the HCT116 and DLD-1 cell lines; and T. Moore from Open Biosystems for help with assembling library pools. G.H. is a fellow of the Helen Hay Whitney Foundation. X.L.A. is supported by a National Research Service Award fellowship, M.E.S. is supported by an American Cancer Society fellowship, and A.S. is supported by grant T32CA09216 to the MGH Pathology Department. T.F.W. is a fellow of the Susan G. Komen Foundation and is supported by grant PDF0403175. This work is supported by grants from NIH and the U.S. Department of Defense to G.J.H., J.W.H., and S.J.E. G.J.H. has a paid consulting relationship with Open Biosystems.

Supporting Online Material
www.sciencemag.org/cgi/content/full/319/5863/620/DC1
Materials and Methods
SOM Text
Figs. S1 to S3
Tables S1 to S6
References
Data Sets S1 to S9

14 August 2007; accepted 20 December 2007
10.1126/science.1149200

Cathepsin K–Dependent Toll-Like Receptor 9 Signaling Revealed in Experimental Arthritis

Masataka Asagiri,[1,2] Toshitake Hirai,[1,4] Toshihiro Kunigami,[1,4] Shunya Kamano,[1,5] Hans-Jürgen Gober,[1] Kazuo Okamoto,[1] Keizo Nishikawa,[1] Eicke Latz,[6] Douglas T. Golenbock,[6] Kazuhiro Aoki,[3] Keiichi Ohya,[3] Yuuki Imai,[7,9] Yasuyuki Morishita,[8] Kohei Miyazono,[8] Shigeaki Kato,[7,9] Paul Saftig,[10] Hiroshi Takayanagi[1,2]*

Cathepsin K was originally identified as an osteoclast-specific lysosomal protease, the inhibitor of which has been considered might have therapeutic potential. We show that inhibition of cathepsin K could potently suppress autoimmune inflammation of the joints as well as osteoclastic bone resorption in autoimmune arthritis. Furthermore, *cathepsin K*$^{-/-}$ mice were resistant to experimental autoimmune encephalomyelitis. Pharmacological inhibition or targeted disruption of cathepsin K resulted in defective Toll-like receptor 9 signaling in dendritic cells in response to unmethylated CpG DNA, which in turn led to attenuated induction of T helper 17 cells, without affecting the antigen-presenting ability of dendritic cells. These results suggest that cathepsin K plays an important role in the immune system and may serve as a valid therapeutic target in autoimmune diseases.

Both innate and adaptive immune systems contribute to the inflammation seen in autoimmune diseases, but the molecular mechanism underlying this process is not completely understood (*1*, *2*). The cathepsins constitute a family of lysosomal cysteine proteases that were initially recognized as nonspecific scavengers of cellular proteins and that were also found to display cell type–specific functions (*3*, *4*). Cathepsins L and S are fundamental in processing of major histocompatibility complex (MHC) class II antigens and MHC class II trafficking and maturation (*3*, *4*). In contrast, cathepsin K is highly expressed in osteoclasts and is involved in degradation of bone matrices such as type I collagen (*5*). The loss-of-function mutation in the *cathepsin K* gene in humans causes pycnodysostosis, a rare genetic disorder characterized by impaired osteoclastic bone resorption (*6*). In mice, the targeted disruption of *cathepsin K* similarly results in the pycnodysostotic phenotype (*4*, *5*, *7*). Among matrix-degrading enzymes expressed in osteoclasts, cathepsin K is the only one for which an essential role in bone resorption has been clearly demonstrated in both mice and humans (*8*). Thus, cathepsin K remains a potential therapeutic target for the treatment of bone diseases such as osteoporosis and autoimmune arthritis, in which osteoclast activity is increased (*9*, *10*).

Through screening, we obtained a potent orally active cathepsin K inhibitor named NC-2300 (Fig. 1A and figs. S1 to S3), which suppresses osteoclastic bone resorption both in vivo and in vitro (figs. S1 and S4). Computer-assisted simulation of the cathepsin K/NC-2300 complex indicated that NC-2300 blocks the active-site cleft where Cys^{25} and His^{162} of cathepsin K form the catalytic site (Fig. 1B and fig. S5). To test the effects of the inhibitor on disease models, we treated adjuvant-induced arthritis (AIA) in rats with oral administration of NC-2300 and compared the results with the effects of alendronate, which is one of the bisphosphonate compounds used clinically as an inhibitor of osteoclastic bone resorption. Bone loss in arthritis occurs mainly in two forms: bone erosion at the inflamed joints and periarticular osteoporosis (*11*). Radiological analysis revealed that NC-2300, but not alendronate, markedly suppressed bone erosion (Fig. 1C), although bone mineral density analysis showed that both compounds had a comparable inhibitory effect on periarticular osteoporosis (fig. S6A). NC-2300 also ameliorated paw swelling (Fig. 1D) and improved locomotive activity (fig. S6B) without affecting the onset rate of arthritis. NC-2300 reduced inflammation even when administered after the onset of disease (fig. S7). These results indicate that cathepsin K also functions in cells other than osteoclasts, allowing it to participate in autoimmune inflammation.

In AIA, local injection of adjuvant stimulates antigen presentation by dendritic cells (DCs), leading to T cell autoimmunity, the production of inflammatory cytokines by macrophages, and osteoclast-mediated bone destruction (*9*, *12*, *13*). The adjuvant effects are mainly dependent on the pathogen-associated molecular patterns (PAMPs)–induced activation of Toll-like receptor (TLR) signaling (*14*, *15*). Therefore, we next analyzed the expression and function of cathepsin K in T cells, macrophages, and DCs. Cathepsin K mRNA was barely detected in nonadherent bone marrow (BM) cells or splenic T cells (Fig. 2A), and NC-2300 showed no effects on T cell activation (fig. S8A). Although macrophages have been reported to express cathepsin K (*4*), NC-2300 had no effects on the activation of BM-derived macrophages stimulated by PAMPs (fig. S8B). BM-derived DCs (BM-DCs) did express a detectable level of cathepsin K mRNA, although this was much lower than expression in osteoclasts (Fig. 2A). Nevertheless, cathepsin K activity was confirmed in DCs and was inhibited by NC-2300 (Fig. 2B).

To investigate whether cathepsin K has a role in antigen presentation in DCs, DCs were cultured with fluorescein isothiocyanate (FITC)–labeled ovalbumin. The uptake of ovalbumin-FITC was observed by flow cytometry in NC-2300–treated DCs as well as in nontreated cells (Fig. 2C). In addition, NC-2300–treated DCs stimulated proliferation of splenic T cells from ovalbumin-specific DO11.10 TCR transgenic mice to an extent similar to that of nontreated DCs (Fig. 2D). These results suggest that cathepsin K activity is not required for the antigen uptake, processing, or presentation by

[1]Department of Cell Signaling, Graduate School, Tokyo Medical and Dental University, Tokyo 113-8549, Japan. [2]Center of Excellence Program for Frontier Research on Molecular Destruction and Reconstruction of Tooth and Bone, Tokyo Medical and Dental University, Tokyo 113-8549, Japan. [3]Department of Hard Tissue Engineering, Section of Pharmacology, Graduate School, Tokyo Medical and Dental University, Tokyo 113-8549, Japan. [4]Nippon Chemiphar Co., Ltd., Saitama 341-0005, Japan. [5]Department of Orthopaedic Surgery, Juntendo University School of Medicine, Tokyo 113-8421, Japan. [6]Division of Infectious Diseases and Immunology, University of Massachusetts Medical School, Worcester, MA 01605, USA. [7]Institute of Molecular and Cellular Biosciences, University of Tokyo, Tokyo 113-0032, Japan. [8]Department of Molecular Pathology, Graduate School of Medicine, University of Tokyo, Tokyo 113-0033, Japan. [9]Exploratory Research for Advanced Technology, Japan Science and Technology Agency, Saitama 332-0012, Japan. [10]Biochemical Institute, Christian-Albrechts-University Kiel, D-24098 Kiel, Germany.

*To whom correspondence should be addressed. E-mail: taka.csi@tmd.ac.jp

DCs. Considering the crucial role of cathepsins L and S in antigen presentation (*3*, *4*, *16*), these results also indicate that the effects of NC-2300 on these cathepsins are negligible.

Complete Freund's adjuvant (CFA) is composed of killed mycobacteria, which contain various PAMPs including TLR2, TLR4, and TLR9 agonists (*14*, *17*). Therefore, we tested the responses of DCs to these PAMPs with or without cathepsin K inactivation. Enzyme-linked immunosorbent assay revealed that the production of cytokines such as interleukin-12 (IL-12) and IL-23 by DCs was significantly inhibited by NC-2300 when stimulated with oligodeoxynucleotides containing unmethylated CpG motif (CpG: the TLR9 ligand), but not with Malp2 and peptidoglycan (PGN) (the TLR2 ligands) or lipopolysaccharide (LPS: the TLR4 ligand) (Fig. 2E). CpG-induced expression of IL-6, IL-12, and IL-23 in BM-DCs was down-regulated at the mRNA level (Fig. 2F), and IFN-β production by Flt3L-induced BM-DCs in response to CpG was suppressed by NC-2300 (Fig. 2F). These results suggest that cathepsin K plays an important role in the gene induction program regulated by TLR9 signaling.

Deoxyribonuclease treatment of the mycobacterial components in CFA greatly reduces the severity of AIA without affecting the induction efficiency, and this reduction is recovered by supplementation with CpG DNA (*18*, *19*), indicating that TLR9-mediated immune responses determine the severity of autoimmune inflammation. Because mycobacterial DNA can be detected weeks after CFA inoculation (*19*), CpG DNA may augment autoimmune inflammation throughout the course of arthritis. These observations lend support to the notion that cathepsin K–dependent TLR9 signaling contributes to autoimmune inflammation.

How does cathepsin K regulate TLR9 signaling? After being taken up into the cells, CpG DNA locates within the endosomal compartment, where CpG DNA binds to TLR9 (*14*, *18*). The binding of CpG with TLR9 results in the conformational change of TLR9 (*20*), leading to activation of MyD88 and downstream signaling such as the mitogen-activated protein kinase, interferon regulatory factor (IRF), and nuclear factor kappa B (NF-κB) pathways (*14*). Activation of these pathways leads to the production of inflammatory cytokines and up-regulation of cell-surface molecules such as CD40, CD80, and CD86 in DCs (*2*, *21*). Compounds that block endosomal acidification such as chloroquine inhibit CpG-driven signaling (*14*, *18*). A normal number of BM-DCs were generated in BM cells derived from *cathepsin K*$^{-/-}$ mice (*5*, *22*), and they exhibited a normal morphology (Fig. 3A), suggesting that cathepsin K is dispensable for the DC differentiation. CpG-induced, but not LPS-induced, phosphorylation of extracellular-signal regulated kinases 1 and 2 (ERK 1/2) in DCs was suppressed by cathepsin K inactivation (Fig. 3B). CpG-induced activation of IRF and NF-κB was also suppressed by cathepsin K inactivation in DCs (Fig. 3C). In addition, NC-2300 reduced expression of CD40, CD80, and CD86 in DCs (Fig. 3D). CpG-induced, but not LPS-induced, production of cytokines such as IL-12 and IL-6 in *cathepsin K*$^{-/-}$ DCs was significantly suppressed (Fig. 3E). Thus, cathepsin K inactivation leads to the blockade of essentially all the downstream pathways of TLR9 signaling in DCs, suggesting that cathepsin K plays a critical role in the signaling events proximal to TLR9. However, the endocytosis of CpG was not affected in *cathepsin K*$^{-/-}$ DCs (Fig. 3F) and the endosomal acidification was not inhibited by NC-2300 (fig. S9), whereas chloroquine suppressed the cathepsin K activity in DCs (fig. S10).

It remains to be elucidated how cathepsin K regulates CpG-TLR9 signaling in the endosome, but the results of pharmacological inhibition indicate that the proteolytic activity of this enzyme is crucial for the mechanism. It is conceivable that cathepsin K may be involved in the degradation of proteins that inhibit the interaction between CpG and TLR9, or cathepsin K–mediated proteolysis may result in the conformational change of TLR9 that augments its signal transduction (*20*). Because fluorescence resonance energy transfer analysis showed that the CpG-induced conformational change of TLR9 was not affected in human embryonic kidney (HEK) 293 cells by NC-2300 (fig. S11), we cannot rule out the possibility that cathepsin K degrades a cytoplasmic protein that modifies the proximal TLR9 signaling. The observation that *cathepsin K*$^{-/-}$ DCs responded normally to TLR3 or TLR7/8 stimulation suggests that the role of cathepsin K is TLR9-specific in DCs (fig. S12).

To clearly demonstrate that cathepsin K plays a critical role in autoimmune inflammation in an osteoclast-independent manner, we subjected *cathepsin K*$^{-/-}$ mice to experimental autoimmune encephalomyelitis (EAE), in which TLR9 signaling plays an important role (*23*, *24*). The frequency of the onset of EAE was not different between control and *cathepsin K*$^{-/-}$ mice, but the severity of the paralytic symptoms was much lower in the *cathepsin K*$^{-/-}$ mice than in control mice (Fig. 3G, top). Histological analysis of spinal cords demonstrated a marked decrease in inflammation (Fig. 3G, HE staining), T cell infiltration (Fig. 3G, anti-CD3 staining), and demyelination (Fig. 3G, LFB staining) in *cathepsin K*$^{-/-}$ mice. Because T helper 17 (T_H17) cells play an essential role in the autoimmune inflammation in EAE (*25*), we examined the effect of cathepsin K inactivation on the ability of DCs to induce

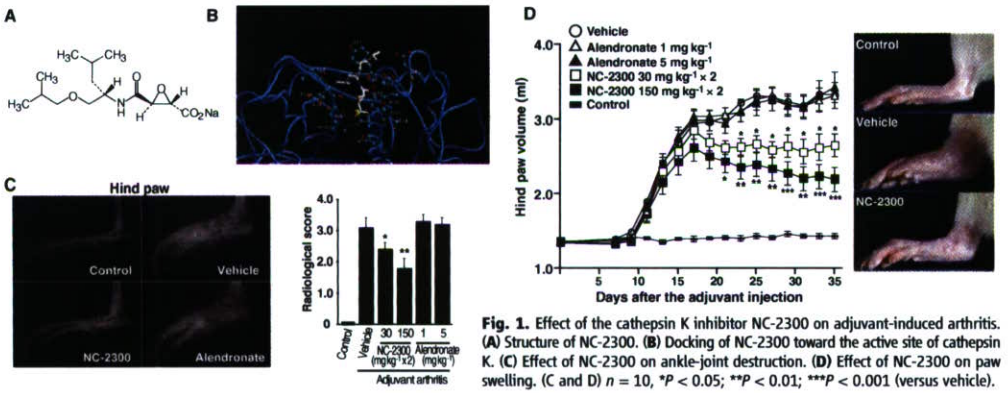

Fig. 1. Effect of the cathepsin K inhibitor NC-2300 on adjuvant-induced arthritis. **(A)** Structure of NC-2300. **(B)** Docking of NC-2300 toward the active site of cathepsin K. **(C)** Effect of NC-2300 on ankle-joint destruction. **(D)** Effect of NC-2300 on paw swelling. (C and D) $n = 10$, $^*P < 0.05$; $^{**}P < 0.01$; $^{***}P < 0.001$ (versus vehicle).

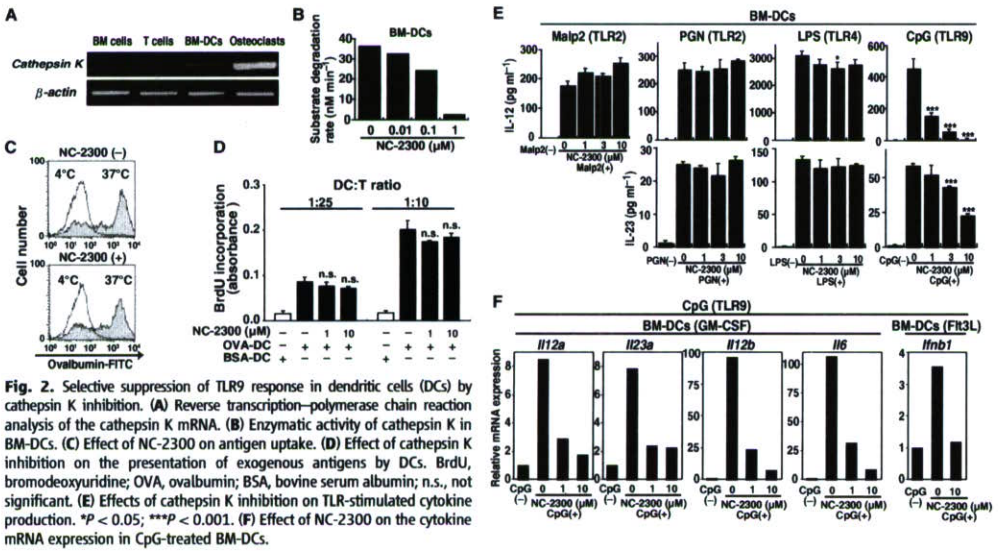

Fig. 2. Selective suppression of TLR9 response in dendritic cells (DCs) by cathepsin K inhibition. **(A)** Reverse transcription–polymerase chain reaction analysis of the cathepsin K mRNA. **(B)** Enzymatic activity of cathepsin K in BM-DCs. **(C)** Effect of NC-2300 on antigen uptake. **(D)** Effect of cathepsin K inhibition on the presentation of exogenous antigens by DCs. BrdU, bromodeoxyuridine; OVA, ovalbumin; BSA, bovine serum albumin; n.s., not significant. **(E)** Effects of cathepsin K inhibition on TLR-stimulated cytokine production. $^*P < 0.05$; $^{***}P < 0.001$. **(F)** Effect of NC-2300 on the cytokine mRNA expression in CpG-treated BM-DCs.

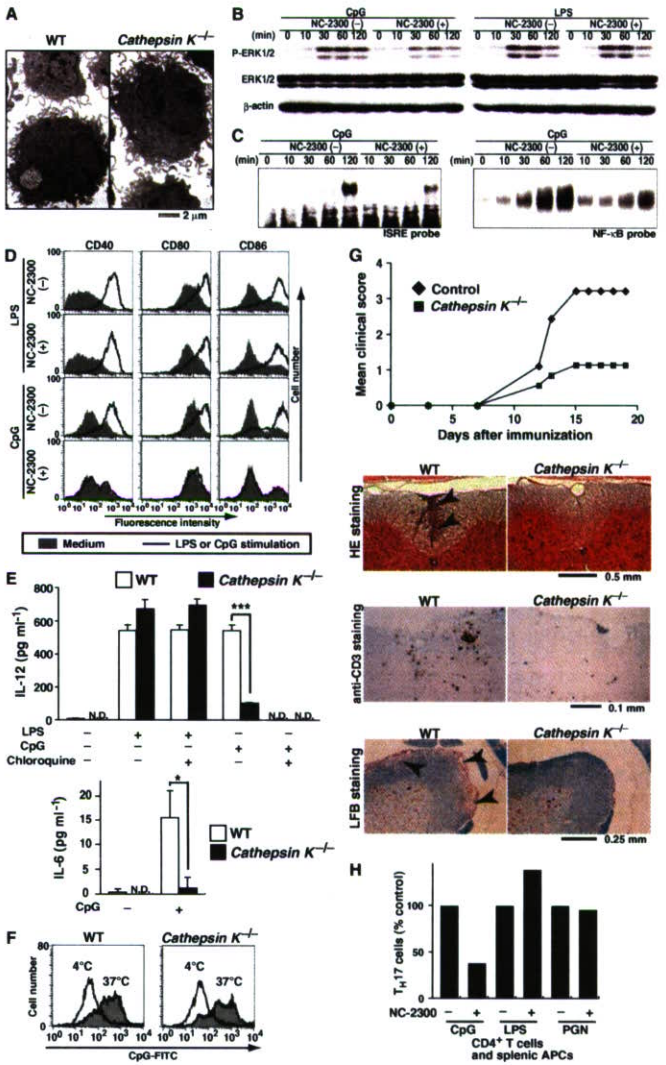

Fig. 3. Cathepsin K regulation of TLR9-mediated immune responses and autoimmune inflammation. **(A)** Electron micrographs of WT and *cathepsin K*$^{-/-}$ BM-DCs. **(B)** Suppression of ERK phosphorylation by NC-2300 in CpG-stimulated DCs. **(C)** Effect of NC-2300 on CpG-induced activation of transcription factors, IRF (left) and NF-κB (right) (electrophoretic mobility shift assay). ISRE, IFN-stimulated response element. **(D)** Impaired TLR9-mediated expression of cell-surface molecules in NC-2300–treated DCs. **(E)** Cytokine production in WT or *cathepsin K*$^{-/-}$ DCs in response to LPS or CpG. N.D., not detected. $^*P < 0.05$; $^{***}P < 0.001$. **(F)** Uptake of CpG in *cathepsin K*$^{-/-}$ DCs. **(G)** Severity of EAE in *cathepsin K*$^{-/-}$ mice. Clinical scores (top). Lumbar spinal cord sections stained with hematoxylin and eosin (HE), immunostained for CD3, and stained with luxol fast blue (LFB) (bottom). Arrowheads indicate inflammatory cellular infiltrates (HE) and demyelinated areas (LFB). **(H)** Cathepsin K inactivation results in defective T_H17 polarization in response to CpG, but not to LPS or PGN.

T_H17 cells. The ability of DCs to induce T_H17 cells was markedly inhibited by cathepsin K inactivation when stimulated with CpG, but not with LPS or PGN (Fig. 3H). Taken together with the results on the role of cathepsin K in CpG-induced cytokine expression in DCs, the impaired induction of T_H17 cells by cathepsin K inactivation was caused, at least in part, by the reduced DC expression of cytokines that are involved in the induction and expansion of T_H17 cells such as IL-6 and IL-23 (*25*, *26*).

Our results show that cathepsin K, which was thought to be an osteoclast-specific enzyme, plays a critical role in the immune system. Cathepsin K functions under the acidified conditions in the endosome, where engagement of CpG by TLR9 occurs, and plays an important role in the signaling events proximal to TLR9. Thus, careful attention should be paid to the side effects of cathepsin K inhibitors on the immune system in the treatment of osteoporosis, whereas they may have dual benefits in the treatment of autoimmune arthritis, the pathogenesis of which is dependent on both DCs and osteoclasts (*9*).

References and Notes

1. J. Banchereau, V. Pascual, A. K. Palucka, *Immunity* **20**, 539 (2004).
2. R. M. Steinman, D. Hawiger, M. C. Nussenzweig, *Annu. Rev. Immunol.* **21**, 685 (2003).
3. V. Turk, B. Turk, D. Turk, *EMBO J.* **20**, 4629 (2001).
4. K. Honey, A. Y. Rudensky, *Nat. Rev. Immunol.* **3**, 472 (2003).
5. P. Saftig *et al.*, *Proc. Natl. Acad. Sci. U.S.A.* **95**, 13453 (1998).
6. B. D. Gelb, G. P. Shi, H. A. Chapman, R. J. Desnick, *Science* **273**, 1236 (1996).
7. W. Chen *et al.*, *Hum. Mol. Genet.* **16**, 410 (2007).
8. M. Asagiri, H. Takayanagi, *Bone* **40**, 251 (2007).
9. H. Takayanagi, *Nat. Rev. Immunol.* **7**, 292 (2007).
10. Y. Yasuda, J. Kaleta, D. Brömme, *Adv. Drug Deliv. Rev.* **57**, 973 (2005).
11. S. Ochi *et al.*, *Proc. Natl. Acad. Sci. U.S.A.* **104**, 11394 (2007).
12. R. Holmdahl *et al.*, *Immunol. Rev.* **184**, 184 (2001).
13. A. Marshak-Rothstein, *Nat. Rev. Immunol.* **6**, 823 (2006).
14. S. Akira, S. Uematsu, O. Takeuchi, *Cell* **124**, 783 (2006).
15. A. Iwasaki, R. Medzhitov, *Nat. Immunol.* **5**, 987 (2004).
16. R. J. Riese *et al.*, *J. Clin. Invest.* **101**, 2351 (1998).
17. S. B. Su *et al.*, *J. Immunol.* **175**, 6303 (2005).
18. A. M. Krieg, *Annu. Rev. Immunol.* **20**, 709 (2002).
19. A. Ronaghy *et al.*, *J. Immunol.* **168**, 51 (2002).
20. E. Latz *et al.*, *Nat. Immunol.* **8**, 772 (2007).
21. I. Mellman, R. M. Steinman, *Cell* **106**, 255 (2001).
22. T. Nakamura *et al.*, *Cell* **130**, 811 (2007).
23. M. Prinz *et al.*, *J. Clin. Invest.* **116**, 456 (2006).
24. B. M. Segal, J. T. Chang, E. M. Shevach, *J. Immunol.* **164**, 5683 (2000).
25. H. Park *et al.*, *Nat. Immunol.* **6**, 1133 (2005).
26. E. Bettelli *et al.*, *Nature* **441**, 235 (2006).

27. We thank K. Takeda, M. Yamamoto, H. Oda, S. Imajoh-Ohmi, M. Matsuura, K. Nishioka, T. Kanda, K. Sato, S. Hida, Y. Iwai, H. Hemmi, H. Yanai, S. Kano, Y. Omatsu, T. Onodera, T. Honda, and A. Suematsu for discussion and assistance. This work was supported in part by a Grant-in-Aid for Creative Scientific Research from the Japan Society for the Promotion of Science (JSPS); grants for the Genome Network Project from the Ministry of Education, Culture, Sports, Science and Technology of Japan (MEXT); Grants-in-Aid for Scientific Research from JSPS and MEXT; Health Sciences Research Grants from the Ministry of Health, Labor and Welfare of Japan; and grants from the Deutsche Forschungsgemeinschaft and the NIH.

Supporting Online Material

www.sciencemag.org/cgi/content/full/319/5863/624/DC1
Materials and Methods
Figs. S1 to S12
References

5 September 2007; accepted 14 December 2007
10.1126/science.1150110

Systemic Leukocyte-Directed siRNA Delivery Revealing Cyclin D1 as an Anti-Inflammatory Target

Dan Peer,[1] Eun Jeong Park,[1] Yoshiyuki Morishita,[1] Christopher V. Carman,[2] Motomu Shimaoka[1]*

Cyclin D1 (CyD1) is a pivotal cell cycle–regulatory molecule and a well-studied therapeutic target for cancer. Although CyD1 is also strongly up-regulated at sites of inflammation, its exact roles in this context remain uncharacterized. To address this question, we developed a strategy for selectively silencing CyD1 in leukocytes in vivo. Targeted stabilized nanoparticles (tsNPs) were loaded with CyD1–small interfering RNA (siRNA). Antibodies to β_7 integrin (β_7 I) were then used to target specific leukocyte subsets involved in gut inflammation. Systemic application of β_7 I-tsNPs silenced CyD1 in leukocytes and reversed experimentally induced colitis in mice by suppressing leukocyte proliferation and T helper cell 1 cytokine expression. This study reveals CyD1 to be a potential anti-inflammatory target, and suggests that the application of similar modes of targeting by siRNA may be feasible in other therapeutic settings.

RNA interference (RNAi) has emerged as a powerful strategy for suppressing gene expression, offering the potential to dramatically accelerate in vivo drug target validation, as well as the promise to create novel therapeutic approaches if it can be effectively applied in vivo (*1*). Cyclin D1 (CyD1) is a key cell cycle–regulating molecule that governs the proliferation of normal and malignant cells (*2*, *3*). In inflammatory bowel diseases, colon-expressed CyD1 is aberrantly up-regulated in both epithelial and immune cells (*4*, *5*). Although CyD1 has also been implicated in promoting epithelial colorectal dysplasia and carcinogenesis, it is not clear whether leukocyte-expressed CyD1 contributes directly to the pathogenesis of inflammation and whether it might serve as a therapeutic target.

To address these questions, we used RNAi silencing of CyD1 in an experimental model of intestinal inflammation. A major limitation to the use of RNAi in vivo is the effective delivery of siRNAs to the target cells (*6*, *7*). RNAi in leukocytes, a prime target for anti-inflammatory therapeutics, has remained particularly challenging, as these cells are difficult to transduce by conventional transfection methods and are often disseminated throughout the body, thus requiring systemic delivery approaches (*8*). One possibility is to use integrins, which are an important family of cell-surface adhesion molecules, as targets for siRNA delivery (*8*). Specifically, we have shown that antibody-protamine fusion proteins directed to the lymphocyte function-associated antigen–1 (LFA-1) integrin selectively delivered siRNAs to leukocytes, both in vitro and in vivo (*8*). However, whether an integrin-directed siRNA delivery approach can induce

[1]Immune Disease Institute and Department of Anesthesia, Harvard Medical School, 200 Longwood Avenue, Boston, MA 02115, USA. [2]Department of Medicine, Beth Israel Deaconess Medical Center, and Harvard Medical School, 330 Brookline Avenue, Boston, MA 02215, USA.

*To whom correspondence should be addressed. E-mail: shimaoka@cbrinstitute.org

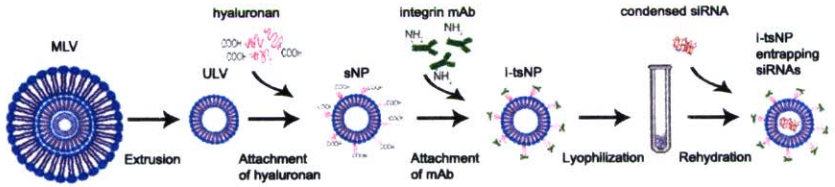

Fig. 1. The processes involved in generating I-tsNPs. Multilamellar vesicle (MLV) [prepared as described in (*9*)] is extruded to form a unilamellar vesicle (ULV) with a diameter of ~100 nm. Hyaluronan is covalently attached to DPPE in the ULV. A monoclonal antibody (mAb) to the integrin is covalently attached to hyaluronan, generating I-tsNP. siRNAs are entrapped by rehydrating lyophilized β_7 I-tsNP with water containing protamine-condensed siRNAs.

Oncogene (2005) 24, 3206–3215

www.nature.com/onc

Domain-specific function of ShcC docking protein in neuroblastoma cells

Izumi Miyake[1,2], Yuko Hakomori[1], Yoko Misu[2], Hisaya Nakadate[2], Nobuo Matsuura[2], Michiie Sakamoto[3] and Ryuichi Sakai*,[1]

[1]*Growth Factor Division, National Cancer Center Research Institute, 5-1-1 Tsukiji, Chuo-ku, Tokyo 104-0045, Japan;* [2]*Department of Pediatrics, Kitasato University School of Medicine, 1-15-1 Kitasato, Sagamihara-shi, Kanagawa 228-8555, Japan;* [3]*Department of Pathology, Keio University School of Medicine, 35 Shinanomachi, Shinjuku-ku, Tokyo 160-8582, Japan*

ShcC is a family member of the Shc docking proteins that possess two different phosphotyrosine-binding motifs and conduct signals as Grb2-binding substrates of various receptor tyrosine kinases. We have recently shown that some neuroblastoma cell lines, such as NB-39-nu cells, express a protein complex of hyperphosphorylated ShcC and anaplastic lymphoma kinase (ALK), which is self-activated by gene amplification. Here, we demonstrate that the expression of a mutant ShcC lacking Grb2-binding sites, 3YF-ShcC, significantly impaired the survival, differentiation and motility of NB-39-nu cells by blocking the ERK and Akt pathways. On the other hand, cells overexpressing ShcC or 3YF-ShcC, but not a mutant ShcC that lacks SH2, showed decreased anchorage independency and *in vivo* tumorigenicity, suggesting a novel ShcC-specific suppressive effect through its SH2 domain on cell transformation. Notably, overexpression of ShcC suppressed the sustained phosphorylation of Src family kinase after cell detachment, which might be independent of phosphorylation of Grb2-binding site. It was indicated that the Src/Fyn-Cas pathway is modulated as a target of these suppressive effects by ShcC. Reciprocal change of ShcC expression and phosphorylation observed in malignant neuroblastoma cell lines might be explained by these phosphotyrosine-dependent and -independent functions of ShcC.

Oncogene (2005) **24,** 3206–3215. doi:10.1038/sj.onc.1208523
Published online 21 February 2005

Keywords: ShcC; neuroblastoma; dominant-negative form; SH2 domain; Src family kinase

Introduction

The Shc family of docking proteins plays an essential role in leading cellular signaling to specific downstream molecules such as the Ras-ERK pathway and the phosphatidylinositol 3-kinase (PI3K)-Akt pathway when recruited towards phosphotyrosine residues of various activated RTKs. In mammals, three *shc* genes have been identified, and their products have been termed ShcA/Shc, ShcB/Sli/Sck and ShcC/Rai/N-Shc (Nakamura *et al.*, 1996a; O'Bryan *et al.*, 1996b; Pelicci *et al.*, 1996). ShcA is ubiquitously expressed in most organs except the adult neural system, whereas ShcB and ShcC proteins are selectively expressed in the neural system within adult mouse tissues.

The Shc family molecules have a unique PTB-CH1-SH2 modular organization. Two phosphotyrosine-binding modules, PTB and SH2 domains, recognize phosphotyrosine-containing polypeptides such as cytoplasmic domains of various activated RTKs (Pelicci *et al.*, 1992; van der Geer *et al.*, 1995). The CH1 domain has several tyrosine phosphorylation sites that recruit other SH2-containing adaptor molecules such as Grb2 (van der Geer *et al.*, 1996; Thomas and Bradshaw, 1997) and a proline-rich stretch of ShcA composing the binding site for the SH3 domains of other proteins including Src, Fyn and Lyn (Weng *et al.*, 1994; Wary *et al.*, 1998). There might be difference in the molecular functions of each Shc family member, although there is not much information on individual roles of Shc families in the neural system and neuronal tumors.

We have recently shown that the expression and tyrosine phosphorylation of Shc family proteins, especially ShcC, are observed in most neuroblastoma cells. Stable association of constitutively activated anaplastic lymphoma kinase (ALK) with the ShcC has been observed in several neuroblastoma cell lines that have extremely high phosphorylation levels of ShcC (Miyake *et al.*, 2002). These cell lines showed malignant phenotypes as for tumorigenicity in nude mice or soft agar colony assay, and notably, ShcC expression is low compared with other neuroblastoma in spite of significantly high phosphorylation state. The *ALK* gene locus was significantly amplified in these cell lines, which results in the constitutive activation of the ALK and most prominent tyrosine phosphorylation of ShcC among several known binding partners of ALK such as PLCγ and IRS-1 (Miyake *et al.*, 2002).

ALK protein has the typical structure of an RTK classified into the insulin receptor superfamily. It is dominantly expressed in the normal neural system (Iwahara *et al.*, 1997; Morris *et al.*, 1997), although the biological role of this protein in neuronal cells has not yet been clearly identified. We detected remarkable amplification of the *ALK* gene in three out of 13 neuroblastoma cell lines (Miyake *et al.*, 2002) and a less

*Correspondence: R Sakai; E-mail: rsakai@gan2.res.ncc.go.jp

Received 12 October 2004; revised 30 December 2004; accepted 12 January 2005; published online 21 February 2005

significant gain of copy numbers in eight out of 85 primary neuroblastoma tissues (Hakomori *et al.*, manuscript in preparation), most of which accompany the amplification of the *N-myc* gene. The three *ALK*-amplified neuroblastoma cell lines showed constitutive activation of full-length ALK and the increased local concentration of receptor tyrosine kinases appeared to interfere with signals from other RTKs. It is possible that ALK-ShcC signal activation has additional effects on the malignant tumor progression of neuroblastoma, probably similar to the mechanism reported in EGFR and Neu/ErbB2 (Andrechek *et al.*, 2000; Pawson *et al.*, 2001).

To clarify the role of hyperphosphorylated ShcC in neuroblastoma cells, the 3YF-ShcC mutant, which has phenylalanines at three Grb2-binding tyrosines (Y221/222/304) of ShcC, was utilized in this study in the expectation of a dominant-negative effect specific for signals originating from the ShcC-Grb2 complex. The biological effects of the 3YF-ShcC mutant as well as wild-type ShcC and the ΔSH2 ShcC mutant, which lacks the SH2 domain, were analysed to elucidate both Grb2-dependent and -independent functions of ShcC in neuroblastoma.

Results

Suppression of ERK1/2 and Akt activation in NB-39-nu cells by expression of 3YF-ShcC

A neuroblastoma cell line, NB-39-nu, was used in this study because it shows high tumorigenicity and anchorage independency with prominent phosphorylation level of ShcC caused by constitutively activated ALK kinase. The expression level of ShcC is relatively low among the neuroblastoma cell lines examined in our previous study. T7-tagged ShcC constructs containing the full length of human ShcC cDNA (ShcC-wt), a tyrosine-to-phenylalanin mutant for all three putative Grb2-binding sites (3YF-ShcC), and the SH2-deletion mutant (ΔSH2-ShcC) were subcloned into a mammalian expression vector, pcDNA3.1. Multiple independent clones of NB-39-nu cell lines stably expressing these ShcC mutants at comparable levels were selected and submitted to biochemical and biological analysis. Results of representative clones are shown in Figure 1a, although basically same results were obtained from other independent clones (data not shown). Tyrosine phosphorylation of the 3YF-ShcC was significantly suppressed suggesting that the three tyrosines lost in this mutant are the main phosphorylation sites of ShcC in NB-39-nu (Figure 1a). As expected, the complex formation of 3YF-ShcC with Grb2 was impaired, regardless of EGF stimulation, compared with that of ShcC-wt and ΔSH2-ShcC (Figure 1c). The activation level of ERK1/2 at 5 min after the EGF stimulation was decreased by expression of 3YF-ShcC, while expression of ShcC-wt or ΔSH2-ShcC did not affect the levels of ERK1/2 activation compared with the control cells transfected only by expression vector (mock) (Figure 1d). The phosphorylation level of Akt at Ser-473 was also suppressed by expression of 3YF-ShcC, although not at a similar level as that of cells treated with Wortmannin (Sigma), a PI3K inhibitor (Figure 1e). These analyses were performed using at least two independent clones. It was confirmed that 3YF-ShcC-expression has a dominant-negative effect on the PI3K/Akt pathway as well as the Ras/ERK pathway in this neuroblastoma cell line.

Expression of 3YF-ShcC increased susceptibility to retinoic acid (RA)-induced apoptosis in NB-39-nu cells

There were no obvious differences in growth rate among the NB-39-nu clones expressing each ShcC mutant (Figure 2a), whereas the rate of [^{3}H]-thymidine incorporation of the cell lines expressing 3YF-ShcC was slightly lower than that of other cells (Figure 2b).

The cytological analyses of the cells cultured with 10 μM of all-*trans*-RA revealed that 3YF-ShcC expressing cells were more susceptible to RA-induced apoptosis than the control or ShcC-wt-expressing cells (Figure 3a). Treatment of NB-39-nu cells, especially ShcC-wt-expressing cells, with RA at a lower concentration of 2.5 or 5 μM induced mild neurite formation, flattened, substrate-adherent cells resembling epithelial cells within 48 h (Figure 3b), which is known to be a characteristics of RA-induced morphologic differentiation (Sidell *et al.*, 1983). In contrast, this type of differentiation was not observed in 3YF-ShcC-expressing cells. Along with the suppressive effects of 3YF-ShcC to the Akt pathway (Figure 1e), these results suggest that phosphorylated ShcC plays significant role in survival signals through the putative Grb2-binding sites in NB-39-nu cells.

ShcC plays a distinct role in the migration of ALK-ShcC-activated neuroblastoma cells

Expression of 3YF-ShcC significantly suppresses cell migration ability as shown by the wound-healing assay (Figure 4a). A modified Boyden chamber cell-migration assay without Matrigel using fibronectin as a chemoattractant showed the results consistent with those obtained in the wound-healing assay (Figure 4b). A similar assay with Matrigel coating on a chamber filter to evaluate the chemotactic invasive activity of each transfectant also showed decreased invasive activity in 3YF-ShcC-expressing cells (Figure 4c). In contrast, ShcC-wt expression increased the migration ability of NB-39-nu cells both in wound healing assay and modified Boyden chamber assay without Matrigel (Figure 4a, b), while the ΔSH2-ShcC expression presented no remarkable effects on the cell motility. The invasive activity of ShcC-wt-expressing cells was not significantly high compared to that of the control or of the ΔSH2-ShcC-expressing cells (Figure 4c).

Expression of ShcC-wt or 3YF-ShcC has a negative effect on the transforming activity of NB-39-nu cells

Cells expressing ShcC-wt or 3YF-ShcC tend to grow to confluence with a monolayer appearance, making a clear

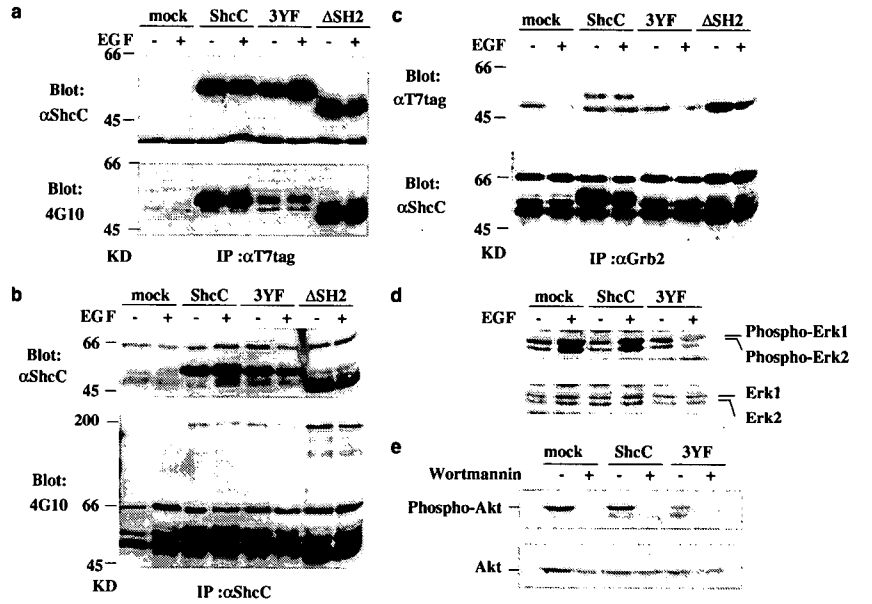

Figure 1 NB-39-nu cells stably expressing ShcC mutants analysed by immunoblotting. (**a**) Expression (upper panel) and tyrosine phosphorylation (lower panel) of ectopic ShcC mutant proteins (mock: control, ShcC: ShcC-wt, 3YF: 3YF-ShcC and ΔSH2: ΔSH2-ShcC) in the NB-39-nu cells. (**b**) Expression (upper panel) and tyrosine phosphorylation (lower panel) of both endogenous ShcC and ectopic ShcC mutants in NB-39-nu cells. (**c**) The complex formation of Grb2 with ShcC (lower panel) or ectopic ShcC mutants (upper panel) was analysed. (**d**) The activation of ERK1/2 in ShcC mutant cells. (**e**) Akt (Ser473) phosphorylation in ShcC mutant cells in a tissue culture medium with 10% fetal calf serum (FCS). For the negative control, the cells were treated with 1 μM of Wortmannin for 2 h. EGF stimulations were performed as described in Materials and methods. Lysates were duplicated and detected by the antibodies shown in the figure

difference from original NB-39-nu cells that tend to form cell aggregations on the culture dishes (Figure 5a). In addition, control NB-39-nu cells and ΔSH2-ShcC-expressing cells form a considerable number of colonies in soft agar (Figure 5b), which is significantly suppressed by the expression of ShcC-wt or 3YF-ShcC (Figure 5b). These results indicate that ShcC-wt or 3YF-ShcC have inhibitory effect on the transforming activity of NB-39-nu cells, especially anchorage-independent growth. Since the overexpression of ShcC had no significant effect on the activation of ERK1/2 or Akt in our experiment, it was suggested that a unique signaling pathway rather than classical Grb2-Ras pathway is involved in this phenomenon.

Src family kinases (SFKs) are well known to be associated with the ability to induce cellular transformation including anchorage independency (Parsons and Weber, 1989; Windham *et al.*, 2002). During the investigation of ShcC mutant cells in the suspension state, we noticed that the sustained activation of both Fyn and c-Src observed in the control cells and ΔSH2-ShcC-expressing cells was suppressed by the expression of ShcC-wt or 3YF-ShcC (Figure 6a, b) at 24 h after cell detachment. Especially, the condition of phosphorylation of Fyn at suspension culture well correlated with anchorage independency of NB-39-nu sublines (Figure 6a). Tendency of phosphorylation of Src Tyr-416, which indicates the kinase activation of SFKs, is consistent with these results (Figure 6c). Phosphorylation of Cas, a main substrate of SFKs, in a suspended condition has recently been associated with the anchorage-independent growth of cancer-like lung adenocarcinoma (Wei *et al.*, 2002). Sustention and temporary elevation of the Cas phosphorylation was also observed specifically in the original NB-39-nu cells, control and ΔSH2-ShcC-expressing cells, whereas there was a marked decrease of the phosphorylation level of Cas in ShcC-wt- and 3YF-ShcC-expressing cells (Figure 6d, e). Treatment of NB-39-nu control cells with PP2, a Src-specific inhibiter, suppressed the phosphorylation of Cas both in an attached and suspended condition, suggesting that the anchorage-independent phosphorylation of Cas is associated with the activity of the SFKs (Figure 6f).

The activation of ERK1/2 or Akt was similarly suppressed by suspension culture for 24 h regardless of the expression of each ShcC mutants although the basal

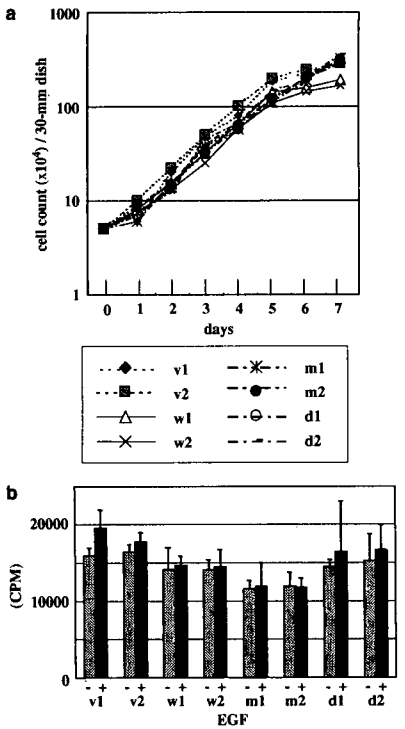

Figure 2 Growth rate and proliferation ability of ShcC mutant cells *in vitro*. (**a**) ShcC mutant cells cultured in a normal medium with 10% FCS by 30-mm dishes were counted at the indicated time points. The results represent the average values (±s.d.) of three replicated experiments for each clone. (**b**) ShcC mutant cells stimulated with none (gray bar) or EGF (black bar) were treated with [^{3}H]thymidine to the culture medium as described in Materials and methods. The graph represents the average values (±s.d.) from an experiment performed in triplicate. NB-39-nu clones are described as: v1 and v2 (control), w1 and w2 (expressing ShcC-wt), m1 and m2 (expressing 3YF), d1 and d2 (expressing ΔSH2)

level is lower in 3YF-ShcC clones (Supplementary Figure A). There were no difference in phosphorylation level of FAK and paxillin, which plays an important role in regulating the signals from the extracellular matrix (ECM) and organizing the actin-cytoskeleton, by expressing ShcC-wt, showing a similar level of decrease in the suspended condition (Supplementary Figure B). In summary, it was confirmed in this system that the constitutive activation of SFKs, such as Fyn and c-Src, and phosphorylation of Cas in suspended cells, but not other components of integrin signals such as FAK, is strictly linked to the anchorage independency of NB-39-nu cells, closely related with ShcC mutants expression. Furthermore, we detected interaction between ShcC-wt and some of SFKs following the stimulation (Figure 6g), indicating a novel biological interaction of ShcC with SFK, as suggested for ShcA in integrin pathway (Wary *et al.*, 1996; Giancotti, 1997)

Loss of tumorigenicity of NB-39-nu-expressing ShcC-wt or 3YF-ShcC in mouse subcutaneous tissues

To investigate these antitransforming effects of ShcC-wt and 3YF-ShcC *in vivo*, the tumorigenicity of NB-39-nu cells expressing each mutant in nude mice was evaluated. Tumors generated by eight independent injections of each mutant were analysed in weight and histology at 4 weeks after subcutaneous injection. The results revealed a marked reduction in sizes of tumors from the cells expressing either ShcC-wt or 3YF-ShcC at this time, but not of tumors from the control cells or cells expressing ΔSH2-ShcC (Figure 7a).

The tumors from the control, ShcC-wt-expressing and ΔSH2-ShcC-expressing cells presented a hypervascular appearance (Figure 7a: upper panel), which has the histological characteristics of almost equal-sized cells with a regular arrayed pattern, high nuclear-to-cytoplasmic (N/C) ratio and chromatin-rich nucleuses (Figure 7b). On the other hand, the tumors from the 3YF-ShcC-expressing cells were hypovascular and histologically distinct from the other mutants, showing rather unequal-sized cells with an irregular arrayed pattern, a lower N/C ratio, few mitosis and decreased nucleus density. In accordance with this, staining by a proliferation marker, Ki-67, or a mitotic activity marker, cyclin A, markedly decreased in the tumors from 3YF-ShcC-expressing cells (Figure 7b), showing that the cell cycle progression was significantly suppressed by 3YF-ShcC *in vivo*, compared with the analysis by [^{3}H]-tymidine incorporation *in vitro* (Figure 2b). TUNEL staining showed no marked difference in cell apoptosis among each tumor tissue (data not shown). These results suggest that the antitumorigenic activity of the 3YF-ShcC-expressing cells *in vivo* accompanies the regulation of cell proliferation, which is distinct from the impairment of tumorigenicity by expression of ShcC-wt.

Discussion

In our previous report, the biological effects of constitutively activated signals of ALK-ShcC on the tumorigenesis of neuroblastoma cells remain to be investigated. Here, we demonstrated that the proliferation, survival and cell migration of these neuroblastoma cells were dependent on the signals via ShcC-Grb2 pathway, downstream of ALK. Additionally, overexpressed ShcC has a suppressive effect on the anchorage-independent growth of these cells via its SH2 domain and this regulation is closely associated with the regulation of c-Src and Fyn tyrosine kinases.

The fact that 3YF-ShcC significantly suppressed the activity of both ERK1/2 and Akt, suggesting that ShcC, among signaling pathways originating from activated ALK, predominantly regulates these signals through

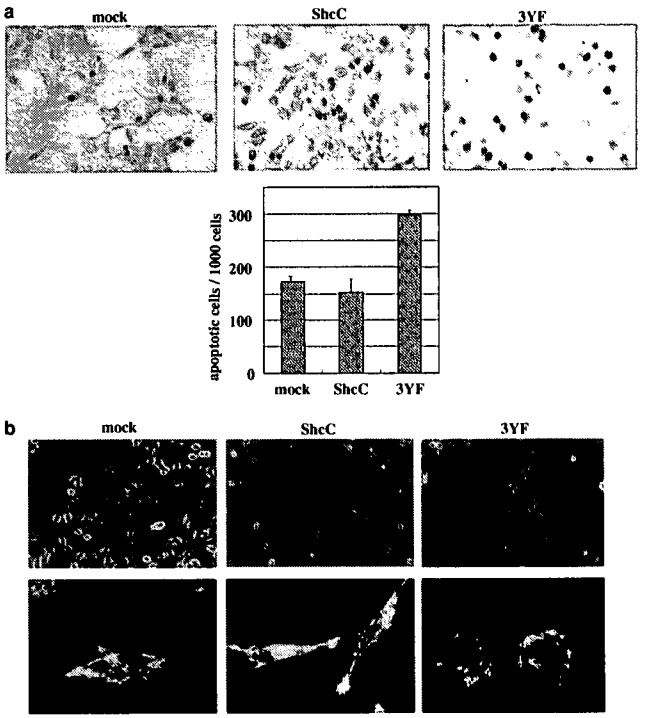

Figure 3 Effects of ShcC mutants on apoptosis and differentiation of NB-39-nu cells induced by all-*trans* retinoic acid (RA). (**a**) TUNEL analysis of ShcC mutant cells were performed as described in Materials and methods. Bar: 100 μm (upper panel). TUNEL-positive cells, the prominent dark positive cells, are counted for every 1000 cells for each slide, and three different slides were analysed for each sample. The graph represents the results (expressed as mean±s.d.) of three observations (lower panel). (**b**) RA-induced morphological change of NB-39-nu cells expressing ShcC mutants. The cells were grown for 48 h in RPMI 1640 with 10% FCS containing 2.5 μM of RA and examined by phase-contrast microscopy (upper panel). Actin filaments stained with FITC-labeled phalloidin were visualized with a confocal fluorescence microscope (lower panel)

binding to Grb2. Our recent study also shows that the suppression of activated ALK using the RNA interference technique (RNAi) reduces the phosphorylation of ShcC, ERK1/2 and Akt, and induces the apoptotic cell death of NB-39-nu cells (Hakomori *et al.*, manuscript in preparation). The ERK and Akt pathways are key regulators of cell proliferation, survival and differentiation. Cells expressing 3YF-ShcC become more susceptible to RA-induced apoptosis presumably due to inhibition of the Akt pathway. It has recently been shown that ShcC is physiologically involved in the regulation of the PI3K/Akt pathway as a downstream effecter of the ligand-stimulated Ret receptor in neuroblastoma cells (Pelicci *et al.*, 2002). This study confirms that the survival of NB-39-nu cells is regulated by the signals downstream of ShcC. The 3YF-ShcC also causes inhibition of cell motility, while overexpressed ShcC significantly increases the ability of cell migration, indicating that ShcC positively affects the regulation of cell migration. Previously, ShcA was shown to be closely related with cell motility via the MAPK pathway (Collins *et al.*, 1999; Gu *et al.*, 1999), but the association of ShcC with the ability of cell migration has not been investigated.

The expression of 3YF-ShcC had a suppressive effect on the proliferation of NB-39-nu cells cultured *in vitro* and more significantly on the cell cycle progression of the nude mouse tumor. These data suggest that ShcC positively regulates the cell proliferation of neuronal tumor cells as well as ShcA, which has been reported to affect the tumor growth in nude mice using breast cancer cell lines (Stevenson *et al.*, 1999).

The overexpression of ShcC-wt endowed NB-39-nu cells with several characteristics. Other than the enhancement of cell migration and neurite outgrowth, which is consistent with previous study (Collins *et al.*, 1999; Pelicci *et al.*, 2002), the observation that ShcC-wt-expressing cells were impaired for anchorage-indepen-

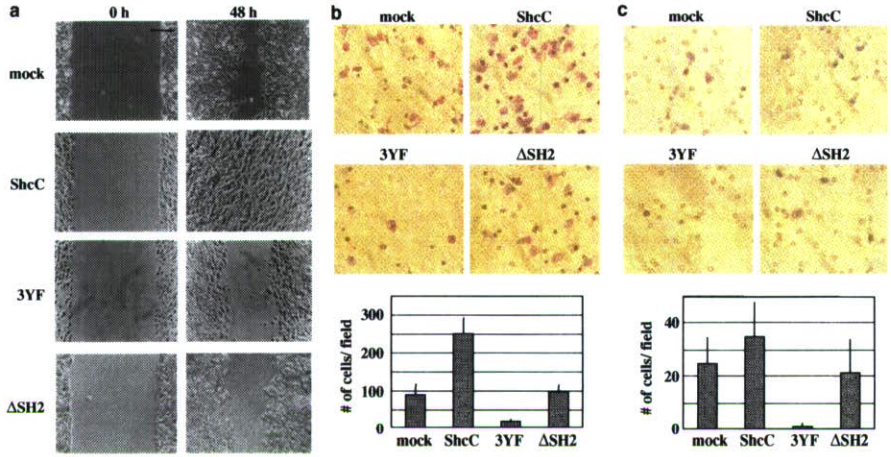

Figure 4 Expression of ShcC-wt significantly promotes the ability of cell migration in NB-39-nu cells. (**a**) Wound-healing assay for ShcC mutant cells. Photographs of the cells taken 48 h after wounding under a microscope. Bar: 200 μm. (**b**) Photographs (upper panel) and graph (lower panel) of ShcC mutant cells that have migrated through the filter by modified Boyden chamber cell migration assay. The graph represents the results (expressed as mean $\pm$s.d.) of the experiments performed in triplicate. (**c**) Photographs (upper panel) and a graph (lower panel) of the results from cell invasion assay

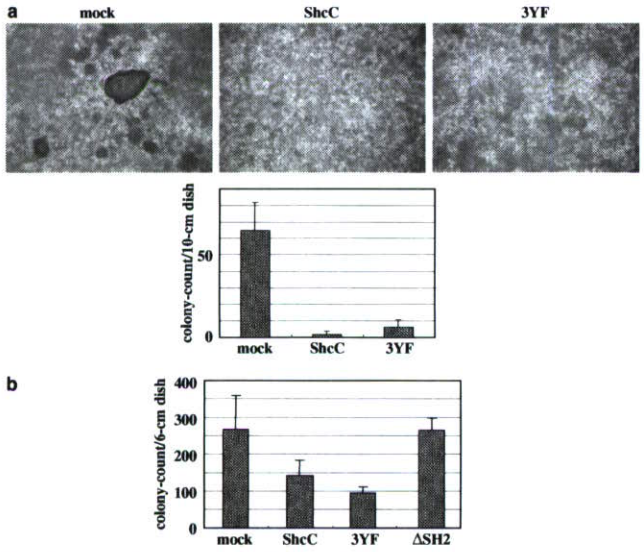

Figure 5 Evaluation of *in vitro* transforming activity in NB-39-nu cells expressing ShcC mutants. (**a**) Tendency for ShcC mutant cells to form cell aggregations on the dish surface as described in Materials and methods. Photographs of each dish were taken with a microscope at a magnification of $\times$40 (upper panel). The graph represents the mean values ($\pm$s.d.) of three independent experiments (lower panel). (**b**) Anchorage-independent growth of ShcC mutant cells was evaluated by assaying colony formation in soft agar (performed as described in Materials and methods). The results represent the average values ($\pm$s.d.) of three replicated experiments

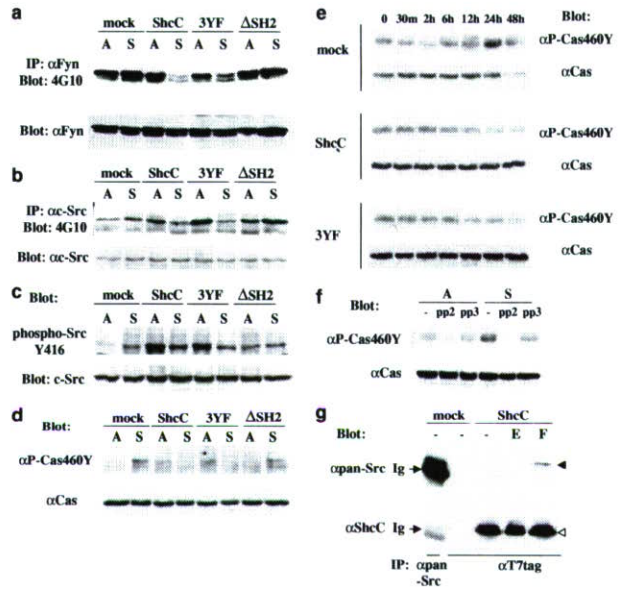

Figure 6 Anchorage-independent activation of Src family kinases (SFKs) and tyrosine phosphorylation of Cas in NB-39-nu is affected by the expression of ShcC. The cell suspension culture of ShcC mutant cells was essentially performed as described in Materials and methods. **A**: attached cells. **S**: cells in a suspended condition. Lysates were duplicated and detected by immunoprecipitation and Western analysis. (**a**, **b** and **c**) Cells cultured for 24 h in adherent or suspended conditions were analysed with the antibodies against each Src family kinase shown in the figure. Anti-phospho-Src Y416 recognizes all Src family members phosphorylated at the tyrosine corresponding to Tyr416 of avian Src. (**d**) Same analysis performed as (**a**) (**b**) and (**c**) using the antibodies against for phospho-460Y of Cas (αP-Cas460Y) and Cas protein (αCas). (**e**) Time course of tyrosine phosphorylation of Cas in each ShcC mutant cells cultured in suspension for the indicated time periods. (**f**) Effect of Src inhibitor, PP2, on the tyrosine phosphorylation of Cas in NB-39-nu control cells. The cells cultured for 24 h were harvested following treatment with 10 μM of PP2 for 2 h. As a negative control, the same dose of PP3 was used in place of PP2. (**g**) ShcC forms complex with SFKs following the stimulation of fibronectin. Lysates of mock cells and ShcC-wt cells were analysed after the stimulation with EGF or fibronectin as described in Materials and methods. -: serum free without stimulation; E: stimulated by EGF; F: stimulated by fibronectin. Ig: immunoglobulin. Anti-pan-Src antibody (SRC2) reacts with c-Src p60, Yes p62, Fyn p59, c-Fgr p55 and c-Src2. closed arrowhead: SFK; open arrowhead: p52 ShcC

dent growth and tumorigenicity suggests a novel function of ShcC. Taking into account that the expression of 3YF-ShcC but not ΔSH2-ShcC showed similar effects, the SH2 domain of ShcC may be responsible for this unique function of ShcC, distinct from ShcA. In addition, the least changes in ERK1/2 or Akt activation by overexpression of ShcC-wt suggest that this function might be independent of phosphorylation of Grb2-binding sites or the activation levels of downstream targets. There are reports showing different binding specificity towards phosphotyrosine-containing motifs among Shc families (O'Bryan *et al*., 1996a, b; Pelicci *et al*., 1996). It is crucial to identify the molecules associating with the SH2 domain of ShcC in neuroblastoma cells to elucidate the mechanism of these SH2-mediated effects of ShcC.

The smaller size of the nude mouse tumors due to the expression of ShcC-wt, regardless of mild changes in cell proliferation as both tumor tissue and culture cells, may also reflect suppression of anchorage independency (Freedman and Shin, 1974; Kumar, 1998), which results in the loss of the majority of the injected cells by anoikis before they start forming tumors. The anchorage independency of NB-39-nu mutants well corresponded to the sustained phosphorylation levels of c-Src, Fyn and Cas after cell detachment, suggesting that the expression of ShcC-wt has a negative effect on anchorage independency due to the suppression of the SFK-Cas pathway (Figure 6). It is possible that ShcC-SH2 plays a competitive role with YDYV in the Src-binding domain of Cas, judging from the consensus motifs binding to ShcC-SH2 (O'Bryan *et al*., 1996a, b), although this association was not detected by usual immunoprecipitation experiments (data not shown). On the other hand, the fact that ShcC forms the complex with SFK in this study indicates that there might be a role of association between SFK and ShcC in the regulation of tyrosine kinase activity of SFK. The fact that malignant neuroblastoma cell lines with hyperphosphorylated ShcC frequently have lower expression level